# WAVE OVERTOPPING AT RUBBLE MOUND BREAKWATERS WITH A NON-RESHAPING BERM

AN EXPERIMENTAL RESEARCH

M.Sc. Thesis

J.C. Krom
December 2012

Delft University of Technology
*Faculty of Civil Engineering and Geosciences*
*Department of Hydraulic Engineering*

Van Oord
*Dredging and Marine Contractors*

*Front cover image:*

*Original picture: "Mike" Michael L. Baird (2008).*
*Morro Bay Winter Storm February 24th 2008. Online image.*
*Retrieved October 18th 2012 from: http://www.flickr.com/photos/mikebaird/2289247641*
*Minor digital enhancements were made.*

*Note: This document has been designed for full colour double-sided printing*

# COLOPHON

M.Sc. Thesis
Subject: "Wave overtopping at rubble mound breakwaters with a non-reshaping berm"
Rotterdam, December 2012

A dissertation submitted in partial fulfilment of the requirements for the degree of Master of Science in Civil Engineering, track Hydraulic Engineering, specialisation Coastal Engineering.

**Institutes**

Delft University of Technology
*Faculty of Civil Engineering and Geosciences*
*Department of Hydraulic Engineering*
*P.O. Box 5048*
*2600 GA, Delft*
*The Netherlands*

Van Oord
*Dredging and Marine Contractors*
*P.O. Box 8574*
*3009 AN,*
*Rotterdam*
*The Netherlands*

**Author**

J.C. Krom
Email: jankees_krom@hotmail.com
Study number: 1304011

**Graduation committee**

| | |
|---|---|
| Prof. dr. ir. W.S.J. Uijttewaal | *Environmental Fluid Mechanics, TU Delft* |
| Ir. J.P. van den Bos | *Hydraulic Engineering, TU Delft/ Hydronamic, Royal Boskalis Westminster* |
| Ir. H.J. Verhagen | *Hydraulic Engineering, TU Delft* |
| Ir. G.M. Smith | *Estimating & Engineering, Van Oord* |
| Ir. W.J. Ockeloen | *Maritime & Waterways, Royal HaskoningDHV* |

# ABSTRACT

This thesis focuses on wave overtopping at rubble mound breakwaters with a non-reshaping berm. The research was aimed at gaining insight into the influence of a permeable berm on the overtopping behaviour. Moreover it was desired to validate existing prediction methods for the spatial distribution of overtopping for breakwaters with a non-reshaping berm.

Wave overtopping was investigated by means of a physical model. The breakwater scale model was divided into 8 collection bins. Overtopped volumes were collected and pumped into floating tanks further down the flume. After the experiment the mass of the floating tanks was measured and the mean overtopping discharge could be determined for 8 horizontal positions on the breakwater. The measured total overtopping discharges cannot be predicted accurately by existing prediction methods. On the basis of experimental data a new prediction method was proposed that achieves an excellent fit for total overtopping. The crest freeboard definition was adjusted to account for the permeability of the crest. The reduction factor accounting for slope roughness was made dependent on the Iribarren number. For Iribarren numbers higher than 6, this method calculates no reduction of overtopping due to slope roughness. The effect of a permeable berm on total overtopping was found to be remarkably different from the effect of an impermeable berm. Permeable berms below Still Water Level (SWL) lead to less reduction of overtopping than impermeable berms below SWL. Berms above SWL lead to wave breaking on the slope in front of the berm. Contrarily to impermeable berms above SWL, a permeable berm above SWL leads to significant reduction of overtopping.

The measured spatial distribution of overtopping is associated with a lot of seemingly random behaviour. Large differences were found with the experimental data of Lioutas (2010). It is suspected that the used experiment setup gives rise to significant model effects for the spatial distribution of overtopping. An experiment setup was recommended that is expected to more accurately model the behaviour of the prototype situation. Data on the spatial distribution of overtopping could not accurately be predicted by existing prediction methods. In some cases existing prediction methods provided an upper limit for overtopping (Juul Jensen, 1984) but none led to a good fit with the experimental data. A new reduction factor was found that reduces the amount of scatter and provides a conservative prediction of the experimental data.

**Keywords**
Wave Overtopping, Spatial Distribution, Rubble Mound Breakwaters, Non-reshaping Permeable Berm, Physical Experiments, Prediction Method

# PREFACE

This thesis is the final report of a research project carried out to obtain the degree of Master of Science at Delft University of Technology. In this report the findings of a study into the behaviour of overtopping at breakwaters with a non-reshaping berm are presented. Physical experiments were conducted at the Laboratory of Fluid Mechanics at Delft University of Technology. The study was carried out in cooperation with the Engineering Department of Van Oord.

The facilities and support of both Van Oord and Delft University of Technology are greatly appreciated. Ever since my childhood I've been fascinated by the behaviour of flowing water. At first glance the water surface may look irregular and unpredictable, yet for a keen observer patterns and general trends become clear. In this experimental study I had the chance to perform scientific research while gaining a more practical insight into the interaction between waves and breakwater.

I would like to thank Sander de Vree for his daily technical support during the experimental phase. The members of the graduation committee are acknowledged for their advice and the enthusiasm with which they supervised this research. From Delft University of Technology: Wim Uijttewaal, Henk Jan Verhagen and Jeroen van den Bos. From Van Oord: Greg Smith. From Royal HaskoningDHV: Wouter Ockeloen.

I also would like to thank Anestis Lioutas for his support. The discussions we had regarding the experiment setup and the interpretation of the results were highly appreciated.

Finally I would like to thank my family, friends and colleagues for their support during the research.

Jan Kees Krom
Rotterdam, December 2012

# TABLE OF CONTENTS

# LIST OF FIGURES

# LIST OF TABLES

# LIST OF SYMBOLS

| | | |
|---|---|---|
| A | Empirical coefficient | [-] |
| $A$ | Erosion area in cross-section (Van der Meer, 1988) | [m²] |
| $A_C$ | Armour freeboard of structure | [m] |
| a | Coefficient of friction for laminar part (Forchheimer, 1901) | [s/m] |
| a | Empirical coefficient (Owen, 1980) | [-] |
| $a$ | Wave amplitude | [m] |
| B | Empirical coefficient | [-] |
| $B$ | Berm width | [m] |
| $B_*$ | Dimensionless berm width (Lykke Andersen, 2006) | [-] |
| $B^*$ | Horizontal distance from intersection of the SWL and the sea side slope to the very end of the crest (Juul Jensen, 1984) | [m] |
| b | Coefficient of friction for turbulent part (Forchheimer, 1901) | [s²/m²] |
| b | Empirical coefficient (Owen, 1980) | [-] |
| C | Empirical coefficient | [-] |
| $C_r$ | Reduction factor for overtopping $= q(x)/q_{tot}$ | [-] |
| c | Coefficient for inertial resistance (Forchheimer, 1901) | [s²/m] |
| $c_{pl}$ | Empirical coefficient for plunging waves (Van der Meer, 1988) | [-] |
| $c_s$ | Empirical coefficient for surging waves (Van der Meer, 1988) | [-] |
| D | Empirical coefficient | [-] |
| $D_n$ | Nominal stone diameter | [m] |
| $D_{n50}$ | Median nominal stone diameter $= (M_{50}/\rho_s)^{1/3}$ | [m] |
| $D_{n50,armour}$ | Median nominal stone diameter of the armour layer | [m] |
| $D_x$ | Diameter of stone that exceeds the x% value of the sieve curve | [m] |
| $D_{x,B}$ | Diameter of stone that exceeds the x% value of the sieve curve, base layer. | [m] |
| $D_{x,F}$ | Diameter of stone that exceeds the x% value of the sieve curve, filter layer | [m] |
| $d_B$ | Berm elevation | [m] |
| $d_{B*}$ | Dimensionless berm elevation (Lykke Andersen, 2006) | [-] |
| $E(f)$ | Variance density spectrum | [m²s] |
| Fr | Froude number | [-] |
| $F$ | Exceedance probability of travel distance (Lykke Andersen, 2006) | [-] |
| $f$ | Wave frequency $= 1/T$ | [1/s] |
| $f_{dB\geq 0}$ | Empirical coefficient describing the influence of a berm | [-] |
| $f_{dB<0}$ | Empirical coefficient describing the influence of a berm | [-] |
| $f_{PM}$ | Peak frequency of a Pierson-Moskowitz spectrum | [1/s] |
| $f_{H0}$ | Factor accounting for the influence of stability numbers (Lykke Andersen, 2006) | [-] |
| $f_{peak}$ | Peak frequency of a wave spectrum | [1/s] |
| $G_C$ | Crest width | [m] |
| $G_*$ | Dimensionless crest width (Lykke Andersen, 2006) | [-] |
| $g$ | Gravitational acceleration | [m/s²] |
| $H_0$ | Stability number $= \frac{H_s}{\Delta D_{n50}}$ | [-] |
| $H_0T_0$ | Dynamic stability number | [-] |
| $H_{1/3}$ | Average of the highest 1/3 of wave heights | [m] |
| $H_{1/1000}$ | Average of highest 1/1000 of wave heights | [m] |
| $H_{m0}$ | Significant wave height from spectral analysis $= 4\sqrt{m_0}$ | [m] |
| $H_{rms}$ | Root mean square wave height | [m] |

| | | |
|---|---|---|
| $H_s$ | Significant wave height | [m] |
| $H^*$ | Dimensionless wave height (Van Kester, 2009) | [-] |
| $H_d^*$ | Threshold value for overtopping behind the crest (Van Kester, 2009) | [-] |
| $H^*T^*$ | Dimensionless presentation of wave flux (Van Kester, 2009) | [-] |
| $h$ | Water depth; water depth at structure toe | [m] |
| $h_{ex}$ | Extraction depth of collection bins | [m] |
| $I$ | Hydraulic pressure gradient | [-] |
| k | Empirical coefficient (Lioutas, 2012) | [-] |
| $L$ | Wave length measured in direction of wave propagation | [m] |
| $L_0$ | Deep water wave length $= gT_0^2/2\pi$ | [m] |
| $L_{0m}$ | Deep water mean wave length $= gT_m^2/2\pi$ | [m] |
| $L_{0p}$ | Deep water peak wave length $= gT_p^2/2\pi$ | [m] |
| $L_{Berm}$ | Berm width parameter | [m] |
| $L_{m-1,0}$ | Wave length based on $T_{m-1,0}$ | [m] |
| $L_{0p}$ | Deep water peak wave length $= gT_p^2/2\pi$ | [m] |
| $M_n$ | Mass of particle for which n % of granular material is lighter | [kg] |
| $m_n$ | $n^{\text{th}}$ moment of spectrum | [$m^{2+n}s$] |
| $N$ | Number of incoming waves during storm period | [-] |
| $N_x$ | Prototype-to-model scale ratio for parameter $x$ | [-] |
| $n_v$ | Porosity | [-] |
| $P$ | Wave energy flux | [J/ms] |
| $P$ | Notional permeability of structure (Van der Meer, 1988) | [-] |
| $q$ | Mean overtopping discharge per meter structure width | [$m^3/m/s$] |
| $q_{bc}$ | Mean overtopping discharge directly behind the crest | [$m^3/m/s$] |
| $q_{tot}$ | Mean total overtopping discharge | [$m^3/m/s$] |
| $q(x)$ | Mean overtopping discharge at location $x$ | [$m^3/m/s$] |
| $q^*$ | Dimensionless overtopping discharge | [-] |
| $q_d^*$ | Threshold value for overtopping behind the crest (Steenaard, 2002) | [-] |
| $q_i$ | Overtopping intensity (Juul Jensen, 1984) | [$m^3/m^2/s$] |
| $q_J^*$ | Dimensionless overtopping discharge (Juul Jensen, 1984) | [-] |
| $q_{tot,S}^*$ | Dimensionless total overtopping discharge (Steenaard, 2002) | [-] |
| $R_C$ | Crest freeboard of structure | [m] |
| $R_{u2\%}$ | Run-up height exceeded by 2% of the waves | [m] |
| $R_*$ | Dimensionless crest freeboard (Lykke Andersen, 2006) | [-] |
| $R^*$ | Dimensionless crest freeboard | [-] |
| $r_B$ | Berm width parameter | [-] |
| $r_{db}$ | Berm elevation parameter | [-] |
| $S$ | Characteristic value of damage level (Van der Meer, 1988) | [-] |
| $s$ | Wave steepness $= H/L$ | [-] |
| $s_{0m}$ | Deep water mean wave steepness $= H/L_{0m}$ | [-] |
| $s_{0p}$ | Deep water peak wave steepness $= H/L_{0p}$ | [-] |
| $s_{m-1,0}$ | Wave steepness based on $L_{m-1,0}$ , $= H/L_{m-1,0}$ | [-] |
| $T$ | Wave period | [s] |
| $T_0$ | Dimensionless wave period $= \sqrt{g/D_{n50}}$ | [-] |
| $T_0^*$ | Dimensionless wave period transition (Lykke Andersen, 2006) | [-] |
| $T_m$ | Mean wave period | [s] |
| $T_{m-1,0}$ | Spectral wave period $= m_{-1}/m_0$ | [s] |
| $T_{m0,1}$ | Spectral wave period $= m_0/m_1$ | [s] |
| $T_p$ | Spectral peak wave period | [s] |
| $T_z$ | Mean zero-crossing wave period | [s] |

| | | |
|---|---|---|
| $u_{drain}$ | Drainage capacity in the collection bins | [m/s] |
| $u_f$ | Filter velocity | [m/s] |
| $u_p$ | Flow velocity in the pores | [m/s] |
| $x$ | Distance behind the crest | [m] |
| $x$ | Distance from seaward end of the crest | [m] |
| $x^*$ | Dimensionless distance behind the crest | [-] |
| $y$ | Vertical distance between crest wall elevation and position of the tanks (Lykke Andersen, 2006) | [m] |
| $\Delta$ | Relative density $= \frac{\rho_s - \rho_w}{\rho_w}$ | [-] |
| $\alpha$ | Angle between overall structure slope and the horizontal | [°] |
| $\alpha$ | Energy scale of a wave spectrum | [-] |
| $\alpha_{PM}$ | Energy scale of a Pierson-Moskowitz spectrum | [-] |
| $\beta$ | Angle of wave attack relative to the normal of the structure | [°] |
| $\beta$ | Empirical constant, equal to the distance for which the overtopping intensity decreases with a factor 10 (Juul Jensen, 1984) | [m] |
| $\gamma$ | Peak-enhancement factor for wave spectrum | [-] |
| $\gamma_b$ | Reduction factor to account for influence of the berm | [-] |
| $\gamma_c$ | Reduction factor to account for distance from the crest | [-] |
| $\gamma_f$ | Reduction factor to account for slope roughness | [-] |
| $\gamma_v$ | Reduction factor to account for vertical wall on the crest | [-] |
| $\gamma_\beta$ | Reduction factor to account for oblique waves | [-] |
| $\mu$ | Dynamic viscosity | [kg/ms] |
| $\mu(x)$ | Mean value of $x$ | [] |
| $\nu$ | Kinematic viscosity | [m²/s] |
| $\xi$ | Breaker parameter; Iribarren number $= \frac{\tan(\alpha)}{\sqrt{s}}$ | [-] |
| $\xi_{cr}$ | Critical value for the breaker parameter (Van der Meer, 1988) | [-] |
| $\xi_{m-1,0}$ | Breaker parameter based on $T_{m-1,0}$ , $= \frac{\tan(\alpha)}{\sqrt{2\pi H / g T_{m-1,0}^2}}$ | [-] |
| $\rho_w$ | Specific density of water | [kg/m³] |
| $\rho_s$ | Specific density of rock | [kg/m³] |
| $\sigma$ | Peak-width parameter | [-] |
| $\sigma_a$ | Peak-width parameter for $f < f_{peak}$ | [-] |
| $\sigma_b$ | Peak-width parameter for $f < f_{peak}$ | [-] |
| $\sigma(x)$ | Standard deviation of $x$ | [] |

# CHAPTER 1. INTRODUCTION

In this thesis the behaviour of overtopping at rubble mound breakwaters with a non-reshaping berm is discussed. First a brief introduction to overtopping and breakwaters in general is given in section 1.1. The problem definition is formulated in section 1.2. Section 1.3 presents the research objectives. The methodology that was used to conduct the research is discussed in section 1.4. To conclude the structure of the report is described in section 1.5.

## 1.1 GENERAL INFORMATION

### 1.1.1 COASTAL DEFENCE STRUCTURES

Across the globe coastal defence structures are constructed to regulate the interaction between land and sea. The term coastal defence structures covers a large variety of structures, among which sloping dikes, breakwaters, sea walls and flood gates. Here 2 of these types are discussed, being 1) sloping dikes, historically often applied to protect European and in particular Dutch coastlines from flooding, and 2) breakwaters, generally constructed to protect a harbour basin from severe wave action.

Breakwaters are either rubble mound breakwaters, consisting of large quantities of loose elements, or monolithic breakwaters, large solid blocks that are positioned on a foundation. In this research rubble mound breakwaters are considered.

Both sloping dikes and rubble mound breakwaters are covered with some kind of armour protection, to withstand wave attack and prevent erosion of the structure. One of the key differences between the structure types is the hydraulic permeability of the core. Wave energy is hardly able to penetrate the core of a sloping dike. Sloping dikes are considered impermeable. The core of a breakwater is more permeable and here energy dissipation occurs during wave attack. Breakwater cores therefore are considered permeable. For a more extensive discussion of structure permeability refer to subsection 2.1.1. A second difference is the roughness of the structures. Sloping dikes are generally built using placed blocks, leading to a rather smooth surface whereas breakwaters have an armour layer consisting of rubble mound or concrete elements that generally leads to a very irregular surface. The roughness of the armour slope has a significant effect on both run-up and overtopping. For further information about roughness refer to subsection 2.1.1.

An example of a breakwater is printed in Figure 1.1-1. This breakwater in South Africa protects the harbour basin of the East London port from a severe wave climate. While the waves break on the breakwater the harbour basin behind it is relatively calm. The ship wreck on the southern breakwater illustrates the harsh sea states that the region is confronted with. The breakwater was designed to withstand wind-generated waves with a significant wave height of 8.5 m.


FIGURE 1.1-1: BREAKWATER AT PORT ENTRANCE OF EAST LONDON, SOUTH AFRICA. GOOGLE EARTH. ONLINE IMAGE. RETRIEVED OCTOBER 26TH 2012 FROM GOOGLE EARTH.

Rubble mound breakwaters exist in a large variety of configurations. The Rock Manual (2007) describes the configurations depicted in Figure 1.1-2.

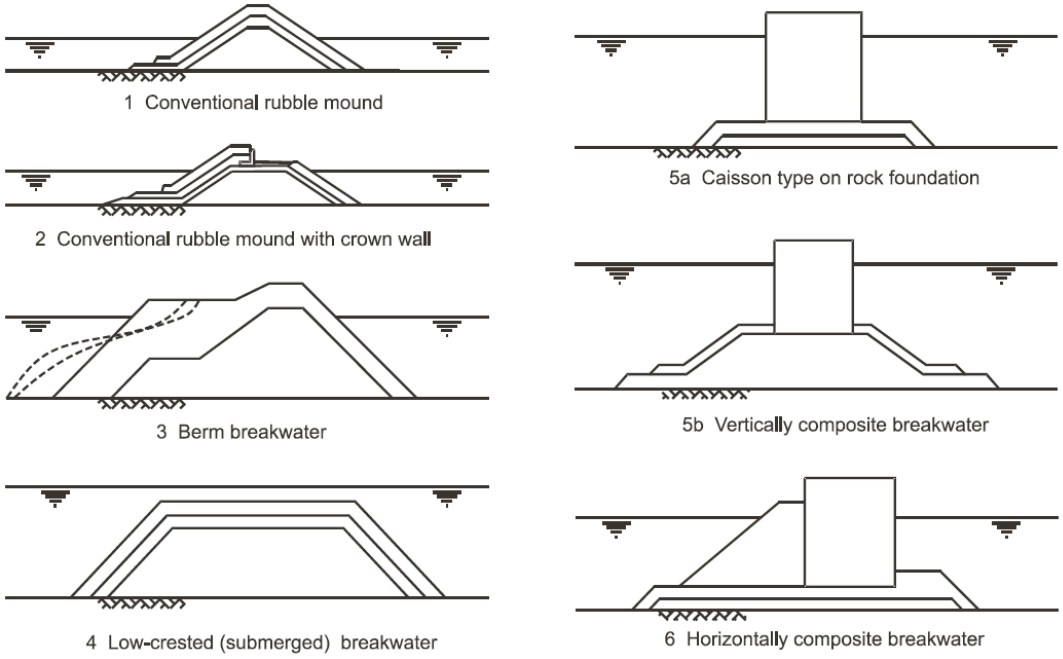


FIGURE 1.1-2: TYPICAL CROSS-SECTIONS OF VARIOUS TYPES OF RUBBLE MOUND BREAKWATERS (ROCK MANUAL, 2007)

In this thesis the focus lies specifically on non-reshaping berm breakwaters; the solid line in configuration 3 in Figure 1.1-2. In literature this type of breakwater is sometimes also addressed as a breakwater with a berm. No reshaping takes place after construction. The berm leads to reduction of the wave energy so that the main slope of the breakwater is confronted with less violent wave attack. Therefore stones used in the armour layer of the upper slope can be can be significantly smaller (Van Gent, Smith, & Van der Werf, 2012). Moreover the run-up height also is decreased, allowing for a lower crest height. Breakwaters with a berm are therefore often an attractive option for recreational areas.

Two other types of berm breakwaters exist that are designed for more movement of the armour layer. The cross-section of a reshaped statically stable berm breakwater transforms during a storm when material from the berm is moved offshore. With this type eventually the individual stones are stable. The cross-section of a dynamically stable reshaping berm breakwater also gets changed during a storm, resulting in a naturally stable S-profile, but here the individual stone are still moving up and down the slope. Averaged over time (multiple wave periods) however, there is no movement.

The armour layer of conventional rubble mound breakwaters generally is designed using the armour stability formula of Van der Meer (1988). An adjusted version of this method is demonstrated in section 3.2.

When one wants to design a berm breakwater a design procedure should be chosen. The following procedure was used for the Sirevåg breakwater in Norway (Sigurdarson et al., 2003).

1. Is it economical to design a conventional rubble mound structure following the Van der Meer method? Check if all quarried material can be used in the project or sold to other projects.
2. Is it more economical to design a statically stable non-reshaping berm breakwater with the largest stone class similar to Van der Meer criteria or with $H_0 = \frac{H_s}{\Delta D_{n50}}$ up to about 2. The demand for large stones is usually less in option 2 than in option 1. If there is a quarry available to dedicate to the project, then option 2 is often more economical, usually for design wave height higher than $H_s$ = 2 to 3 m.
3. If large stones, relative to the design wave height, are not available, then a wider and more voluminous berm breakwater of the statically stable reshaped type should be chosen.
4. If option 1 to option 3 are not possible, then a dynamically stable berm breakwater design should be investigated. This could be a suitable structure for a trunk section connecting an island to the shore, but is not suitable for a head section.

Dynamically stable reshaping berm breakwaters have a larger volume but still can be economically attractive because smaller armour stones can be used.

In this thesis the most stable berm breakwater type is considered; a berm breakwater with a non-reshaping berm.

### 1.1.2 DEFINITION OF WAVE OVERTOPPING

Wave overtopping is a hydraulic phenomenon related to the interaction between coastal defence structures and wave action. Cost effective design of coastal structures commonly leads to a crest height that is higher than the run-up height of a large part of the wave spectrum, while the highest waves of the spectrum can still overtop the structure. Consequently a portion of the water associated with the highest waves will be transported over the crest. This water is referred to as wave overtopping. The different steps in the wave breaking process are depicted in Figure 1.1-3.

There are multiple causes for wave overtopping. EurOtop (2007) denotes three causes, being 1) wave run-up or surge action, leading to an almost continuous flow over the crest, 2) wave breaking on the seaward face of the slope, producing significant volumes of splash water which will partly be transported over the crest, and 3) wave spray produced by the interaction between wind and waves directly seaward of the coastal defence structure.

Wave overtopping is often referred to as "green water" when more or less complete sheets of water flow over the crest, as would be the case for the first cause. "White water" on the other hand denotes wave overtopping due to cause 2 and 3. The latter two processes lead to much air entrainment in the overtopping water, hence the name "white water".

The main parameter when assessing wave overtopping is the mean discharge per meter of width, $q$. This parameter is generally measured in $m^3/s$ per meter crest width or l/s per meter crest width. Wave overtopping is highly time dependent; the instantaneous overtopping discharge can be much larger than the mean discharge, but will then be followed by a relatively long period of little or no overtopping discharge.

Overtopping is a highly complex process that depends on a large variety of parameters. Scatter of an order 10 in experiment results is not uncommon.

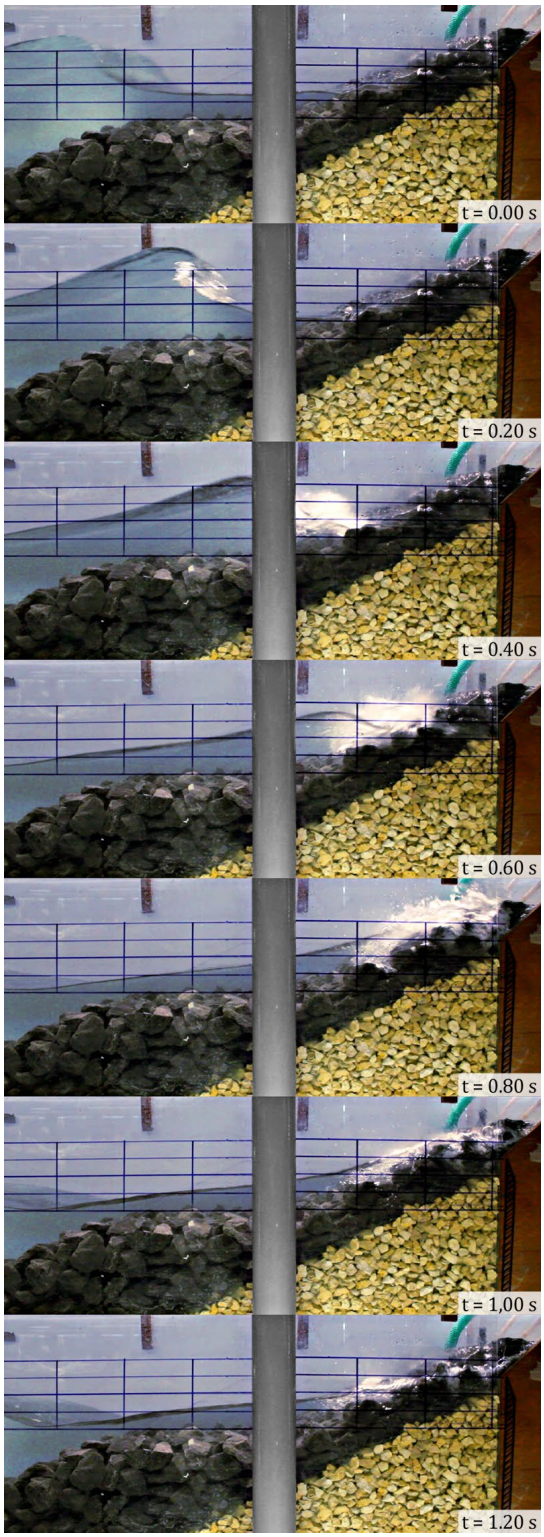


FIGURE 1.1-3: WAVE BREAKING ON A RUBBLE MOUND BREAKWATER WITH A BERM

### 1.1.3 HAZARDS DUE TO WAVE OVERTOPPING

Wave overtopping can bring inconvenience or harm to people and property in various forms. EurOtop (2007) mentions four general categories under which the dangers of wave overtopping can be placed:

1. Direct hazard of injury or death to people immediately behind the defence.
2. Damage to property, operation and/or infrastructure in the area defended, including loss of economic, environmental or other resource, or disruption to an economic activity or process.
3. Damage to defence structure(s), either short-term or longer-term, with the possibility of breaching and flooding.
4. Low depth flooding (inconvenient but not dangerous).

FIGURE 1.1-4: FLOODING CAUSED BY OVERTOPPING.
ONLINE IMAGE. RETRIEVED OCTOBER 26TH 2012 FROM
WWW.RESEARCH.PLYMOUTH.AC.UK/CERG/FIELD_OF_WORK/EPIRUS.HTM

### 1.1.4 TOLERABLE WAVE OVERTOPPING

Wave overtopping is not necessarily dangerous. A certain amount of overtopping may be permitted in extreme situations. Guidelines were developed indicating maximum values of mean wave overtopping discharges, depending on the purpose the land should fulfil, refer to Table 1-1.

TABLE 1-1: ALLOWABLE OVERTOPPING DISCHARGES (ALLSOP, FRANCO, BELLOTTI, BRUCE, & GEERAERTS, 2005)

| | $q$ [$m^3/m/s$] |
|---|---|
| **Pedestrians** | |
| Unsafe for unaware pedestrians, no clear view of the sea, relatively easily upset or frightened, narrow walkway or proximity to edge | $3 \cdot 10^{-5} < q$ |
| Unsafe for aware pedestrians, clear view of the sea, not easily upset or frightened, able to tolerate getting wet, wider walkway | $1 \cdot 10^{-4} < q$ |
| Unsafe for trained staff, well shed and protected, expected to get wet, overtopping flows at lower levels only, no falling jet, low danger of fall from walkway | $1 \cdot 10^{-3}$ to $0.01 < q$ |
| **Vehicles** | |
| Unsafe for driving at moderate or high speed, impulsive overtopping fiving falling or high velocity jets | $1 \cdot 10^{-5}$ to $5 \cdot 10^{-5} < q$ |
| Unsafe for driving at low speed, overtopping by pulsating flows at low levels only, no falling jets | $0.01$ to $0.05 < q$ |
| **Marinas** | |
| Sinking of small boats set 5-10 m from wall, damage to larger yachts | $0.01 < q$ |
| Significant damage or sinking of larger yachts | $0.05 < q$ |
| **Buildings** | |
| No damage | $q < 1 \cdot 10^{-6}$ |
| Minor damage to fitting etc. | $1 \cdot 10^{-6} < q < 3 \cdot 10^{-5}$ |
| Structural damage | $3 \cdot 10^{-5} < q$ |
| **Embankment seawalls** | |
| No damage | $q < 2 \cdot 10^{-5}$ |
| Damage if crest not protected | $2 \cdot 10^{-3} < q < 0.02$ |
| Damage if back slope not protected | $0.02 < q < 0.05$ |
| Damage even if fully protected | $0.05 < q$ |
| **Revetment seawalls** | |
| No damage | $q < 0.05$ |
| Damage if promenade not paved | $q < 0.2$ |
| Damage even if promenade paved | $0.2 < q$ |

### 1.1.5 OVERTOPPING FOR BREAKWATERS WITH A NON-RESHAPING BERM

Existing literature on overtopping covers either impermeable structure with a berm, or permeable structures without a berm. The rough, permeable character of a berm constructed in front of a breakwater may very well lead to different overtopping behaviour. Therefore it is unsure if existing prediction methods can calculate the effect of a permeable berm on wave overtopping with a reasonable degree of accuracy.

In design practice a breakwater with a berm is quite commonly applied. It is therefore important to investigate the predictive power of existing prediction methods for this kind of structure.

### 1.1.6 SPATIAL DISTRIBUTION OF WAVE OVERTOPPING

The wave overtopping discharge will decrease when moving farther land inward. Part of the overtopping water infiltrates into the backfill material while the remaining part travels onward. This is a very complex process where wave conditions and structure parameters can be expected to all play a significant role.

In comparison with the existing knowledge on total overtopping, literature covering the spatial distribution of overtopping is rather limited. Some research has been carried out (e.g. Juul Jensen (1984), Lykke Andersen (2006), Lioutas, Smith, and Verhagen (2012)) but the relations found do not include all parameters that can be expected to have an influence (e.g. backfill porosity or wave steepness).

In design practice an overtopping criterion will not be imposed at the crest of the coastal defence structure. A walkway or other facility will be built at a certain distance from the crest, and the actual mean overtopping discharge should be calculated for that particular position. Therefore overtopping prediction methods should properly cover the spatial distribution of wave overtopping.

## 1.2 PROBLEM DEFINITION

Previous sections have illustrated the importance of adequate prediction methods for wave overtopping. Knowledge about overtopping behaviour is not complete for breakwaters with a non-reshaping berm. The following two problems can be observed:

- Existing literature on overtopping covers either impermeable structure with a berm, or permeable structures without a berm. For breakwaters with a non-reshaping berm it is expected the roughness and permeability of the berm lead to different overtopping behaviour.
- Current prediction methods for the spatial distribution of overtopping have not been verified to be accurate for breakwaters with a non-reshaping berm.

## 1.3 RESEARCH OBJECTIVE

The objective of this research can be stated as follows:

> *To provide insight in the overtopping phenomenon for rubble mound breakwaters with a non-reshaping berm. If existing prediction methods do not accurately describe the relations found, it is the intention to recommend a method that has an increased predictive power. In the end the aim is to provide more accurate guidance in the design practice of breakwaters. Both the total overtopping volume and the spatial distribution of overtopping will be investigated.*

## 1.4 RESEARCH METHODOLOGY

Overtopping at rubble mound breakwaters is a highly complex process. Accurate analytical methods are not available. Research investigating overtopping can typically be divided into two categories; physical-model tests where a scale model is built and the overtopped water is collected, or numerical tests where overtopping is investigated using mathematical models to properly simulate wave propagation and other main processes (e.g. Peng and Zou (2011)). In numerical modelling it is inevitable to make simplifications in terms of geometry and governing physical processes. Currently numerical modelling cannot be used to efficiently and accurately model overtopping at rubble mound breakwaters. Therefore in the current research overtopping is investigated using physical model tests.

The research objective has been approached in sequential steps. The steps taken in order to properly conduct the experimental research are listed below.

- Existing literature related to overtopping was studied in order to understand the physical process and identify the essential parameters involved.
- A laboratory plan was composed for the execution of the experiments in the laboratory. The scale model and experiment setup were introduced and an overview all test series to be conducted was presented.
- Experiments were executed using the same measuring system as Lioutas (2010). Water was collected in multiple collection bins and pumped into floating tanks to ensure the Still Water Level (SWL) in front of the breakwater remains constant. First validation tests were run to ensure experiment similarity. Thereafter the experiments for breakwaters with a non-reshaping berm were carried out.
- Results were gathered and evaluated in relation to existing prediction methods.
- In the end conclusions were drawn and recommendations for further research were formulated.

## 1.5 STRUCTURE OF THE REPORT

The structure of the report follows to a large extent the research methodology. Chapter 2 begins by discussing existing literature, and looks at the relevancy for the current research. In Chapter 3 the experimental part of this study is described. Results of the experiments are compared with existing prediction methods in Chapter 4 and Chapter 5, for total overtopping and the spatial distribution of overtopping respectively. During the experiments it became clear the experiment setup may give rise to significant model effects. Therefore the experiment setup is discussed in Chapter 6. Finally, in Chapter 7 conclusions and recommendations are drawn.

# CHAPTER 2. THEORETICAL BACKGROUND

In this chapter existing literature is discussed that is related to overtopping. First in section 2.1 the physical and hydraulic parameters are presented. Then in sections 2.2 and 2.3 literature is discussed, for total overtopping and the spatial distribution of overtopping respectively. Section 2.4 provides conclusions that can be drawn from the discussed literature.

## 2.1 PHYSICAL AND HYDRAULIC PARAMETERS

In this section the main parameters that are relevant for the wave overtopping process are discussed. The parameters have been defined in coherence with EurOtop (2007).

### 2.1.1 PHYSICAL DIMENSIONS OF BREAKWATERS

#### CREST

The crest freeboard, $R_C$, is the vertical distance between the crest elevation and Still Water Level (SWL). The armour freeboard, $A_C$, is the vertical distance between the top of the armour layer and SWL. $G_C$ depicts the width of the horizontal part of the crest.

The crest height is defined as the elevation of the most seaward point at which run-up water cannot run down anymore. In literature there is some ambiguity about which elevation should be used for permeable crests. Historically the TAW (2002) formulae use the top of the armour layer as crest height, as they were developed for impermeable structures. For permeable structures TAW (2002) and EurOtop (2007) recommend not taking into account the armour layer; the top of the underlying filter layer should be used as crest elevation. When a wave wall is constructed behind the armour layer, the top of the wave wall should be taken as crest height.

Lioutas et al. (2012) concluded from experiments that $R_C = A_C - 0.9 \cdot D_{n50,armour}$ should be used, to properly account for the permeability of the armour layer.

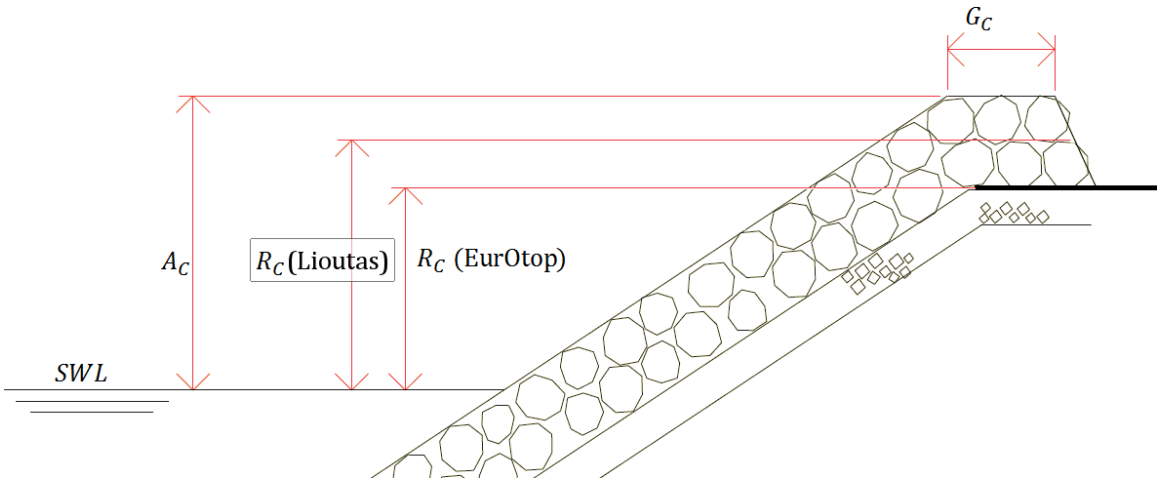


FIGURE 2.1-1: CREST FREEBOARD, ARMOUR FREEBOARD AND CREST WIDTH

### SEAWARD SLOPE

A part of a structure is referred to as a slope when the slope of that part is at least 1:8 and at most 1:1. If a slope is gentler than 1:8 the slope is considered as a foreshore. In design often a slope as steep as possible is chosen to make a cost-effective design. Hydraulic and structural boundary conditions or requirements will determine the final design; in practice slopes steeper than 1:1.5 are not built using rubble mound material.

### BERM

A berm is a part of a structure in which the slope varies between horizontal and 1:15. A berm is parameterised by the width of the berm, $B$, and by $d_B$, the vertical difference between the middle of the berm and the still water level (SWL). If the width of the berm, $B$, is larger than $0.25 \cdot L_0$ the structure is regarded as a foreshore rather than a berm (EurOtop, 2007).

### PERMEABILITY AND POROSITY

Porosity ($n_v$) is defined as the percentage of voids as part of the total volume. This parameter mainly depends on the shape, grading and method of placement of the armour stones on the slope. Loose material is always porous. For rock and concrete armour the porosity may range roughly between 30-55%. Sand has a porosity of roughly 30%-45%.

Permeability can be defined as the ability of a porous material to allow fluids to pass through it. When assessing groundwater flows sand may be regarded as rather permeable. In the wave breaking process however sand is regarded as non-permeable. This difference comes about due to the change in time scale. The process of waves rushing in and breaking on a structure with a core of sand is too quick for the water pressures to propagate into the sand. This causes overpressures just above the sandy core that can lead to decreased stability of the armour elements. In wave-structure calculations a sandy core therefore is regarded as impermeable. A breakwater core is regarded as permeable because larger rock material is used and up-rushing waves can penetrate the under layers, which leads to increased dissipation of wave energy.

### ROUGHNESS

A rough slope can decrease wave run-up and consequently overtopping since it causes dissipation of wave energy. Sloping dikes are generally built using placed blocks, leading to a rather smooth surface whereas breakwaters have an armour layer consisting of rubble mound or concrete elements that generally leads to a very irregular surface. In overtopping formulae the roughness generally is accounted for by means of the reduction factor $\gamma_f$.

## 2.1.2 HYDRAULIC PARAMETERS

### WAVE HEIGHT

Wave run-up and overtopping formulae use the incident significant wave height $H_{m0}$ at the toe of the structure. Significant wave height is the average of the highest one third waves of a time record, $H_{1/3}$. From a wave spectrum the spectral wave height can be calculated, $H_{m0} = 4\sqrt{m_0}$. Here $m_n$ is defined as the $n^{th}$-moment of the variance spectrum (Holthuijsen, 2007), see Equation 2.1-1. In deep water, both definitions result in almost the same value, but in shallow water situations differences are observable of 10-15 % (EurOtop, 2007).

The moment of a wave spectrum is given by Equation 2.1-1.

$$m_n = \int_0^\infty f^n E(f)\mathrm{df} \qquad \textit{Equation 2.1-1}$$

### WAVE PERIOD

From a wave spectrum or wave record various wave periods can be defined. Commonly used wave periods are the peak period $T_p$ (the period associated with the peak of the spectrum), the average wave period $T_m$ and the significant wave period $T_{1/3}$ (the average wave period of the highest 1/3 of the waves).

The wave period used for some wave run-up and overtopping formulae is the spectral period $T_{m\text{-}1,0}$ (=$m_{\text{-}1}/m_0$). This period gives more weight to the longer periods in the spectrum than other averaged periods. In particular the longer waves are of importance for run-up and overtopping. For single peaked spectra a fixed ratio exists between $T_p$ and $T_{m\text{-}1,0}$; $T_p$=1.1·$T_{m\text{-}1,0}$ (EurOtop, 2007).

### WAVE STEEPNESS

Wave steepness is defined as the ratio of wave height to wave length. The deep water wave steepness is for example $s_0$=$H_{m0}/L_0$. A wave steepness $s_0$=0.01 indicates a typical swell sea while a wave steepness of $s_0$=0.04-0.06 characterises a typical wind sea.

A shallow foreshore can cause a typical wind wave spectrum to have a very low wave steepness. Due to depth-induced breaking the wave height will reduce significantly while the wave period will be nearly unaffected (EurOtop, 2007). The maximum wave steepness for an individual wave is $s_{0,\max} \approx 0.14$ (Holthuijsen, 2007).

### WAVE LENGTH

The wave length of a wave is defined as the product of the wave period and the wave propagation speed, $L = c \cdot T$. In deep water (i.e. $h/L$>0.5) the wave period is $T = T_0$ and the propagation speed is $c_0 = \frac{g}{2\pi} T_0$ . At deep water the wave length therefore is $L_0 = \frac{g}{2\pi} T_0^2$.

*Note: The flume used for these experiments does not suffice the criterion for deep water but due to the relatively short distance waves have to travel, no influence of shoaling or transformation of the spectrum is expected. Therefore the formula for deep water wave lengths is used to calculate the wave length from a measured wave period.*

### BREAKER PARAMETER

The breaker parameter is also referred to as the surf similarity parameter or Iribarren number, $\xi$. In deep water conditions the breaker parameter is defined as:

$$\xi_0 = \frac{\tan(\alpha)}{\sqrt{s_0}} = \frac{\tan(\alpha)}{\sqrt{H/L_0}} = \frac{\tan(\alpha)}{\sqrt{(2\pi \cdot H)/(g \cdot {T_0}^2)}} \qquad \textit{Equation 2.1-2}$$

The breaker parameter is commonly used to describe the way a wave will break when approaching the coast. The interaction between the slope, characterized by a certain slope angle, and the waves leads to a specific type of wave breaking.

Since the breaker parameter is calculated based on the wave period, different breaker parameters can be calculated that are based on different definitions of the wave period.

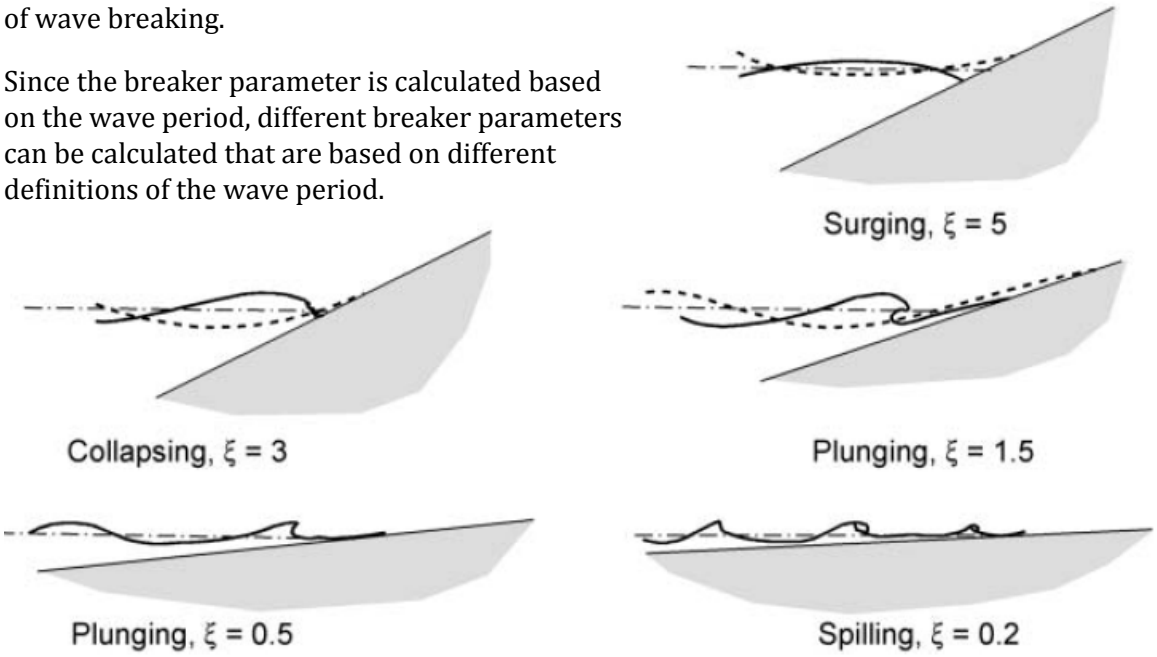


FIGURE 2.1-2: TYPES OF WAVE BREAKING FOR REGULAR WAVES (SCHIERECK, 2001)

For most stability and overtopping prediction methods the spectral wave period $T_{m\text{-}1,0}$ is used. $\xi_{m\text{-}1,0}$ is defined as printed in Equation 2.1-3.

$$\xi_{m-1,0} = \frac{\tan(\alpha)}{\sqrt{s_{m-1,0}}} = \frac{\tan(\alpha)}{\sqrt{H_{m0}/L_{m-1,0}}} = \frac{\tan(\alpha)}{\sqrt{(2\pi \cdot H_{m0})/(g \cdot {T_{m-1,0}}^2)}} \qquad \textit{Equation 2.1-3}$$

### WAVE SPECTRUM

The wave spectrum gives a complete description of the surface elevation of a sea state in a statistical sense (Holthuijsen, 2007). A spectrum defines the wave energy distribution over all frequencies observed in the sea state. Typically a JONSWAP (JOint North Sea WAve Project) spectrum is encountered when assessing a not fully developed sea state. Multiple studies have shown that the JONSWAP spectrum is valid for both fetch-limited conditions as for storm conditions. Since coastal structure design is frequently based on storm conditions, the JONSWAP spectrum is often chosen as the design spectrum.

A Pierson-Moskowitz spectrum describes the sea state for fully developed seas, see Equation 2.1-4. During research on the JONSWAP spectrum the shape of the Pierson-Moskowitz spectrum was down-scaled and its peak was enhanced with a so-called peak enhancement factor. See Equation 2.1-5 for the expression of the JONSWAP spectrum.

$$E_{PM}(f) = \alpha_{PM} \cdot g^2 \cdot (2\pi)^{-4} \cdot f^{-5} \cdot \exp\left[-\frac{5}{4}\left(\frac{f}{f_{PM}}\right)^{-4}\right] \qquad \textit{Equation 2.1-4}$$

where:

| | | | |
|---|---|---|---|
| $\alpha_{PM}$ | = | energy scale | [-] |
| $f_{PM}$ | = | peak frequency | [$s^{-1}$] |
| $g$ | = | gravitational acceleration | [$m/s^2$] |

$$E_{JONSWAP}(f) = \alpha \cdot g^2 \cdot (2\pi)^{-4} \cdot f^{-5} \cdot \exp\left[-\frac{5}{4}\left(\frac{f}{f_{peak}}\right)^{-4}\right] \cdot \underbrace{\gamma^{\exp\left[-\frac{1}{2}\left(\frac{\frac{f}{f_{peak}}-1}{\sigma}\right)^2\right]}}_{G(f)= \; peak-enhancement\ factor}$$

*Equation 2.1-5*

$$\sigma = \begin{cases} \sigma_a & \text{for } f < f_{peak} \\ \sigma_b & \text{for } f > f_{peak} \end{cases} \qquad \textit{Equation 2.1-6}$$

where:

| | | | |
|---|---|---|---|
| $\alpha$ | = | energy scale | [-] |
| $f_{peak}$ | = | peak frequency | [$s^{-1}$] |
| $g$ | = | gravitational acceleration | [$m/s^2$] |
| $\gamma$ | = | peak-enhancement factor | [-] |
| $\sigma_a, \sigma_b$ | = | peak-width parameters | [-] |

Average values of the parameters present in Equation 2.1-5 are: $\gamma = 3.3$, $\sigma_a = 0.07$ and $\sigma_b = 0.09$ for normal wind waves. The shape of a JONSWAP spectrum is indicated in Figure 2.1-3.

These parameter values are not valid for swell conditions. Goda (1985) presented values so that the JONSWAP spectrum can be used to characterise a swell sea state; $\gamma = 9$, $\sigma_a = 0.07$ and $\sigma_b = 0.09$.

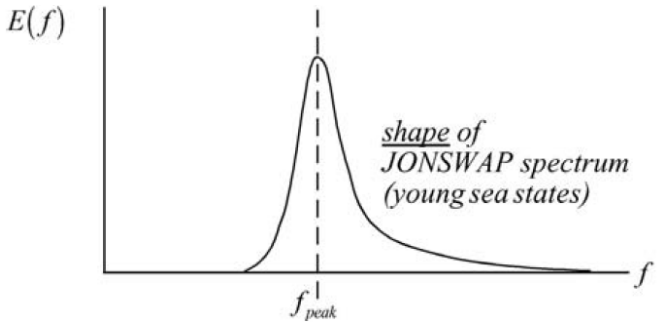


FIGURE 2.1-3: JONSWAP SPECTRUM (HOLTHUIJSEN, 2007)

## 2.2 TOTAL OVERTOPPING

The total overtopping is defined as the entire amount of water that passes the seaward edge of the crest. During the experiments conducted in the research it was observed that quite a lot of overtopping water actually moves through the crest, rather than over the crest. Therefore in this thesis when addressing total overtopping the amount of water plunging over and through the armour layer is considered, refer to Figure 2.2-1.

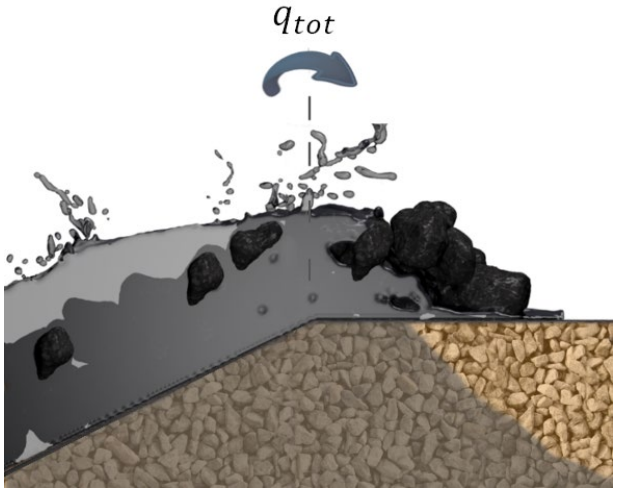


FIGURE 2.2-1: IMPRESSION OF TOTAL OVERTOPPING

Analytical methods for wave overtopping are not able to include all influencing factors of the overtopping process. Attempts have been made by for instance Shi-igai and Kono (1970) – as discussed in TAW (1974) – who considered wave overtopping on levees as a succession of different states of steady flow, that could be described with a weir-discharge formula.

Later in time research moved to experiments that resulted in empirical prediction methods. The results of the experiments were plotted along specific dimensionless axes such that scatter in the data was minimized. The curve that accurately described the data would then be suggested as prediction method.

All current prediction methods stem from the same principle. An exponential function is chosen to relate a dimensionless form of the average wave overtopping discharge $q$ [$m^3$/s per meter crest width] to a dimensionless form of the freeboard $R_C$ [m], see Equation 2.2-1.

$$q^* = A \cdot e^{B \cdot R_C^*} \qquad \textit{Equation 2.2-1}$$

Here A and B are empirical coefficients accounting for wave conditions and structure dimensions.

Per prediction method specific choices have been made as to the way dimensionless numbers are formed. Also the validity of the empirical coefficients is different per prediction method. In Owen (1980) specific coefficients are provided per breakwater configuration whereas in TAW (2002) the same empirical coefficients can be used for all configurations.

### 2.2.1 OWEN (1980)

For smooth slopes the formula of Owen (1980) is recommended by British guidelines (EurOtop, 2007). Being originally developed to describe mean wave overtopping at smooth impermeable slopes and smooth bermed impermeable slopes, the formula takes into account the roughness, the structure configuration and the steepness of the waves, see Equation 2.2-2. Originally Owen (1980) tested three different slopes; 1:1, 1:2 and 1:4.

$$\frac{q_{tot}}{T_m \cdot g \cdot H_{m0}} = \mathrm{a} \cdot \exp\left(-\mathrm{b} \cdot \frac{R_C}{T_m \cdot \sqrt{g \cdot H_{m0}}} \cdot \frac{1}{\gamma_f}\right) \qquad \textit{Equation 2.2-2}$$

where:

| | | | |
|---|---|---|---|
| a, b | = | empirical coefficients | [-] |
| $g$ | = | gravitational acceleration | [m/s²] |
| $H_{m0}$ | = | spectral significant wave height | [m] |
| $q_{tot}$ | = | mean overtopping discharge at the crest | [m³/m per s] |
| $R_C$ | = | crest freeboard | [m] |
| $T_m$ | = | spectral wave period at the toe | [s] |
| $\gamma_f$ | = | influence factor to account for roughness, see section 2.2.2.4. | [-] |

The empirical coefficients a and b depend on the structure configuration, see Table 2-1. A berm is taken into account by adjusting the values of the empirical coefficients. See e.g. Rock Manual (2007) section 5.1.1.3.

TABLE 2-1: OWEN'S COEFFICIENTS FOR NON-DEPTH LIMITED WAVES AND STRAIGHT SLOPES

| Seawall Slope | a | b |
|---|---|---|
| **1:2** | 9.39E-3 | 21.6 |
| **1:2.5** | 1.03E-2 | 24.5 |
| **1:3** | 1.09E-2 | 28.7 |
| **1:3.5** | 1.12E-2 | 34.1 |
| **1:4** | 1.16E-2 | 41.0 |
| **1:4.5** | 1.20E-2 | 47.7 |
| **1:5** | 1.31E-2 | 55.6 |

Owen's method was found applicable for $0.05 < \frac{R_C}{T_m \cdot \sqrt{g \cdot H_s}} < 0.60$ and $0.035 < s_{0m} < 0.055$ (Rock Manual, 2007). Swell waves are not properly covered. Hawkes, Coates, and Jones (1998) introduced an adjustment factor that reduces the predicted overtopping discharge based on the Iribarren number. For $\xi_m > 4.3$ this reduction is 0.1. This means that for surging waves the original method of Owen is on average an order 10 off.

The prediction method of Owen is not suitable for permeable rubble mound structures. Experiments performed by Pearson et al. (2004) indicated that instead the general trend of the TAW (2002) prediction method was followed.

### 2.2.2 TAW (2002)

The TAW (2002) prediction method was originally introduced for impermeable structures. In design practice however it is quite commonly used to determine the overtopping for breakwaters. TAW (2002) notes that for permeable structures the permeable crest should not be taken into account for the crest freeboard.

In this prediction method distinction is made between breaking ($\gamma_b \xi_{m-1,0} \lesssim 2.0$) and non-breaking ($\gamma_b \xi_{m-1,0} \gtrsim 2.0$) wave conditions. For breaking conditions the overtopping increases for higher values of the breaker number $\xi_{m-1,0}$. When $\gamma_b \xi_{m-1,0} \gtrsim 2.0$ theoretically no breaking takes place. From this point on the Iribarren number does not have an effect on the total overtopping.

In comparison with Owen the crest freeboard and mean overtopping discharge are made dimensionless in a different way. Where Owen already includes the wave period in the dimensionless overtopping and dimensionless freeboard, in the TAW formulae the Iribarren number is used to take this into account. An elegant benefit of the TAW formula is that the values of the empirical coefficients do not depend on the structure configuration.

#### 2.2.2.1 BREAKING WAVES

For breaking waves ($\gamma_b \xi_{m-1,0} \lesssim 2.0$) the wave overtopping formula is presented in Equation 2.2-3.

$$\frac{q_{tot}}{\sqrt{g \cdot H_{m0}^3}} = \frac{\mathrm{A}}{\sqrt{\tan(\alpha)}} \cdot \gamma_b \cdot \xi_{m-1,0} \cdot \exp\left(-\mathrm{B} \cdot \frac{R_C}{H_{m0}} \frac{1}{\xi_{m-1,0} \cdot \gamma_b \cdot \gamma_f \cdot \gamma_\beta \cdot \gamma_v}\right) \qquad \textit{Equation 2.2-3}$$

where:

| | | | |
|---|---|---|---|
| A, B | = | empirical coefficients, see section 2.2.2.3 | [-] |
| $g$ | = | gravitational acceleration | [m/s²] |
| $H_{m0}$ | = | spectral significant wave height | [m] |
| $q_{tot}$ | = | mean overtopping discharge at the crest | [m³/m per s] |
| $R_C$ | = | crest freeboard | [m] |
| $s_{m-1,0}$ | = | wave steepness = $2\pi H_{m0}/(gT_{m-1,0}^2)$ | [-] |
| $\tan(\alpha)$ | = | seaward slope | [-] |
| $T_{m-1,0}$ | = | spectral wave period at the toe | [s] |
| $\gamma_b, \gamma_f, \gamma_\beta, \gamma_v$ | = | influence factors to account for a berm, roughness, angle of incident waves, a vertical wall on the crest, refer to section 2.2.2.4 | [-] |
| $\xi_{m-1,0}$ | = | breaker parameter = $\tan(\alpha) / \sqrt{s_{m-1,0}}$ | [-] |

The dimensionless overtopping discharge is depicted in Equation 2.2-4. Equation 2.2-5 shows the dimensionless freeboard.

$$q_{tot}^{*} = \frac{q_{tot}}{\sqrt{g \cdot H_{m0}^{3}}} \frac{\sqrt{\tan(\alpha)}}{\gamma_b \cdot \xi_{m-1,0}} \qquad \textit{Equation 2.2-4}$$

$$R_C^{*} = \frac{R_C}{H_{m0}} \frac{1}{\xi_{m-1,0} \cdot \gamma_b \cdot \gamma_f \cdot \gamma_\beta \cdot \gamma_v} \qquad \textit{Equation 2.2-5}$$

To account for the influences of various circumstances (berm dimensions, oblique waves, etc.) the dimensionless freeboard is increased through dividing the crest freeboard by the associated factors. Refer to section 2.2.2.4 for a detailed description of the reduction factors.

### 2.2.2.2 NON-BREAKING WAVES

For non-breaking waves ($\gamma_b \xi_{m-1,0} \gtrsim 2.0$) the wave overtopping formula is presented in Equation 2.2-6.

$$\frac{q_{tot}}{\sqrt{g \cdot H_{m0}^{3}}} = \mathrm{C} \cdot \exp\left(-\mathrm{D} \cdot \frac{R_C}{H_{m0}} \frac{1}{\gamma_f \cdot \gamma_\beta}\right) \qquad \textit{Equation 2.2-6}$$

Different definitions are used for the dimensionless overtopping discharge and dimensionless freeboard.

$$q_{tot}^{*} = \frac{q_{tot}}{\sqrt{g \cdot H_{m0}^{3}}} \qquad \textit{Equation 2.2-7}$$

$$R_C^{*} = \frac{R_C}{H_{m0}} \frac{1}{\gamma_f \cdot \gamma_\beta} \qquad \textit{Equation 2.2-8}$$

The dimensionless wave overtopping discharge and dimensionless crest height no longer depend on the breaker parameter $\gamma_b \xi_{m-1,0}$. Also $\gamma_v$ is discarded in the calculation of the dimensionless freeboard.

### 2.2.2.3 EMPIRICAL COEFFICIENTS

TAW (2002) introduces the fitting coefficient A, B, C and D, see Table 2-2. For deterministic calculation values for coefficient B and D are proposed of $\mu$-$x\sigma$, with $x$=1. Coefficient values for probabilistic calculation were derived using a statistical analysis of the dataset.

TABLE 2-2: VALUES FOR COEFFICIENTS A, B, C AND D

| Coefficient | Value for deterministic calculation | Values for probabilistic calculation | | |
|---|---|---|---|---|
| | | Distribution | $\mu$ | $\sigma$ |
| **A** | 0.067 | Deterministic | 0.067 | - |
| **B** | 4.3 | Normal | 4.75 | 0.5 |
| **C** | 0.2 | Deterministic | 0.2 | - |
| **D** | 2.3 | Normal | 2.6 | 0.35 |

### 2.2.2.4 REDUCTION FACTORS

The TAW prediction method accounts for various overtopping reducing circumstances. Specific combinations of the reduction factors can lead to a very large decrease of the wave overtopping discharge. Since these combinations are not well tested TAW (2002) recommends to perform further research when $\gamma_b \cdot \gamma_\beta \cdot \gamma_f < 0.4$.

#### INFLUENCE OF BERMS

Impermeable berms are taken into account by means of the reduction factor $\gamma_b$. This factor is calculated with two additional parameters.

$$\gamma_b = 1 - r_B \cdot (1 - r_{db}) \text{ for } 0.6 \leq \gamma_b \leq 1.0 \qquad \textit{Equation 2.2-9}$$

$r_B$ indicates the influence of the width of the berm, *B;* see Equation 2.2-10. The definition of $L_{Berm}$ is depicted in Figure 2.2-2. . $r_B$ essentially takes account of the influence of the berm width on the average slope (De Waal & Van der Meer, 1992).

$$r_B = \frac{B}{L_{Berm}} \qquad \textit{Equation 2.2-10}$$

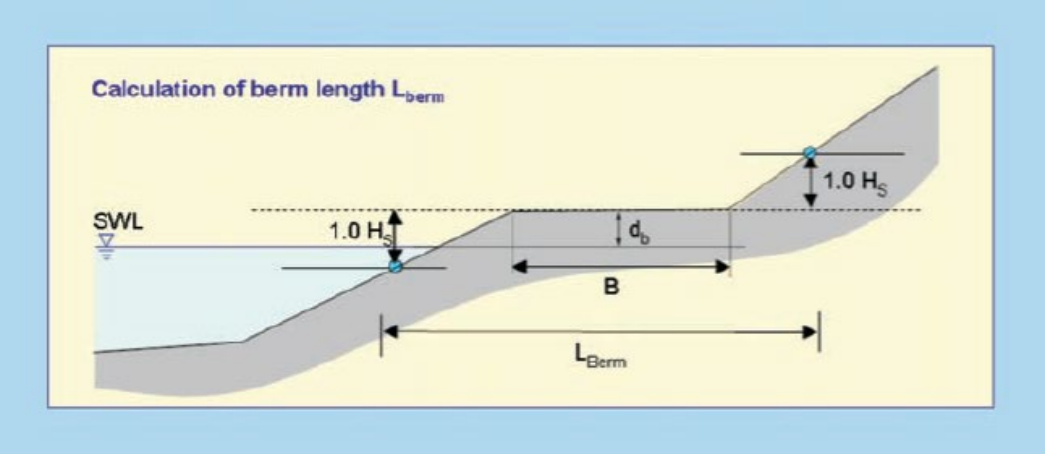


FIGURE 2.2-2: DEFINITION OF $L_{BERM}$ (EUROTOP, 2007)

$r_{db}$ accounts for the vertical difference $d_B$ between the Still Water Level and the middle of the berm and becomes zero if the berm lies on SWL. Reduction of wave overtopping is maximal for a berm positioned at SWL.

$$r_{db} = 0.5 - 0.5 \cdot \cos\left(\pi \frac{d_B}{R_{u2\%}}\right) \text{ for a berm above SWL}$$

$$r_{db} = 0.5 - 0.5 \cdot \cos\left(\pi \frac{d_B}{2 \cdot H_{m0}}\right) \text{ for a berm below SWL} \qquad \textit{Equation 2.2-11}$$

A berm positioned below SWL $- 2 \cdot H_{m0}$ or above SWL $- R_{u2\%}$ has no effect on the wave run-up and wave overtopping. The minimum value for $\gamma_b$ is 0.6.

The definition used for $d_B$ is somewhat counterintuitive. When a berm is constructed above SWL, $d_B$ has a negative value. Figure 2.2-3 was made to help clarify the effect a different berm elevation has on the reduction factor.

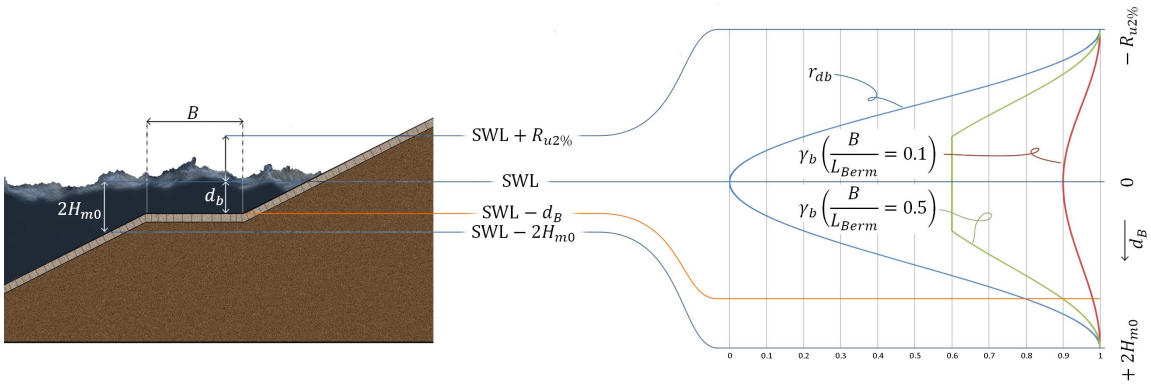


FIGURE 2.2-3: REDUCTION FACTOR TO ACCOUNT FOR A BERM

Historically the $\gamma_b$-factor was first suggested for wave run-up, and later also recommended for wave overtopping, see De Waal and Van der Meer (1992). This may explain that for $d_B < -R_{u2\%}$ no reduction of overtopping is accounted for. The run-up height would not decrease for that configuration, but for wave overtopping some sort of spatial reduction should be taken into account. In the current form of $\gamma_b$ this is not the case.

### INFLUENCE OF SLOPE ROUGHNESS

Bruce, Van der Meer, Franco, and Pearson (2009) presented values of the roughness factor $\gamma_f$ for different kinds of armour units, refer to Table 2-3. The printed results are valid for relatively steep waves with $\gamma_b \cdot \xi_{m-1,0} < 1.8$.

TABLE 2-3: VALUES FOR ROUGHNESS FACTOR $\gamma_f$ FOR $\gamma_b\xi_{m-1,0} < 1.8$

| **Armour unit** | $\gamma_f$ |
|---|---|
| Concrete, asphalt and grass (smooth impermeable slope) | 1 |
| Pitched stone | 0.80-0.95 |
| Rocks - 1 layer on impermeable base | 0.60 |
| Rocks - 2 layers on impermeable base | 0.55 |
| Rocks - 1 layer on permeable base | 0.45 |
| Rocks - 2 layers on permeable base | 0.40 |
| Cubes - 1 layer randomly placed | 0.50 |
| Cubes - 2 layers randomly placed | 0.47 |
| Accropode™ | 0.46 |
| Xbloc® | 0.45 |
| Tetrapods | 0.38 |

For small values of the Iribarren parameter some armour units can lead to very much reduction of the run-up and overtopping. Longer waves encounter less friction. Therefore TAW recommends using the following interpolation. For $\gamma_b \cdot \xi_{m-1,0} < 1.8$ the values found in Table 2-3 can be maintained. When $\gamma_b \cdot \xi_{m-1,0} > 10$ there is no reduction due to roughness, i.e. $\gamma_f = 1$. For $1.8 < \gamma_b \cdot \xi_{m-1,0} < 10$ a linear interpolation is suggested.

#### INFLUENCE OF OBLIQUE WAVES

The factor $\gamma_\beta$ accounts for a reduction of overtopping due to obliquity of the waves. In this research no oblique waves were tested. For more information refer to TAW (2002).

#### INFLUENCE OF VERTICAL WALL

The factor $\gamma_v$ accounts for a reduction of overtopping due to a vertical positioned at the crest. In this research no vertical wall was applied at the crest. For more information refer to TAW (2002).

### 2.2.2.5 RUN-UP

Although not of primary interest in this research, the calculation of $R_{u2\%}$ is presented here since it is used in the calculation of the reduction factor due to a berm, $\gamma_b$. Equation 2.2-12 holds for probabilistic calculation. Since run-up and overtopping are related processes the same $\gamma_b$ term is used as printed in Equation 2.2-9. For berms above SWL an iterative calculation is required since $\gamma_b$ is also a function of $R_{u2\%}$.

$$\frac{R_{u2\%}}{H_{m0}} = \gamma_f \cdot \gamma_\beta \cdot \min \begin{cases} 1.65 \cdot \gamma_b \cdot \xi_{m-1,0} \\ 4.0 - \dfrac{1.5}{\sqrt{\xi_{m-1,0}}} \end{cases} \qquad \textit{Equation 2.2-12}$$

### 2.2.2.6 STRUCTURE PERMEABILITY

Originally the TAW prediction method was developed for smooth impermeable structures. According to Rock Manual (2007) experiments have been conducted to verify the validity of the TAW prediction method for permeable structures. Slight changes to the roughness factor were recommended but the results compared reasonably well with earlier found data for impermeable slopes.

However no experiments have yet been conducted to also study the influence of a permeable berm on the mean overtopping discharge. The current research will give insight into the validity of the prediction method for these configurations.

## 2.2.3 EUROTOP (2007)

The EurOtop manual was presented as a replacement for TAW (2002). Compared with the TAW manual, the EurOtop manual introduces a prediction method specifically for permeable structures.

### 2.2.3.1 PERMEABLE STRUCTURES

The EurOtop manual specifically addresses permeable structures. Essentially the prediction method is similar to the TAW prediction method for non-breaking waves (Equation 2.2-6), with some adjustments. For breakwaters generally steep slopes are used and theoretically no wave breaking will occur. Since the prediction method for non-breaking waves is used, no influence of a berm is accounted for.

The $\gamma_b$-factor is not present in the dimensionless crest freeboard. Equation 2.2-6 is reprinted below.

$$\frac{q_{tot}}{\sqrt{g \cdot H_{m0}^3}} = \mathrm{C} \cdot \exp\left(-\mathrm{D} \cdot \frac{R_C}{H_{m0}} \frac{1}{\gamma_f \cdot \gamma_\beta}\right) \qquad \textit{Equation 2.2-6}$$

The values of the empirical coefficients C and D can be found in Table 2-2. They are the same as in the TAW prediction method.

### CREST FREEBOARD DEFINITION

In the EurOtop manual specific recommendations are made as to which crest freeboard should be used for permeable structures. The EurOtop manual recommends neglecting the permeable armour layer. The predicted amount of overtopping is very sensitive to changes in the crest freeboard. Neglecting the armour layer in the crest freeboard therefore will lead to significantly more overtopping.

### INFLUENCE OF SLOPE ROUGHNESS

In the TAW prediction method for impermeable structures all reduction factors due to roughness are increased for $\gamma_b \cdot \xi_{m-1,0} > 1.8$. In the EurOtop manual however a distinction is made between the interpolated roughness reduction factor, $\gamma_{f,surging}$ (see Equation 2.2-14), and the roughness factor $\gamma_f$ that is originally recommended for $\gamma_b \cdot \xi_{m-1,0} < 1.8$. The EurOtop manual recommends using $\gamma_f$ in all overtopping formulae and only uses $\gamma_{f,surging}$ in the maximum expression for run-up on permeable slopes. It is expected this choice was made based on curve fitting, since theoretically run-up and overtopping are regarded as similar processes. The prediction method for run-up for probabilistic use is printed in Equation 2.2-13. Values for $\gamma_f$ can be found in Table 2-3.

$$\frac{R_{u2\%}}{H_{m0}} = \gamma_\beta \cdot \gamma_b \cdot \min\begin{cases} 1.65 \cdot \gamma_f \cdot \xi_{m-1,0} \\ \gamma_{f,surging} \cdot \left(4.0 - \dfrac{1.5}{\sqrt{\xi_{m-1,0}}}\right) \end{cases} \qquad \textit{Equation 2.2-13}$$

$$\gamma_{f,surging} = \begin{cases} \gamma_f + \left(\gamma_b \cdot \xi_{m-1,0} - 1.8\right) \cdot \dfrac{1-\gamma_f}{8.2} & \text{for } 1.8 < \xi_{m-1,0} < 10 \\ 1 & \text{for } \xi_{m-1,0} > 10 \end{cases} \qquad \textit{Equation 2.2-14}$$

## 2.2.4 LIOUTAS ET AL. (2012)

Lioutas et al. (2012) carried out multiple experiments on a breakwater with a simple straight slope. A comparison was made between the measurements of total wave overtopping and predictions proposed by TAW (2002). A lot of scatter was observed but there was also considerable grouping of data points in the charts. The data points were grouped by wave steepness, longer waves resulted in higher overtopping, and armour slope, steeper slopes tended to lead to higher overtopping discharges than predicted. It was concluded that the TAW (2002) formulae do not properly take into account the breaker parameter.

In order to solve this problem an "intermediate" form of the two TAW-formulae was recommended, see Equation 2.2-15. This new expression was called the "Adjusted TAW" method.

$$\frac{q_{tot}}{\sqrt{g \cdot H_{m0}^3}} = (0.2 - 0.133 \cdot k)\left(\frac{\gamma_b \cdot \xi_{m-1,0}}{\sqrt{\tan(\alpha)}}\right)^k \cdot \exp\left[-(2.6 + 2.15 \cdot k)\frac{R_C}{H_{m0}}\frac{1}{(\xi_{m-1,0} \cdot \gamma_b \cdot \gamma_v)^k \cdot \gamma_f \cdot \gamma_\beta \cdot \gamma_c}\right]$$

*Equation 2.2-15*

For $k = 1$ the formula is equal to the extended TAW formula for breaking waves. When $k = 0$ the formula is equal to the limited TAW formula for non-breaking waves, maximum overtopping. In Lioutas (2010) the $\gamma_b$ and $\gamma_v$ factors were not raised to the power $k$. Mathematically the equation therefore was not a combination of the two TAW formulae. This was corrected in Lioutas et al. (2012). It should be stressed that this choice was made entirely based on mathematics; Lioutas did not test the influence of a berm or vertical wall.

The definition of the crest freeboard was adapted to take into account the permeability of the crest. Lioutas et al. (2012) advise using $R_C = A_C - 0.9 \cdot D_{n50,armour}$.

The fit of the Adjusted TAW formula with the experimental data was significantly better than when the TAW formulae were used. $k$=0.6 was recommended.

## 2.3 LANDWARD SPATIAL DISTRIBUTION OF OVERTOPPING

In literature distinction is made between overtopping just behind the crest, $q_{bc}$, and overtopping more land inward, $q(x)$. The definitions are indicated in Figure 2.3-1. These two overtopping definitions will be treated separately.

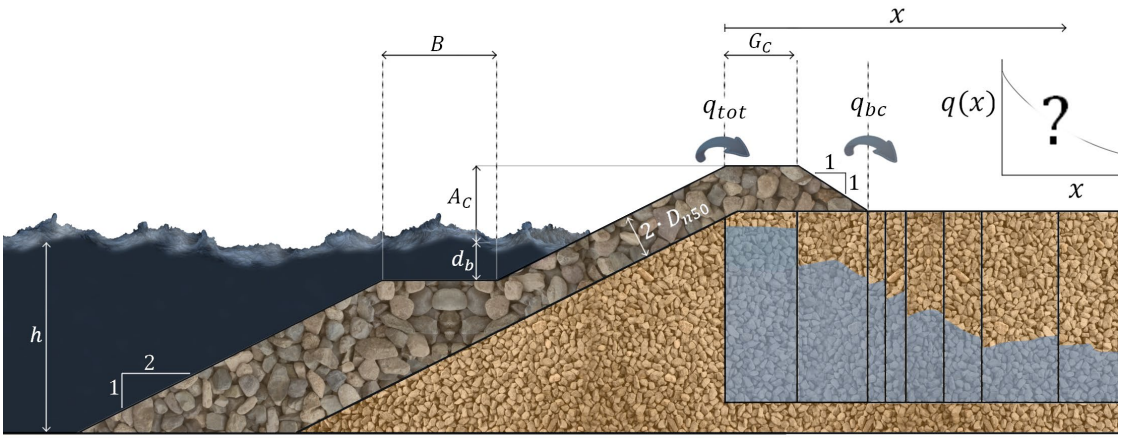


FIGURE 2.3-1: OVERVIEW OF DIFFERENT DEFINITIONS FOR WAVE OVERTOPPING

Most methods discussed in this section relate the overtopping at a certain distance from the crest to the total overtopping. Generally the overtopping is calculated by multiplying the total overtopping with a reduction factor $C_r$. Another method is to insert a reduction factor $\gamma_c$, as was suggested by Lioutas et al. (2012). Here the amount of reduction due to the distance from the crest is made dependent on the other terms in the dimensionless crest freeboard. The terms are compared in a mathematical sense in Appendix C.

### 2.3.1 OVERTOPPING DIRECTLY BEHIND THE CREST

#### 2.3.1.1 BESLEY (1999)

Besley (1999) found that an armour crest could be taken into account by multiplying the overtopping discharge to a reduction factor $C_r$, see Equation 2.3-1 and Equation 2.2-2.

$$C_r = \min\left[3.06 \cdot \exp\left(-1.5 \cdot \frac{G_C}{H_{m0}}\right); 1\right] \qquad \textit{Equation 2.3-1}$$

$$q(x) = C_r \cdot q_{tot} \qquad \textit{Equation 2.3-2}$$

where:

$G_c$ = crest width [m]

No reduction of the mean overtopping discharge is achieved for $G_c/H_{m0}$<0.75. This roughly corresponds to no reduction for crest widths lower than $3D_{n50,armour}$.

Test results in Lykke Andersen and Burcharth (2004) showed that the correction factor of Besley (1999) is not only an improvement to the formula of Owen (1980) but also to the formula proposed by TAW (2002).

### 2.3.1.2 STEENAARD (2002)

Steenaard (2002) also measured the overtopping behind the crest. Hereto he built a standard breakwater configuration with a 1:2 slope and divided the overtopped water into two compartments. One collection tank was filled with the water that infiltrated into the crest while the other compartment contained water that passed the crest.

The experiments were carried out using regular waves and a fixed wave steepness of $s_0$=0.05. During the experiments the following parameters were varied: wave height, crest freeboard and crest width. Eventually a function was presented that predicts the amount of wave overtopping discharge directly behind the crest, see Equation 2.3-3.

$$\frac{q_{bc}}{q_{tot}} = \begin{cases} \dfrac{q_{tot}^* - q_d^*}{q_{tot}^* + 7.0 \cdot 10^{-2}} & Q_{tot}^* > Q_d^* \\ 0 & Q_{tot}^* \leq Q_d^* \end{cases} \qquad \textit{Equation 2.3-3}$$

with:

$$q_{tot}^* = \frac{q_{tot}}{\sqrt{g \cdot {G_C}^3}} \qquad \textit{Equation 2.3-4}$$

where:

| | | | |
|---|---|---|---|
| $G_C$ | = | crest width | [m] |
| $g$ | = | gravitational acceleration | [m/s²] |
| $q_{bc}$ | = | mean overtopping discharge behind the crest | [m³/m per s] |
| $q_{tot}$ | = | mean overtopping discharge at the crest | [m³/m per s] |
| $q_d^* = 0.0081$ | = | threshold value for overtopping behind the crest | [-] |

### 2.3.1.3 VAN KESTER (2009)

Van Kester (2009) built upon the research conducted by Steenaard (2002). Using a more integral approach, Van Kester constructed multiple experiment setups and separately measured overtopping discharges; first the total wave overtopping at the crest, $q_{tot}$, secondly the overtopping directly behind the crest, $q_{bc}$, and finally the spatial distribution of the overtopping behind the crest. Only regular waves were tested in this research.

During the experiments there were some problems with the water depth in front of the breakwater; overtopped water was removed from the system. In his result analysis he therefore calculated an equivalent overtopping discharge to account for the water level decrease.

Van Kester found that the prediction method of Steenaard (2002) did predict the overall trend of his experiments but there was very much scatter. Therefore he introduced a new dimensionless parameter but maintained the general form of the prediction method; see Equation 2.3-5 and Equation 2.3-6. This new formula led to a significantly better fit with the data.

$$\frac{q_{bc}}{q_{tot}} = \begin{cases} \left(\dfrac{H^* - H_d^*}{H^* - 15}\right)^2 & H^* > H_d^* \\ 0 & H^* \leq H_d^* \end{cases} \qquad \textit{Equation 2.3-5}$$

with:

$$H^* = \frac{H \cdot L}{G_C \cdot R_C} \qquad \textit{Equation 2.3-6}$$

where:

| | | | |
|---|---|---|---|
| $G_C$ | = | crest width | [m] |
| $H$ | = | wave height | [m] |
| $H_d^*$ | = | threshold value for overtopping behind the crest | [-] |
| $L$ | = | wave length | [m] |
| $q_{bc}$ | = | mean overtopping discharge behind the crest | [m³/m per s] |
| $q_{tot}$ | = | mean overtopping discharge at the crest | [m³/m per s] |
| $R_C$ | = | freeboard | [m] |

### 2.3.1.4 LIOUTAS ET AL. (2012)

Lioutas used an experiment setup where multiple compartments were made in the breakwater. Per section a pump was installed and the overtopped water was pumped to floating tanks behind the breakwater. Consequently the overtopping discharges could be determined for 7 horizontal positions in total.

Lioutas et al. (2012) tried to describe the wave overtopping discharge directly behind the crest by implementing a new coefficient in the dimensionless crest freeboard of the Adjusted TAW-formula, which was already found for the total wave overtopping, see Equation 2.3-7. The parameter $\gamma_c$ accounts for the reduction due to the distance travelled over the breakwater crest.

$$\frac{q_{tot}}{\sqrt{g \cdot H_{m0}^3}} = (0.2 - 0.133 \cdot k)\left(\frac{\gamma_b \cdot \xi_{m-1,0}}{\sqrt{\tan(\alpha)}}\right)^k \cdot \exp\left[-(2.6 + 2.15 \cdot k)\frac{R_C}{H_{m0}}\frac{1}{{\xi_{m-1,0}}^k \cdot \gamma_b \cdot \gamma_f \cdot \gamma_\beta \cdot \gamma_v \cdot \gamma_c}\right] \qquad \textit{Equation 2.3-7}$$

For overtopping just behind the crest Lioutas recommends $\gamma_c = 0.577$. Plotting the measured overtopping discharges behind the crest against this function showed a reasonably good fit, with maximum deviations of approximately a factor 10. For a highly complex process as overtopping these figures are not uncommon.

In his thesis (Lioutas, 2010) he also looked to the prediction methods that were found by Steenaard (2002) and Van Kester (2009). Steenaard's parameter was found to lead to a rough trend in the data, but the prediction method he suggested could not be justified based on the data set. The parameter $H^*T^*$ introduced by Van Kester did not result in smaller scatter in the data. The differences between regular and irregular waves for overtopping were expected to be the reason for the found deviations.

### 2.3.1.5 LYKKE ANDERSEN (2006)

Specifically for berm breakwaters, both reshaping and non-reshaping, Lykke Andersen (2006) developed a curve fitting formula using the software package WaveLab2. After having done extensive experiments (565 tests) on berm breakwaters with irregular waves, he compared the results with the formula proposed by TAW (2002). Lykke Andersen measured the overtopping discharge at the end of the breakwater crest and therefore applied the correction factor as proposed by Besley (1999) to the TAW-formula. The scatter around the formula was at least a factor 100.

Lykke Andersen used this data as input for a curve fitting routine based on a non-linear least square algorithm utilizing the Levenberg-Marquadt method, minimizing the square of the errors of $\log(q_*)$. This procedure led to Equation 2.3-8.

$$q^* = 1.79 \cdot 10^{-5} \cdot (f_{H0}^{1.34} + 9.22) \cdot s_{0p}^{-2.52} \cdot \exp[-5.63 \cdot R_*^{0.92} - 0.61 \cdot G_*^{1.39} - 0.55 \cdot d_{B*}^{1.48} \cdot B_*^{1.39}] \quad \textit{Equation 2.3-8}$$

where:

$$q^* = \frac{q_{bc}}{\sqrt{g \cdot H_{m0}^3}} \quad \textit{Equation 2.3-9}$$

$$R_* = \frac{R_C}{H_{m0}} \quad \textit{Equation 2.3-10}$$

$$G_* = \frac{G_C}{H_{m0}} \quad \textit{Equation 2.3-11}$$

$$B_* = \frac{B}{H_{m0}} \quad \textit{Equation 2.3-12}$$

$$d_{B*} = \begin{cases} \frac{3 \cdot H_{m0} - h_b}{3 \cdot H_{m0} + R_C} & \text{for } d_B < 3 \cdot H_{m0} \\ 0 & \text{for } d_B \geq 3 \cdot H_{m0} \end{cases} \quad \textit{Equation 2.3-13}$$

$$T_0 = \sqrt{\frac{g}{D_{n50}}} \cdot T_{m0,1} \quad \textit{Equation 2.3-14}$$

$$T_0^* = \frac{19.8 \cdot \exp\left(-\frac{7.08}{H_0}\right) \cdot s_{0m}^{-0.5} - 10.5}{0.05 \cdot H_0} \quad \textit{Equation 2.3-15}$$

$$H_0 = \frac{H_{m0}}{\Delta \cdot D_{n50}} \quad \textit{Equation 2.3-16}$$

$$f_{H0} = \begin{cases} 19.8 \cdot \exp\left(-\frac{7.08}{H_0}\right) \cdot s_{0m}^{-0.5} & \text{for } T_0 \geq T_0^* \\ 0.05 \cdot H_0 T_0 + 10.5 & \text{for } T_0 < T_0^* \end{cases} \quad \textit{Equation 2.3-17}$$

$$s_{0m} = \frac{2\pi \cdot H_{m0}}{g \cdot T_m^2} \quad \textit{Equation 2.3-18}$$

$$s_{0p} = \frac{2\pi \cdot H_{m0}}{g \cdot T_p^2} \quad \textit{Equation 2.3-19}$$

Per parameter a description is provided in the List of Symbols.

Comparison with the original dataset learned that there was indeed a significantly smaller error. The scatter was approximately 10 times smaller than with the TAW-formulae. However the formula is wholly based on curve fitting rather than a physical derivation. A drawback of this prediction method is clearly the relative incomprehensibility, making it not seem to be very attractive for quick design purposes.

## 2.3.2 OVERTOPPING DISTRIBUTION BEHIND THE CREST

### 2.3.2.1 JUUL JENSEN (1984)

Juul Jensen analysed data that was gathered in laboratory tests and also studies on actual projects, performed by the Danish Hydraulic Institute (DHI). The tests involved irregular waves – natural wave records were used as input for the wave generator – and also influence of wind was taken into account.

Overtopping water was collected in separate trays, positioned at different distances behind the breakwater. Seven different breakwater configurations were tested. To investigate the spatial distribution of overtopping Juul Jensen used the parameter *x*, the horizontal distance to the end of the crest.

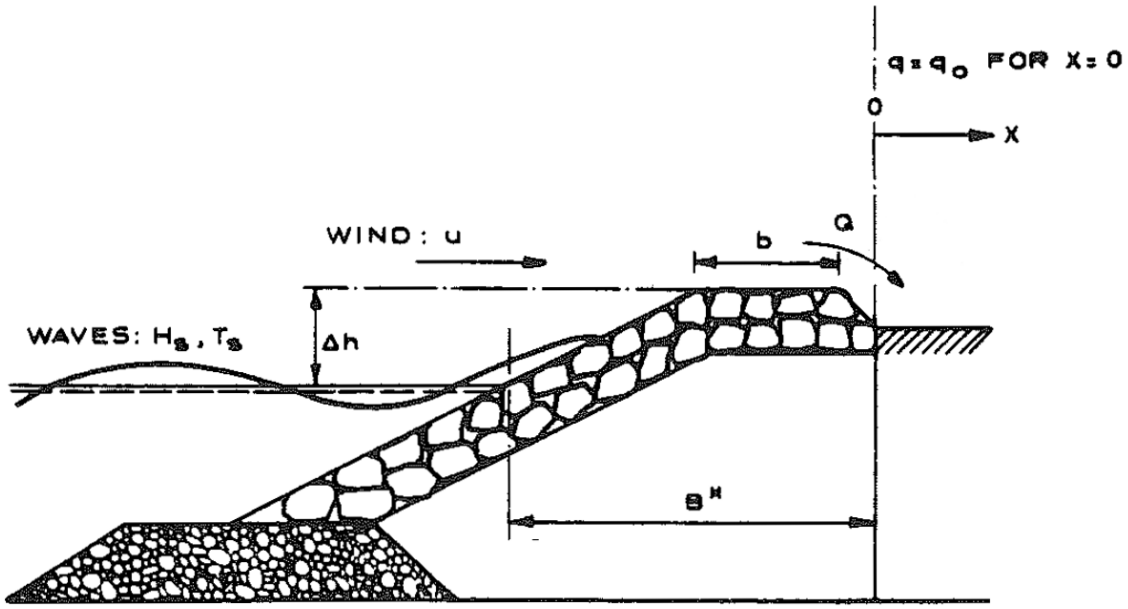


FIGURE 2.3-2: PARAMETERS FOR THE METHOD OF JUUL JENSEN (1984)

The overtopping discharges were made dimensionless using the wave period $T_z$ (mean zero-crossing period) and $B^*$ (the horizontal distance from the intersection of the seaward slope of the breakwater with SWL, to the landward end of the crest). See Equation 2.3-20.

$$q_J^* = q \cdot \frac{T_z}{B^{*2}} \qquad \textit{Equation 2.3-20}$$

The approach Juul Jensen chose to present overtopping in a spatial sense is rather different from other literature. Instead of overtopping discharge per meter crest width, he considered the overtopping intensity per square meter. In this report $q_i$ indicates overtopping intensity and $q$ indicates overtopping discharge.

$$q_i(x) = q_{i,0} \cdot 10^{-\frac{x}{\beta}} \qquad \textit{Equation 2.3-21}$$

where:

| | | | |
|---|---|---|---|
| $q_i(x)$ | = | overtopping intensity at distance x from end of crest | [m³/m²/s] |
| $q_{i,0}$ | = | overtopping intensity at distance x=0, see Figure 2.3-2 | [m³/m²/s] |
| $\beta$ | = | empirical coefficient | [m] |

The coefficient $\beta$ indicates the distance for which the overtopping intensity is decreased with an order 10.

The total overtopping discharge can be calculated by integrating the overtopping intensity from $x = 0$ to $x = \infty$, see Equation 2.3-22. Overtopping discharges at other locations can be calculated by using different boundaries in the integral, see Equation 2.3-23.

$$q_{bc} = \int_{x=0}^{x=\infty} q_{i,0} \cdot 10^{-\frac{x}{\beta}} dx = \frac{q_{i,0} \cdot \beta}{\ln(10)} \qquad \textit{Equation 2.3-22}$$

$$q(x) = \int_{x=\mathrm{x}}^{x=\infty} q_{i,0} \cdot 10^{-\frac{x}{\beta}} dx = \frac{q_{i,0} \cdot \beta}{\ln(10)} \cdot 10^{-\frac{\mathrm{x}}{\beta}} \qquad \textit{Equation 2.3-23}$$

The spatial decrease of overtopping can therefore be written in a similar fashion as Besley (1999).

$$C_r = 10^{-\frac{x}{\beta}} \qquad \textit{Equation 2.3-24}$$

$$q(x) = C_r \cdot q_{bc} \qquad \textit{Equation 2.3-25}$$

In the experiments investigated by Juul Jensen the parameter $\beta/B^*$ remained nearly constant, not depending on wind or wave conditions. Per profile therefore a recommendation for this parameter is given. For profile A – the configuration most similar to the test setup used in the current research – the approximate value of $\beta/B^*$ is 0.40-0.55.

Juul Jensen drew the following general conclusions in his research:

- The amount of overtopping increases rapidly with the parameter $H_s/R_c$. The logarithm of $Q_j^*$ is normally a linearly function of $H_s/R_c$.
- The influence of the wave period differs per structure. However there is a tendency that longer periods cause more overtopping.
- No sharp limit exists between wind-carried spray and mass-overtopping where solid masses of water are passing the crest of the breakwater.
- The wind effect is most pronounced for small values of $H_s/R_c$. For high sea states and/or high water levels (large values of $H_s/R_c$) where mass-overtopping occurs the wind has no influence on the amount of overtopping.

For breakwaters with a non-reshaping berm there is a peculiarity in the prediction method of Juul Jensen. $B^*$ increases with a large increment when the berm elevation is increased from just below SWL to just above SWL. The correctness of this procedure will be investigated after comparison with the experimental data.

### 2.3.2.2 LYKKE ANDERSEN AND BURCHARTH (2006)

The spatial distribution of wave overtopping discharge was investigated by Lykke Andersen and Burcharth (2006) for multiple configurations of rubble mound breakwaters with a crest wall. They focused on the distribution of overtopping travelling through the air and landing on the area behind the crest wall. This distribution was measured using multiple water tanks which were placed just behind the crest wall. Refer to Figure 2.3-3 for an indication of the experiment set-up.

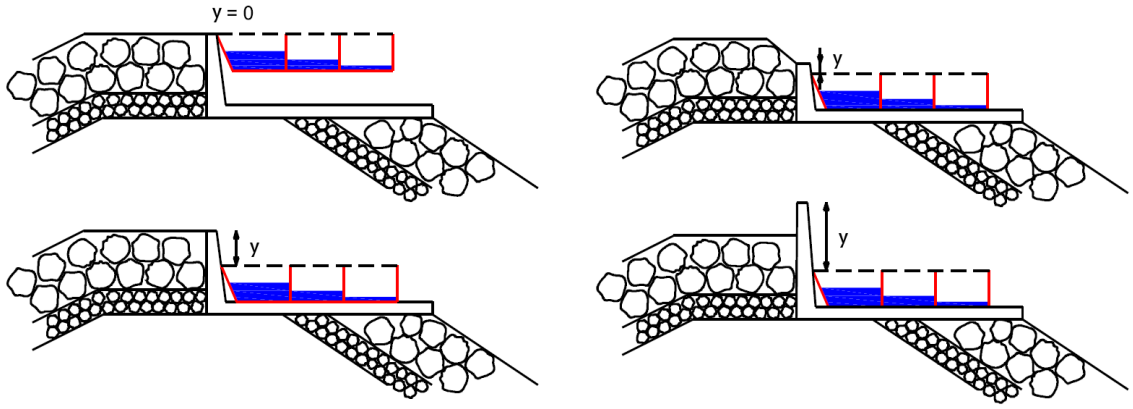


FIGURE 2.3-3: EXPERIMENT CONFIGURATION IN LYKKE ANDERSEN AND BURCHARTH (2006)

They concluded the distribution of the wave overtopping discharge could be described with Equation 2.3-26. The exceedance probability ($F$) of the travel distance is defined as the volume of overtopping water passing a given $x$- and $y$-coordinate, divided by the total overtopping volume. The probability therefore lies between 0 and 1, with $F$=1 at the top of the crest wall.

$$F(x,y) = \exp\left[\frac{-1.3}{H_{m0}} \cdot \left\{\max\left(\frac{x}{\cos(\beta)} - 2.7 \cdot y \cdot s_{0p}^{0.15}; 0\right)\right\}\right] \qquad \textit{Equation 2.3-26}$$

Rewriting leads to an expression to calculate the travel distance of the overtopping, see Equation 2.3-27. Both formulae are valid for slopes of approximately 1:2.

$$\frac{x}{\cos(\beta)} = -0.77 \cdot H_{m0} \cdot \ln(F) + 2.7 \cdot y \cdot s_{0p}^{0.15} \qquad \textit{Equation 2.3-27}$$

For normally incident waves and a wave steepness $s_{0p}$=0.05 this amounts to the information in Table 2-4. $F$ indicates the ratio of overtopping water passing relative to the total overtopping volume.

TABLE 2-4: RESULTS OF LYKKE ANDERSEN AND BURCHARTH (2006)

| $F$ | $x$ ($y$=0) | $x$ ($y$=0.5) | $x$ ($y$=1.0) | $x$ ($y$=2.0) |
|---|---|---|---|---|
| **1** | 0.00·$H_{m0}$ | 0.89· $H_{m0}$ | 1.77· $H_{m0}$ | 3.54· $H_{m0}$ |
| **0.1** | 1.77· $H_{m0}$ | 2.66· $H_{m0}$ | 3.54· $H_{m0}$ | 5.31· $H_{m0}$ |
| **0.01** | 3.55· $H_{m0}$ | 4.43· $H_{m0}$ | 5.32· $H_{m0}$ | 7.09· $H_{m0}$ |

With no drainage facilities, the water that ends up just after the crest wall cannot go anywhere but landward. For the objective of this thesis the experiment setup should be rather different. Not the exact location of where the overtopping water falls down is relevant but merely the mean overtopping discharge at that location. Therefore also water flows over the backfill material should be taken into account.

#### 2.3.2.3 VAN KESTER (2009)

Van Kester (2009) investigated the spatial distribution of wave overtopping for both impermeable and permeable backfill, while using regular waves.

##### IMPERMEABLE BACKFILL

For the impermeable backfill a slope of 3% towards the breakwater was constructed, representing a roadway. The target was to arrive at a reduction factor to be applied to the total overtopping discharge, in a similar fashion as Besley (1999). For impermeable backfill Van Kester (2009) found a strong dependence on the wave energy flux, see Equation 2.3-28.

$$P = \frac{1}{16 \cdot \pi} \cdot \rho \cdot g^2 \cdot H^2 \cdot T \qquad \textit{Equation 2.3-28}$$

Thereafter a new dimensionless number was introduced; the dimensionless factor $x/H_{m0}$ divided by a dimensionless presentation of the energy flux, see Equation 2.3-29, resulting in Equation 2.3-30.

$$H^*T^* = \frac{H_{m0}}{R_C} \cdot T \cdot \sqrt{\frac{g}{R_C}} \qquad \textit{Equation 2.3-29}$$

$$x^* = \frac{x}{H_{m0}} \cdot \frac{1}{(H^*T^*)^n} \qquad \textit{Equation 2.3-30}$$

The exact value of the empirical parameter $n$ was determined using a "trial and error"-method, eventually resulting in smaller scatter of the data points for $n$=6. It is noted that this value will presumably depend on very specific circumstances, being for instance the inside and outside slope, the armour size, permeability of the breakwater, and so forth. Subsequently a trend line through the data was determined, resulting in Equation 2.3-31 for probabilistic design.

$$C_r = \frac{q^*(x)}{q^*_{bc}} = \exp\left(-4 \cdot 10^8 \cdot \frac{x}{H_{m0}} \cdot \frac{1}{(H^*T^*)^6}\right) \qquad \textit{Equation 2.3-31}$$

where:

$$q^*(x) = \frac{q(x)}{\sqrt{g \cdot H_{m0}^3}} \qquad \textit{Equation 2.3-32}$$

$$q^*_{bc} = \frac{q_{bc}}{\sqrt{g \cdot H_{m0}^3}} \qquad \textit{Equation 2.3-33}$$

#### PERMEABLE BACKFILL

For the permeable core much smaller differences were found in the data points, but again no unique relation between $R_C$ and $x/H_{m0}$ could be observed. Therefore the same approach as for the impermeable core was chosen. When plotting $C_r$ to $x^*$ as defined by Equation 2.3-30 the narrowest dataset was achieved using $n$=3 whereas for impermeable backfill $n$=6 was found. Fitting a trend line to this data led to Equation 2.3-34 for probabilistic design.

$$C_r = \frac{q^*(x)}{q^*_{bc}} = \exp\left(-1.64 \cdot 10^5 \cdot \frac{x}{H_{m0}} \cdot \frac{1}{(H^*T^*)^3}\right) \qquad \textit{Equation 2.3-34}$$

where $q^*(x)$ and $q^*_{bc}$ are defined as in Equation 2.3-32 and Equation 2.3-33 respectively.

#### IRREGULAR WAVES

Van Kester (2009) also performed a few tests using irregular waves. After analysis of the results he concluded that the same prediction methods may be used but $H_{m0}$ should be substituted by $H_{1/1000}$. For an experiment with a test duration of 30 minutes, this means that the largest wave height of the set should be used instead of the average of the one-third largest wave heights.

It should be stressed that based on this small number of experiments with irregular waves no general conclusion can be drawn.

### 2.3.2.4 LIOUTAS ET AL. (2012)

For the spatial distribution of wave overtopping Lioutas et al. (2012) again tried using the Adjusted TAW formula, supplemented with the parameter $\gamma_c$ accounting for the spatial variation of the overtopping, see Equation 2.3-7. For multiple distances from the crest graphs were plotted and optimal values for $\gamma_c$ were determined, leading eventually to a graph showing $\gamma_c$ seemingly exponentially decaying with distance from the crest. Nevertheless for sake of simplicity a linear trend line was determined, resulting in Equation 2.3-35.

$$\gamma_c = -0.142 \cdot \frac{x}{G_C} + 0.577 \qquad \textit{Equation 2.3-35}$$

In the end Figure 2.3-4 is presented showing a reasonable prediction method. However a clear arch-shape trend can be observed in the data that was a lot less pronounced in the graph for the total wave overtopping. Therefore it is expected some improvement in the expression $\gamma_c$ is possible. Besides for large distance from the crest $\gamma_c$ would become negative, leading to undesired behaviour in the Adjusted TAW formula.

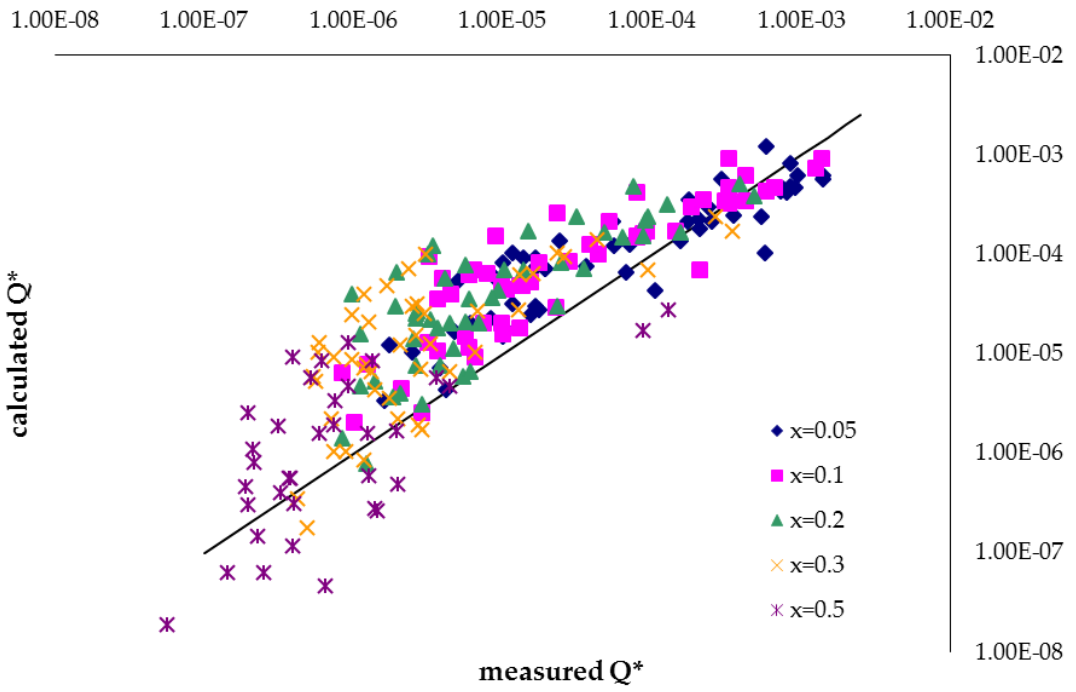


FIGURE 2.3-4: EVALUATION OF THE "ADJUSTED" TAW-FORMULA (LIOUTAS ET AL., 2012)

Also a comparison with the prediction method of Juul Jensen (1984) was drawn. The general trend of the spatial distribution of wave overtopping was also well predicted by this expression, showing similar scatter as the "Adjusted" TAW-formula.

The prediction method of Besley (1999) was not found to be applicable to these measurement results. The scatter in the data was just too large to discern a clear trend.

Results of Van Kester (2009) were also found to be non-applicable to the experiment results. The scatter in the results was very large and no correlation was visible in the graphs. One reason for this is the difference between regular and irregular wave overtopping.

## 2.4 CONCLUSIONS

### 2.4.1 TOTAL OVERTOPPING

Extensive research has been carried out on total overtopping. The TAW prediction method is recommended by most prominent literature (e.g. The Rock Manual (2007)).

The method includes all parameters that have currently proven to influence the process of wave overtopping. Moreover the parameters of the method are generally well defined which means that no major assumptions have to be made during design.

EurOtop recommends using the TAW formula for non-breaking waves to calculate the mean overtopping discharge for breakwaters. Several adjustments were made regarding the reduction factor for slope roughness and the run-up height.

Lioutas et al. (2012) combined the two TAW formulae and recommended a so called Adjusted TAW prediction method. The current research will include experiments based on the same configuration as Lioutas et al. (2012) used. Therefore it will be interesting to see if the Adjusted TAW formula is also valid for the current experiments.

The data acquired during the experiment phase will be compared with the TAW prediction method, the EurOtop method and the Adjusted TAW method.

### 2.4.2 LANDWARD SPATIAL DISTRIBUTION OF OVERTOPPING

#### 2.4.2.1 WAVE OVERTOPPING DISCHARGE DIRECTLY BEHIND THE CREST

The overtopping discharge directly behind the crest has been studied less extensively than the total overtopping. Different prediction methods exist but none of these include material properties of the breakwater. The permeability and roughness of the used rock material is likely to have an influence on the amount of overtopping that infiltrates in the crest.

For all discussed prediction methods a comparison with the experimental data will be drawn in section 5.2.

#### 2.4.2.2 WAVE OVERTOPPING DISCHARGE DISTRIBUTION BEHIND THE CREST

All discussed prediction methods again are empirical formulae that are based on experiments. Per prediction method it was investigated how the spatial distribution of overtopping was measured in the experiments. For the current research interaction between overtopped water and backfill material behind the crest should be taken into account. For this reason the findings of Lykke Andersen (2006) cannot be used in the current research.

Furthermore the method of Van Kester was presented after experiments with regular waves. The validity of this method to the current experiments, where irregular waves are used, cannot be guaranteed.

The prediction methods of Juul Jensen and Lioutas both were determined after experiments with irregular waves, and interaction of the overtopped water with the backfill material was taken into account. These two methods therefore are expected to be most relevant for the current research.

# CHAPTER 3. PHYSICAL MODEL SETUP

The experimental part of this research was executed in the Hydraulic Laboratory of Delft University of Technology. In this chapter all aspects of the physical model will be discussed. First a prototype is determined that accurately represents a realistic breakwater. Then in section 3.3 requirements are discussed that the scale model should meet. The scale model is presented in section 3.4. Section 3.5 describes the measuring system used in the experiments. Laboratory equipment is discussed in section 3.6. An overview of the physical model setup is given in section 3.7. Finally results of the validation tests are presented in section 3.8.

## 3.1 INTRODUCTION

Since the overtopping process is quite complicated and many parameters are involved (see also section 3.3.2) it is not feasible to investigate the influence of every parameter. The most prominent parameters were selected as experiment variables.

From the literature discussed in section 2.2 it is apparent that four parameters have a major influence on the overtopping process. In coherence with Van Kester (2009) and Lioutas et al. (2012) the following parameters are selected; 1) wave height, 2) wave steepness, 3) freeboard and 4) seaward slope.

Two additional parameters are required to account for the berm; 1) berm width and 2) water depth above the berm, i.e. berm elevation. A horizontal berm was used in the experiments.

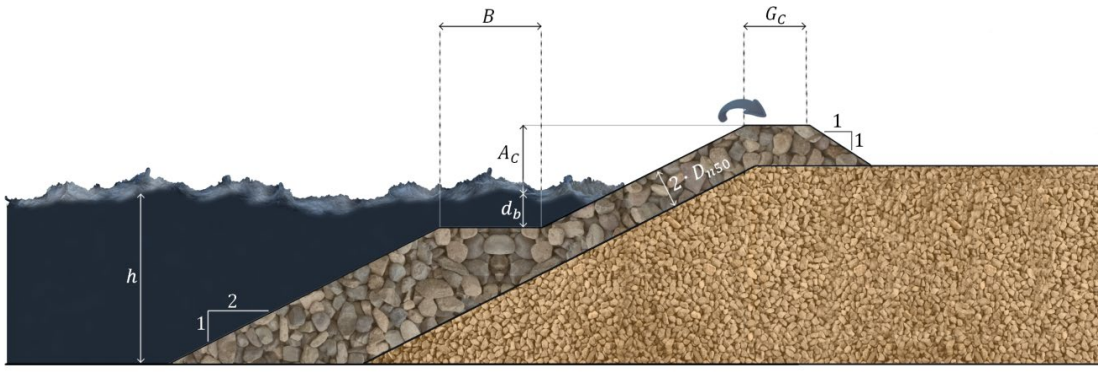


FIGURE 3.1-1: BERM BREAKWATER PARAMETER DEFINITION

The experiment programme that was conducted by Lioutas (2010) covered the area of interest accurately. Therefore this programme was taken as a starting point and modified to also account for the presence of a berm, resulting in the parameters printed in Table 3-1. Figure 3.1-1 visualises the parameters.

TABLE 3-1: PARAMETERS IN THE BREAKWATER CONFIGURATION

| Variable | Description | Unit |
|---|---|---|
| $B$ | berm width | [m] |
| $d_b$ | water depth above berm | [m] |
| $H_{m0}$ | spectral wave height | [m] |
| $A_C$ | armour freeboard | [m] |
| $s_{m-1,0}$ | wave steepness | [-] |
| $\tan(\alpha)$ | seaward slope | [-] |

The permeability of the backfill is expected to have a significant effect on the spatial distribution of the overtopping, because the infiltration rate of overtopped water in the backfill is governed by the backfill permeability. As varying this parameter would lead to too many experiments, the same backfill material was chosen as Lioutas used. For the same reason the seaward slope is not varied; instead a commonly applied slope of 1:2 is chosen.

## 3.2 PROTOTYPE

A prototype is determined that should accurately be represented by the scale model. Already in the prototype some of the boundary conditions posed by the equipment available in the laboratory are taken into account.

For the experiments the "Lange Speurwerk Goot" in the Hydraulic Laboratory of Delft University of Technology was used. The height of the flume is 0.90 m and the wave generator used can produce waves with a wave height up to approximately 0.18 m. This can be translated into the following boundary conditions; $h + A_C \leq$ 0.70 m and $H_{m0} <$ 0.18 m. The equipment that was used is discussed more extensively in section 3.6.

Prototype breakwater configurations and wave conditions are determined as printed in Table 3-2.

TABLE 3-2: PROTOTYPE PARAMETERS FOR BREAKWATERS WITH A BERM

| Variable | Value(s) | | | | Unit |
|---|---|---|---|---|---|
| $B$ | 0 | | 6 | 12 | [m] |
| $d_b$ | 2 | | 0 | -2 | [m] |
| $h$ | 10.0 | | 10.4 | | [m] |
| $H_{m0}$ | 2.4 | 2.8 | 3.2 | 3.6 | [m] |
| $A_C$ | 4.0 | | 3.6 | | [m] |
| $s_{m-1,0}$ | 0.01 | | 0.05 | | [-] |
| $\tan(\alpha)$ | 2 | | | | [-] |

### ARMOUR LAYER

Little information is available for the design of non-reshaping berm breakwaters. The design generally involves small-scale physical model tests, in which multiple iterations can be required before a cost-effective design is found.

PIANC (2003) notes that movement of stones is initiated when $H_0 \cong 1.5 - 2.0$, with $H_0 = \frac{H_s}{\Delta D_{n50}}$. Roughly, this is consistent with the stability prediction formula of Van der Meer (1988).

A conservative design method is to use the stability criterion of Van der Meer (1988). Some research has been carried out on the effect of a berm on the stability of armour elements. Van Gent et al. (2012) concluded from experiments that the stone stability in the upper slope is increased based on the berm elevation, the berm width and the wave steepness.

In this research an adjusted version of the stability criterion of Van der Meer – as discussed in Verhagen, d'Angremond, and Roode (2009) – has been used to determine the armour stone size, see Equation 3.2-1. This is a conservative choice. Because in the current research multiple berm configurations were tested, it was desirable that adaptations could be carried out quickly and the same armour material could be used for all of the configurations. Moreover no damage could be permitted during the tests, for the overtopping should be measured for different wave conditions on the exact same slope.

$$\frac{H_{2\%}}{\Delta \cdot D_{n50}} = c_{pl} \cdot P^{0.18} \cdot \left(\frac{S}{\sqrt{N}}\right)^{0.2} \cdot \left(s_{m-1,0}\right)^{0.25} \cdot \sqrt{\cot(\alpha)} \quad \text{for plunging waves} \qquad \textit{Equation 3.2-1}$$

$$\frac{H_{2\%}}{\Delta \cdot D_{n50}} = c_{s} \cdot P^{-0.13} \cdot \left(\frac{S}{\sqrt{N}}\right)^{0.2} \cdot \left(s_{m-1,0}\right)^{-0.25} \cdot \left(\xi_{m-1,0}\right)^{P-0.5} \quad \text{for surging waves} \qquad \textit{Equation 3.2-2}$$

$$\xi_{cr} = \left[\frac{c_{pl}}{c_s} P^{0.31} \sqrt{\tan(\alpha)}\right]^{\frac{1}{P+0.5}} \qquad \textit{Equation 3.2-3}$$

where:

| | | | |
|---|---|---|---|
| $H_{2\%}$ | = | wave height exceeded by 2% of the waves | [m] |
| $c_{pl}$, $c_s$ | = | empirical coefficients | [-] |
| $S$ | = | damage level $A/(D_{n50})^2$, where $A$=erosion area in cross section | [-] |
| $s_{m-1,0}$ | = | fictitious wave steepness, $\frac{2\pi \cdot H_{2\%}}{g T_{m-1,0}^2}$ | [-] |
| $N$ | = | number of waves | [-] |
| $P$ | = | notional permeability coefficient | [-] |

Table 3-3 illustrates the calculation.

TABLE 3-3: STABILITY OF THE ARMOUR LAYER, PROTOTYPE

| Variable | Value | Unit |
|---|---|---|
| $\cot(\alpha)$ | 2 | [-] |
| $c_{pl}$ | 7.25 | [-] |
| $c_s$ | 1.05 | [-] |
| $D_{n50}$ | 1.14 | [m] |
| $H_{2\%}$ | 5.04 | [m] |
| $H_{m0}$ | 3.6 | [m] |
| $N$ | 1000 | [-] |
| $P$ | 0.5 | [-] |
| $S$ | 2 | [-] |
| $s_{m-1,0}$ | 0.07 | [-] |
| $M_{50}$ | 3923 | [kg] |
| $\Delta$ | 1.65 | [-] |
| $\xi_{cr}$ | 3.94 | [-] |
| $\xi_{m-1,0}$ | 1.89 | [-] |

*Please note that here $s_{m-1,0} = 0.07$ has been used, instead of $s_{m-1,0} = 0.05$ which is typical for wind waves and is used for the experiments. This difference originates from the different wave heights that are used to calculate $s_{m\text{-}1,0}$. Generally $s_{m-1,0} = \frac{2\pi \cdot H_{m0}}{g T_{m-1,0}^2}$ is used, whereas in the stability formula $s_{m-1,0} = \frac{2\pi \cdot H_{2\%}}{g T_{m-1,0}^2}$ should be applied. Since wave heights are generally Rayleigh distributed $H_{2\%} = 1.4 \cdot H_{m0}$ is maintained, leading also to a factor 1.4 in the fictitious wave steepnesses.*

For the required median stone weight the stone class HMA 3000-6000 is chosen. According to EN13383 the median stone weight for this class must lay in the range of 4200-4800 kg, with $D_{n50,armour}$=1.18 m.

### CORE

A simple two-layer breakwater was built in the laboratory to ensure that breakwater configurations could be changed in a short period of time. Therefore the core is positioned directly underneath the armour layer. The rock material used for the core will be larger than in reality.

The Rock manual recommends using an armour sub-layer with a mass ratio of 1/10 compared with the armour layer, in order to avoid any problems due to under-pressure.

## 3.3 SCALING REQUIREMENTS

When a scaled model is built this model should accurately reproduce the prototype. According to Hughes (1993) similitude is achieved “when all major factors influencing reactions are in proportion between prototype and model, while those factors that are not in proportion throughout the modelled domain are so small as to be insignificant to the process”. For smaller scale models the accuracy decreases. A scale model reproduces the prototype accurately when specific criteria of similitude are met.

Criteria of similitude, or scale laws, are mathematical conditions that must be met by the ratios of specific parameters between the prototype and the model. They cannot be altered without altering the underlying physical assumptions.

## 3.3.1 CRITERIA OF SIMILITUDE

### 3.3.1.1 GEOMETRIC SIMILARITY

Two objects or systems are geometrically similar if the ratios of all corresponding linear dimensions are equal. This means that the model represents a geometrical reproduction of the prototype. Geometrically similar models are also called geometrically undistorted models.

### 3.3.1.2 KINEMATIC SIMILARITY

Kinematic similarity in this particular case refers to the motion of fluid particles within the flow regime. Kinematic similarity indicates a similarity of motion between particles in model and prototype. Kinematic similarity is achieved when the ratio between the components of all vectorial motions for the prototype and model is the same for all particles at all times (Hughes, 1993). In a geometrically similar model kinematic similarity results in particle paths that are geometrically similar to the prototype.

Kinematically similar wave motion requires $N_t = \sqrt{N_L}$, based on a scale relationship between the length and the wave period for a small amplitude wave (Hughes, 1993). In fact this criterion of similitude is equal to the Froude criterion.

### 3.3.1.3 DYNAMIC SIMILARITY

Dynamic similarity means that there must be constant prototype-to-model ratios of all masses and forces acting on the system. The forces exerted by the wave motion on an object or boundary are similitude when the dynamic similarity is maintained.

It is impossible to achieve complete similitude where all the force ratios are constant. Therefore similitude requirements were determined, indicating the consequences of violating complete similitude.

The major forces for hydraulic engineering experiments are displayed below, in terms of their physical units.

inertial force: $\overrightarrow{F_i} = \text{mass} \cdot \text{acceleration} = (\rho \cdot L^3)(V^2 \cdot L^{-1}) = (\rho \cdot V^2 \cdot L^2)$ *Equation 3.3-1*

gravity force: $\overrightarrow{F_g} = \text{mass} \cdot \text{gravitational acceleration} = (\rho \cdot g \cdot L^3)$ *Equation 3.3-2*

viscous force: $\overrightarrow{F_\mu} = \text{viscosity} \cdot \text{area} \cdot \frac{\text{velocity}}{\text{distance}} = \mu \cdot L^2 \cdot \frac{V}{L} = \mu \cdot L \cdot V$ *Equation 3.3-3*

surface tension force: $\overrightarrow{F_\mu} = \text{unit surface tension} \cdot \text{length} = \sigma \cdot L$ *Equation 3.3-4*

### FROUDE

The Froude number expresses the relative influence of inertia and gravity forces in a hydraulic flow. The Froude number remains constant between model and prototype if Equation 3.3-5 is fulfilled.

$$\left(\frac{V}{\sqrt{g \cdot L}}\right)_{\text{prototype}} = \left(\frac{V}{\sqrt{g \cdot L}}\right)_{\text{model}} \quad \text{or} \quad \left(\frac{N_V}{\sqrt{N_g \cdot N_L}}\right) = 1 \qquad \textit{Equation 3.3-5}$$

This criterion holds for flow situations where inertia and gravity forces are considered to be the only dominant forces, which is the case for most flows with a free surface. Therefore the Froude law is the most important criterion for the design of a coastal scale model.

### REYNOLDS

The Reynolds number is the ratio between inertia and viscous forces. Reynolds first used this number to distinguish between laminar and turbulent flows. Similitude is achieved when Equation 3.3-6 holds.

$$\left(\frac{\rho \cdot L \cdot V}{\mu}\right)_{\text{prototype}} = \left(\frac{\rho \cdot L \cdot V}{\mu}\right)_{\text{model}} \quad \text{or} \quad \left(\frac{N_\rho \cdot N_L \cdot N_V}{N_\mu}\right) = 1 \qquad \textit{Equation 3.3-6}$$

The Reynolds law is intended for modelling flows where viscous flow predominates. In scale model conditions this criterion is not compatible with the Froude law. This means that viscous forces cannot correctly be modelled simultaneously with gravity forces in the same scale model.

### STROUHAL

The Strouhal number is the ratio of temporal to convective inertial forces. This number is likely to be important in unsteady, oscillating flows. Equation 3.3-7 states that the velocity scale ratio is equal to the length scale ratio divided by the time scale ratio. This is the same definition for velocity scale that arises from consideration of the fundamental dimensions of velocity (Hughes, 1993).

$$\left(\frac{L}{V \cdot t}\right)_{\text{prototype}} = \left(\frac{L}{V \cdot t}\right)_{\text{model}} \quad \text{or} \quad \left(\frac{N_L}{N_V \cdot N_t}\right) = 1 \qquad \textit{Equation 3.3-7}$$

### WEBER

The relative influence of surface tension is given by the ratio of inertia forces to surface tension forces, which is known as the Weber number, Equation 3.3-8.

$$\left(\frac{\rho \cdot L^2 \cdot V^2}{\sigma L}\right)_{\text{prototype}} = \left(\frac{\rho \cdot L^2 \cdot V^2}{\sigma L}\right)_{\text{model}} \quad \text{or} \quad \left(\frac{N_\rho \cdot N_L \cdot N_V^2}{N_\mu}\right) = 1 \qquad \textit{Equation 3.3-8}$$

where:

| | | | |
|---|---|---|---|
| $g$ | = | gravitational acceleration | [LT$^{-2}$] |
| $L$ | = | characteristic length | [L] |
| $V$ | = | characteristic velocity | [LT$^{-1}$] |
| $t$ | = | time | [T] |
| $\sigma$ | = | surface tension | [MT$^{-2}$] |
| $\rho$ | = | fluid density | [ML$^{-3}$] |
| $\mu$ | = | dynamic viscosity | [M$^{-1}$LT] |

The formation of wave spray is strongly dependent upon surface tension effects and ought to scale according to Weber.

### 3.3.2 SIMILARITY FOR RUBBLE MOUND BREAKWATERS

Hydraulic similitude requirements for coastal hydrodynamic models can be derived from continuity and Navier-Stokes equations governing incompressible, free-surface flows (Hughes, 1993). Experience has shown almost every problem may be simplified to an interaction between two major forces. Several criteria have been developed based on the assumption that two forces dominate the water motion with other forces having minor effect.

In Hughes (1993) a dimension analysis is presented as performed by Hudson et al. (1979) for stability of rubble mound breakwaters with a core of quarry run.

A large number of parameters is involved in the wave structure interaction:

| | | | |
|---|---|---|---|
| $h$ | = | Water depth at the toe of the structure | [L] |
| $D$ | = | Percent damage of the cover layer (number of displaced armour units divided by total number of units placed) | [-] |
| $g$ | = | Gravitational acceleration | [LT$^{-2}$] |
| $H$ | = | Wave height | [L] |
| $l_a$ | = | Characteristic linear dimension of armour unit | [L] |
| $V_w$ | = | Water velocity in the vicinity of the cover layer | [LT$^{-1}$] |
| $\alpha$ | = | Seaside slope angle measured from the horizontal | [-] |
| $\beta$ | = | Incident wave angle | [-] |
| $\psi$ | = | Shape of armour unit | [-] |
| $\vartheta$ | = | Bottom slope seaward of structure | [-] |
| $L$ | = | Wave length | [L] |
| $\mu$ | = | Dynamic viscosity of water in vicinity of the breakwater | [M$^{-1}$LT] |
| $\zeta_a$ | = | Linear dimension of surface roughness of units | [L] |
| $\rho_a$ | = | Mass density of armour units | [ML$^{-3}$] |
| $\rho_w$ | = | Mass density of water in vicinity of the breakwater | [ML$^{-3}$] |

Assuming all important parameters are included in the list, he argued there must be a function such that Equation 3.3-9 holds.

$$f(V_w, H, L, h, \beta, \vartheta, g, \rho_w, \rho_a, l_a, \mu, \zeta_a, \alpha, \psi, D) = 0 \qquad \textit{Equation 3.3-9}$$

To this day no mathematical relation has been found however. Determination of correct similitude relationships had to be done using dimensional analysis. The conclusions Hudson drew from the analysis are stated below:

- Rubble-mound structure models must be geometrically undistorted in length scale.
- Flow hydrodynamics in a rubble-mound structure model must conform to the Froude criterion.
- Rubble-mound structure models must have turbulent flow conditions throughout the primary armour layer.
- The relative density of the armour stones should be preserved.

The model used in the current research fulfils every requirement. A possible scale effect is the flow pattern inside the core of the breakwater, though not mentioned by Hudson. In the prototype there is turbulent flow inside the core, but for small scale models the flow might become laminar. This would lead to too large viscous forces corresponding to too small Reynolds numbers. In section 3.4.3 this effect is looked at closer.

### 3.3.3 CONCLUSION

All conditions as formulated by Hudson are met in the model used for the current research. Physical phenomena not addressed in the dimensional analysis of Hudson involve the flow inside the core and the overtopping process.

Already before Hudson, Warnock (1950) concluded the forces associated with surface tension and elastic compression can be safely neglected since they are relatively small in all coastal problems. The overtopping phenomenon, being mainly a free surface flow, is driven by the interaction between gravity and inertial forces. Therefore the Froude scaling law is used in the scaling process.

## 3.4 SCALE MODEL

The final scale model was determined by starting from the prototype, using the scaling process discussed in section 3.3 and taking into account the boundary conditions posed by the laboratory equipment. Table 3-4 presents the scales that were used in the process.

TABLE 3-4: SCALES USED

| | | |
|---|---|---|
| $N_\rho$ [-] | 1 | scale of density |
| $N_L$ [-] | $1/20$ | scale of length |
| $N_V$ [-] | $\sqrt{1/20}$ | scale of velocity |
| $N_t$ [-] | $\sqrt{1/20}$ | scale of time |
| $N_g$ [-] | 1 | scale of gravity |
| $N_\mu$ [-] | 1 | scale of viscosity |
| $N_q$ [-] | $(1/20)^{1.5}$ | scale of overtopping |

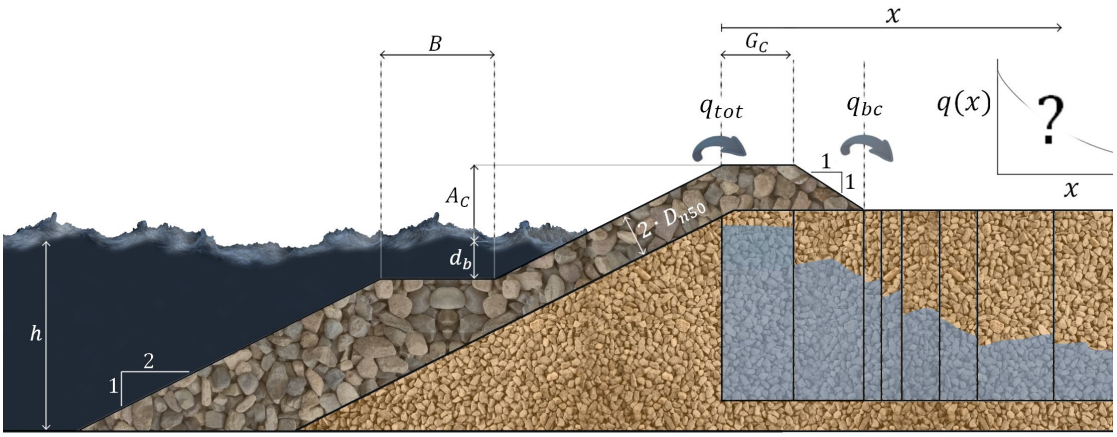


FIGURE 3.4-1: SCALE MODEL

After scaling the breakwater with a berm can be parameterized as displayed in Table 3-5. The final scale model is presented in Figure 3.4-1.

TABLE 3-5: SCALE MODEL PARAMETERS FOR BREAKWATERS WITH A BERM

| Variable | Value(s) | | | | Unit |
|---|---|---|---|---|---|
| $B$ | 0 | | 0.3 | 0.6 | [m] |
| $d_b$ | 0.1 | | 0 | -0.1 | [m] |
| $h$ | 0.50 | | 0.52 | | [m] |
| $H_{m0}$ | 0.12 | 0.14 | 0.16 | 0.18 | [m] |
| $A_C$ | 0.20 | | 0.18 | | [m] |
| $s_{m-1,0}$ | 0.01 | | 0.05 | | [-] |
| $\tan(\alpha)$ | 2 | | | | [-] |

*Please note the elevation of the breakwater crest remains constant. The water level, h, and freeboard, $R_C$, are changed simultaneously. The printed values of $d_B$ are valid for h=0.50 m.*

During the experiments the initial test programme was adjusted because of limitations of the wave generator or overtopping volumes that were in the not suitable for measurement. Section 3.7 gives an impression of the conditions that were actually tested.

A full overview of the parameters per experiment can be found in Appendix K.

## 3.4.1 MATERIALS

### 3.4.1.1 ARMOUR LAYER

The requirements for the stone class HMA 3000-6000 – as posed in EN13383 – were also scaled, see Table 3-6.

TABLE 3-6: ARMOUR STONE WEIGHTS

| | y [-] | | | $M_y$ (Prototype) | $M_y$ (Scale model) |
|---|---|---|---|---|---|
| **ELL** | 0% | - | 5% | 2000 kg | 0.250 kg |
| **NLL** | 0% | - | 10% | 3000 kg | 0.375 kg |
| **NUL** | 70% | - | 100% | 6000 kg | 0.750 kg |
| **EUL** | 97% | - | 100% | 9000 kg | 1.125 kg |

In the laboratory the specified stone class was not available. Therefore a manual selection was made from a grading called "Doornik 56-125 mm". The weight of every individual stone was determined with a balance, eventually resulting in the curve shown in Figure 3.4-2. The light blue shading indicates the requirements a scaled HMA 3000-6000 kg stone class should meet. The selected grading falls just within this area.

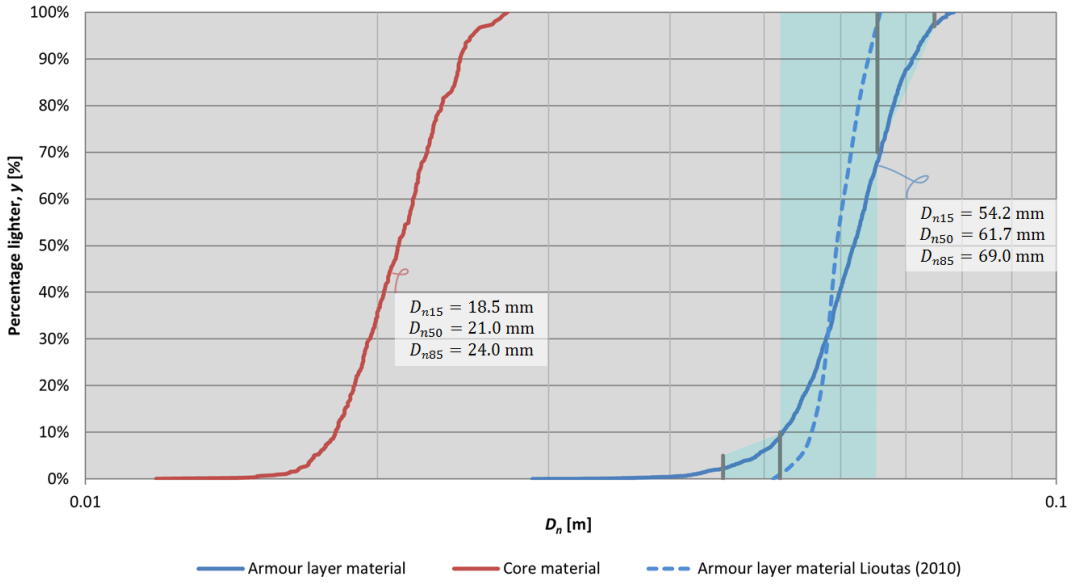


FIGURE 3.4-2: STONE GRADINGS IN THE SCALE MODEL

The density of the armour stones was 2678 kg/m³. The core material had a density of 2658 kg/m³.

### 3.4.1.2 CORE, BACKFILL

The Rock Manual specifies that the mass ratio of subsequent layers of stone should lie between 1/10 and 1/15. In this research the same core material has been applied as in the research of Lioutas (2010). A grading called "Yellow Sun extra split 20-40 mm" was used. The grading is showed in Figure 3.4-2.

The same material was used as backfill. With the pumps the permeability of the backfill could be regulated. The pumps were setup in such a way that the falling velocity of the water was constant in every position in the backfill. See also section 3.6.1.3.

## 3.4.2 STABILITY CHECK

### 3.4.2.1 ARMOUR LAYER

The Froude scaling leads to a correct scaling of the Van der Meer formula for armour slope stability. The selected armour grading results in a stability number $S$=1.21, see Equation 3.4-2. This calculation is done for the highest wind waves tested during the experiments.

$$\frac{H_{2\%}}{\Delta \cdot D_{n50}} = c_{pl} \cdot P^{0.18} \cdot \left(\frac{S}{\sqrt{N}}\right)^{0.2} \cdot \left(s_{m-1,0}\right)^{0.25} \cdot \sqrt{\cot(\alpha)} \qquad \textit{Equation 3.4-1}$$

$$S = \sqrt{N}\left(\frac{H_{2\%}}{\Delta \cdot D_{n50} \cdot c_{pl} \cdot P^{0.18} \cdot \left(s_{m-1,0}\right)^{0.25} \cdot \sqrt{\cot(\alpha)}}\right)^5 \qquad \textit{Equation 3.4-2}$$
$$= \sqrt{1000}\left(\frac{1.4 \cdot 0.18}{1.678 \cdot 0.0617 \cdot 7.25 \cdot (0.5)^{0.18} \cdot (0.07)^{0.25} \cdot \sqrt{2}}\right)^5 = 1.21$$

### 3.4.2.2 FILTER STABILITY

Apart from wave attack, a rock protection can also fail internally as a result of processes related to large pressure gradients inside the protection. Three criterions have to be met (see also Schiereck (2001)).

Stability:

$$\frac{D_{15F}}{D_{85B}} \leq 5 \rightarrow \frac{0.064\ \text{m}}{0.029\ \text{m}} = 2.2 \leq 5 \qquad \textit{Equation 3.4-3}$$

Internal stability in the under layer:

$$\frac{D_{60}}{D_{10}} \leq 10 \rightarrow \frac{0.026\ \text{m}}{0.021\ \text{m}} = 1.2 \leq 10 \qquad \textit{Equation 3.4-4}$$

Permeability:

$$\frac{D_{15F}}{D_{15B}} > 5 \rightarrow \frac{0.064\ \text{m}}{0.022\ \text{m}} = 2.8 \not> 5 \qquad \textit{Equation 3.4-5}$$

The requirement for permeability is not met. However no problems with respect to pressure build up are expected since both armour layer and core are very permeable. Moreover, during the experiments no displacement of core material was observed. Transport of core material can eventually lead to clogging of the armour layer and therefore decrease the permeability.

## 3.4.3 INFILTRATION

In permeable structures breaking waves can partially infiltrate the core. The energy dissipation inside the porous medium and the interactive flow between external and internal wave motion result in wave breaking that is quite different compared with wave breaking on impermeable structures. Therefore it is important to correctly simulate this behaviour in the scale model.

When the flow in the filter layer is simplified to a 1D (Vertical) flow, this flow can be described with the extended Forchheimer equation, see Equation 3.4-6.

$$I = \mathrm{a} \cdot u_f + \mathrm{b} \cdot u_f \cdot |u_f| + \mathrm{c} \frac{\partial u_f}{\partial t} \qquad \textit{Equation 3.4-6}$$

where:

| | | | |
|---|---|---|---|
| a | = | coefficient of friction for laminar part | [s/m] |
| b | = | coefficient of friction for turbulent part | [s²/m²] |
| c | = | coefficient of friction for inertial resistance | [s²/m] |
| $I$ | = | pressure gradient | [-] |
| $u_f$ | = | depth-averaged filter velocity | [m/s] |

Burcharth, Liu, and Troch (1999) mention the last term in Equation 3.4-6 is of minor importance for scaling porous flow in breakwater cores, and can be disregarded. For more information on the extended Forchheimer equation refer to Schiereck (2001).

Shih (1990) proposed the following coefficients of friction.

$$a = \alpha \frac{(1-n)^2}{n^3} \frac{\nu}{g \cdot D_{15}^2} \qquad \textit{Equation 3.4-7}$$

$$b = \beta \frac{1-n}{n^3} \frac{1}{g \cdot D_{15}} \qquad \textit{Equation 3.4-8}$$

With $\nu$ is the kinematic viscosity of the fluid and $n$ is the porosity of the porous medium.

$$\alpha = 1684 + 3.12 \cdot 10^{-3} \cdot \left(\frac{g}{\nu^2}\right)^{\frac{2}{3}} \cdot D_{15}^2 \qquad \textit{Equation 3.4-9}$$

$$\beta = 1.72 + 1.57 \cdot \exp\left(-5.10 \cdot 10^{-3} \cdot \left(\frac{g}{\nu^2}\right)^{\frac{1}{3}} \cdot D_{15}\right) \qquad \textit{Equation 3.4-10}$$

Assuming hydrostatic pressures, the pressure gradient is equal to 1. A porosity of $n = 0.4$ is assumed. $D_{15} = 0.022$ m. This results in $u_f = 0.095$ m/s.
$u_p = \frac{u_f}{n} = 0.237$ m/s.

The Reynolds number for flow around particles in the core is

$$\mathrm{Re} = \frac{u_p \cdot D_{15}}{\nu} = \frac{0.237 \cdot 0.022}{1 \cdot 10^{-6}} = 5232$$

Hughes (1993) prescribed a minimum value for the Reynolds number to ensure turbulent flow in a scale model; the Reynolds number should be at least O($10^4$). For the current scale model the Reynolds number indeed is of the same order of magnitude. Moreover, in the calculation method in Equation 3.4-6 a one dimensional flow is assumed. In reality the flow in the scale model will also have a horizontal component that will lead to more turbulent flow. Therefore it is expected viscous forces will not cause significant scale effects.

## 3.5 MEASURING SYSTEM

The water related to overtopping was collected in eight collection bins which are filled with core material. At the bottom of the tanks an inclination has been made so that the water flows to the inlet point of the pumping system. Eight pumps – one for each collection bin – transport the overtopped water to floating collection tanks at the very end of the wave flume. Eventually by measuring the weight of each collection tank the overtopping discharge for eight locations can be calculated. Figure 3.5-1 illustrates the measuring setup.

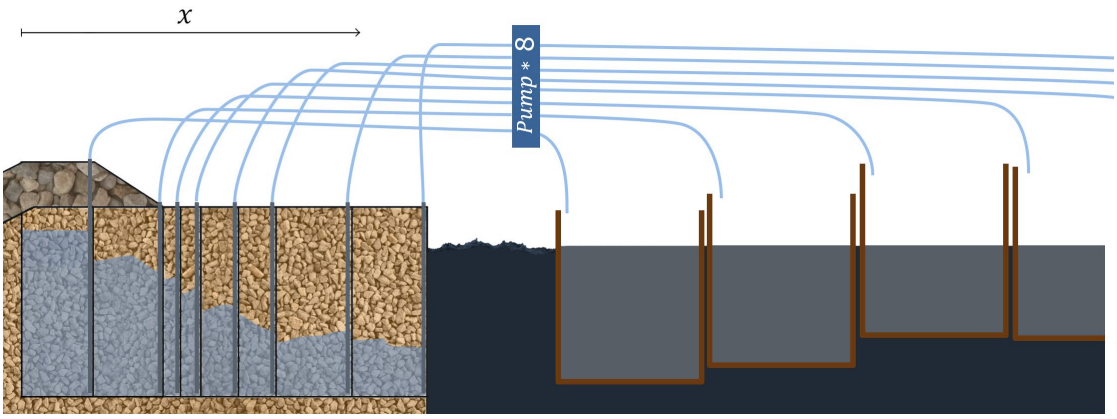


FIGURE 3.5-1: MEASURING SYSTEM

Waves are measured with two sets of three wave gauges. In this manner distinction can be made between the incoming waves and reflecting waves, at two locations in the wave flume. Thereby also the effect of wave propagation in the flume can be discerned.

This measuring system is similar to the one Lioutas et al. (2012) used for his experiments. Especially the floating tanks proved to be a large improvement in comparison with the test setup of Van Kester (2009). Where Van Kester experienced a lowering of the water table due to overtopping "losses" that were not pumped back into the system, in Lioutas' setup the water level was held constant by means of a system of communicating vessels. The breakwater being permeable allowed for water volumes permeating through the structure.

An impression of the measuring system is printed in Figure 3.5-1. The exact same configuration was used as Lioutas (2010), with only one adjustment. The first bin of Lioutas (2010) was split into two bins to make a better distinction of the overtopping infiltrating into the crest of the breakwater. The position of the collection bins is denoted in Table 3-7. Appendix E contains the construction drawings of the collection bin structure.

TABLE 3-7: MEASURING SYSTEM DISTANCES

| | Horizontal position (x) | |
|---|---|---|
| | Seaward end [m] | Landward end [m] |
| **Bin 1** | 0 | 0.18 |
| **Bin 2** | 0.18 | 0.28 |
| **Bin 3** | 0.28 | 0.33 |
| **Bin 4** | 0.33 | 0.38 |
| **Bin 5** | 0.38 | 0.48 |
| **Bin 6** | 0.48 | 0.58 |
| **Bin 7** | 0.58 | 0.78 |
| **Bin 8** | 0.78 | 0.98 |

$x = 0$ at the seaward edge of the crest, see Figure 3.5-1. With the used length scale $N_L$=0.05 a distance of 14 m behind the breakwater crest is covered in prototype scale.

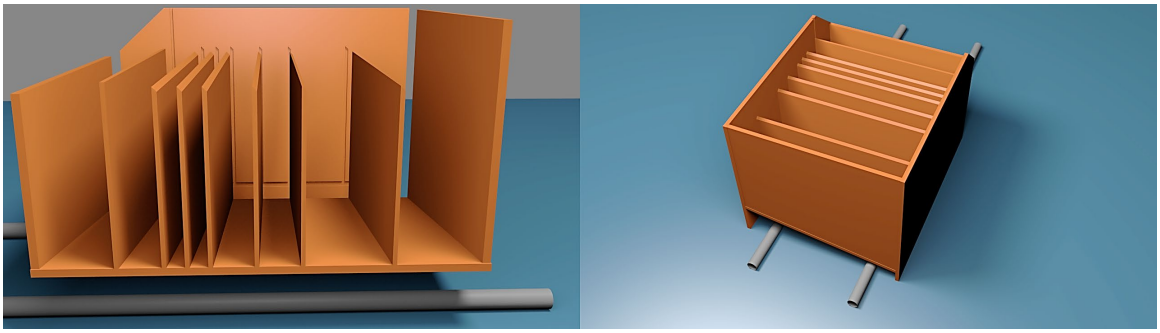

FIGURE 3.5-2: 3D IMPRESSION OF THE COLLECTION BIN STRUCTURE

## 3.6 LABORATORY EQUIPMENT

### 3.6.1 HYDRAULIC EQUIPMENT

#### 3.6.1.1 WAVE FLUME

Experiments were performed in the “Lange Speurwerk Goot” in the Fluid Mechanics Laboratory of Delft University of Technology. The flume can be filled and emptied with pumps and valves on either side of the flume, and a wave generator is present at one side. The main dimensions of this flume are: length = 40 m, width = 0.80 m, height = 0.90 m.

#### 3.6.1.2 WAVE GENERATOR

The wave generator installed in the “Lange Speurwerk Goot” is driven by an electromotor that is controlled by a personal computer. The computer runs software developed by WL|Delft Hydraulics – nowadays part of Deltares – called “Wavegenerator Control”. The program can be used to generate a variety of wave conditions. An input file has to be created by the user, specifying the requested wave height, wave period, wave spectrum, spectrum parameters and duration, see Appendix G. A routine called “Makewave.bat” was then used to generate a steering file that specifies for every time step a voltage that needs to be imposed to the electromotor.

The wave generator is equipped with an Active Reflection Compensator (ARC) that measures reflected waves and corrects the motion of the wave generator accordingly.

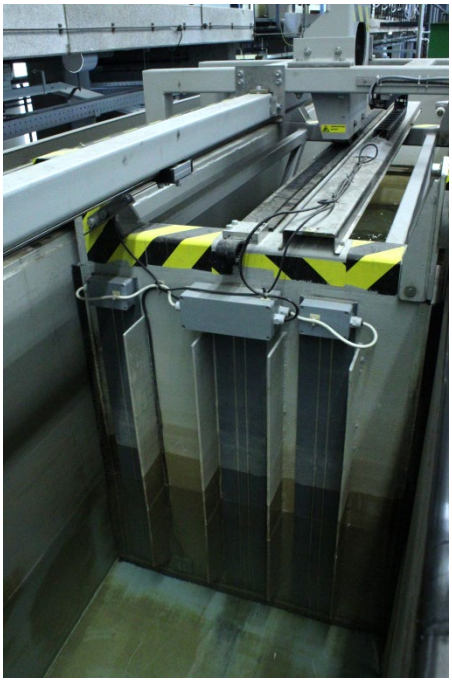

FIGURE 3.6-1: WAVE GENERATOR

The accuracy of the wave generator was better than the one Lioutas (2010) used in his research, but still quite large differences were observed, particularly for large wave heights. Appendix H shows the difference between the requested and generated waves.

### 3.6.1.3 PUMPS

Eight pumps were needed, one for each bin. Since there was not always water in the collection bins, displacement pumps needed to be used. These pumps are designed to displace a certain volume per rotation and can therefore also pump air.

The pump capacity for each bin was scaled to the bin width, resulting in an equal falling velocity for the whole hinterland. A falling velocity of approx. 2.5 mm/s was used.

The pumps used for each bin are displayed in Table 3-8.

TABLE 3-8: OVERVIEW OF THE PUMPS USED

| Bin | Width [m] | Pump type | Pump capacity [l/min] |
|---|---|---|---|
| **1** | 0.18 | F.E.I.T. PVM 0,2 | 25 |
| **2** | 0.10 | Watson Marlow 704U/R | 14 |
| **3** | 0.05 | Watson Marlow 704U/R | 7 |
| **4** | 0.05 | Watson Marlow 704S | 7 |
| **5** | 0.10 | Watson Marlow 620Du (conn. 1) | 4 |
| **6** | 0.10 | Watson Marlow 520 | 2 |
| **7** | 0.20 | Watson Marlow 620Du (conn. 2) | 4 |
| **8** | 0.20 | *Watson Marlow 520* | *2* |

In the laboratory only seven pumps were available. Bin 8 was only occasionally filled with a small amount of water. Therefore after an experiment was completed the pump used for Bin 6 was connected to Bin 8 and the measurement was done.

The pumps connected to Bin 5, Bin 6 and Bin 7 did not have enough pump capacity to ensure an equal falling velocity of the water in comparison with Bins 1-4. Therefore the test would be stopped when Bin 5 started overflowing.

The Watson Marlow 620Du has two connections; one connection was used for Bin 5 and the second connection was used for Bin 7.

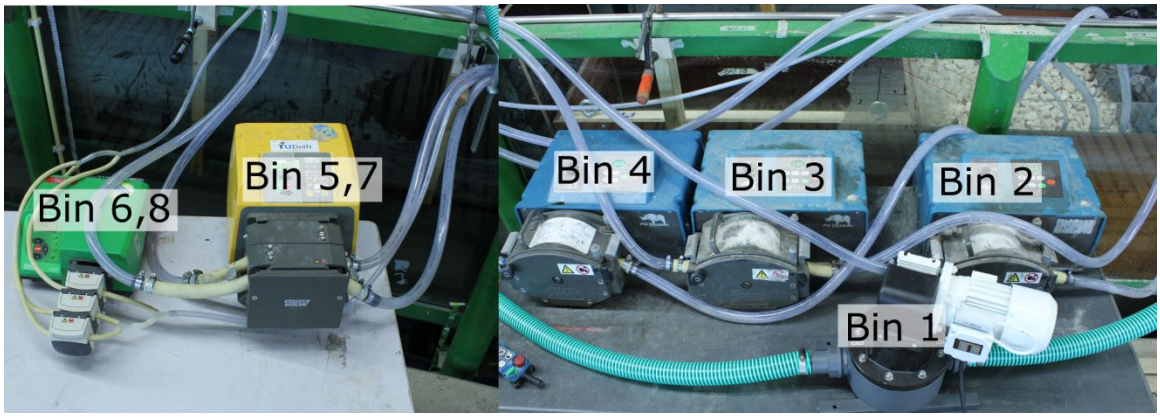


FIGURE 3.6-2: PUMPS USED DURING THE EXPERIMENTS

### 3.6.1.4 FLOATING TANKS

To collect the overtopped water floating tanks were constructed from whitewood and concrete form plywood. An overview of the available floating tanks is provided in Table 3-9. Table 3-10 shows which floating tanks were used per collection bin.

TABLE 3-9: OVERVIEW OF THE FLOATING TANKS

| Type | Quantity | Width [m] | Length [m] | Height [m] |
|---|---|---|---|---|
| **A** | 1 | 0.60 | 1.20 | 0.60 |
| **B** | 7 | 0.60 | 0.75 | 0.60 |
| **C** | 1 | 0.60 | 0.60 | 0.35 |
| **D** | 1 | 0.60 | 0.60 | 0.25 |

TABLE 3-10: OVERVIEW OF THE FLOATING TANKS PER BIN

| Bin | Floating tanks |
|---|---|
| **1** | 1 x Type A, 1 x Type B |
| **2** | 2 x Type B |
| **3** | 1 x Type B |
| **4** | 1 x Type B |
| **5** | 1 x Type B |
| **6** | 1 x Type B |
| **7** | 1 x Type C |
| **8** | 1 x Type D |

## 3.6.2 MEASURING INSTRUMENTS

### 3.6.2.1 WAVE GAUGES

In the flume two sets of three gauges were deployed. One set is put just before the breakwater, at a distance of approximately 0.90 m, while the other is placed quite close to the wave generator, at a distance of approximately 17 m from the breakwater.


FIGURE 3.6-3: WAVE GAUGES

This measuring instrument works as follows. Two conducting metal bars stick into the water. A generator induces a voltage difference between the two bars, as a result of which a current flows through the bars. At the water level the current can short-circuit from one bar to another, leading to less resistance and a higher current. The higher the water level, the less resistance due to the bars is experienced. A computer can consequently determine the water level from a measured voltage.

The water level measurement of the wave gauges is interpreted by a Matlab code. Appendix J describes this process.

#### 3.6.2.2 BALANCE

The weight of the floating tanks was measured using a balance that could be attached to the crane. A "Bosche KHW" balance was used.

FIGURE 3.6-4: BALANCE

### 3.6.3 EXPERIMENT INACCURACY

#### 3.6.3.1 MEASUREMENT INACCURACY

Whenever measuring equipment is involved no single quantity can be determined with absolute accuracy. Therefore for each measurement that was made an accuracy is given, either based on specifications of the equipment or on practical experience gained during the experiments, see Table 3-11.

TABLE 3-11: MEASUREMENT ACCURACIES

| **Measurement** | **Inaccuracy** |
|---|---|
| weight of the collection tanks | |
| *using the crane balance* | +/- 0.3 kg |
| *small volumes, using buckets and a small balance* | +/- 0.05 kg |
| wave height | - |
| wave period | - |
| experiment duration | +/- 5 s |
| water depth | +/- 1 mm |

Very small overtopped volumes were collected in a bucket and measured on a hand scale, leading to smaller measurement inaccuracies. Here the main inaccuracy was the water volume in the pumps and tubes. Also up to 50 ml of water could arrive in the bucket while no water had infiltrated in the corresponding bin. It is expected this is water from a foregoing test that very slowly ended up at the inlet point of the pump.

It was experienced that overtopped volumes lower than 100 ml of water could not be measured accurately. Moreover these values are too much disturbed by the influence of remaining water in the pumps and tubes.

### 3.6.3.2 BREAKWATER CONFIGURATION ACCURACY

Also for the construction of the scaled breakwater accuracies have to be taken into account. Just as in reality the armour stone sizes are rather large with respect to the armour layer. Therefore a survey method should be chosen as to how the top level of the different layers is defined. In these experiments an armour layer thickness of 12 cm was desired. Hereto the stones were placed in such a manner that the spherical foot staff was approximately at the 12 cm line. For more information about survey methods, refer to the Rock Manual section 9.9.8.

The core layer could be constructed within 2.5 mm inaccuracy. Because of the larger stones the armour layer was built within 5.0 mm inaccuracy.

No adaptations to the crest were made during the experiments. The inaccuracy for the crest freeboard is therefore determined only by the water depth: +/- 1 mm.

### 3.6.3.3 CONCLUSION

An indication of the measuring errors is presented in Figure 3.6-5. It can be concluded that errors in the breakwater profile lead to little uncertainty for the position of a measurement on the horizontal axis. The inaccuracies related to the measurements of the overtopped water can be neglected for larger overtopping volumes, since the error bars are so small that they are not even visible. For smaller overtopping volumes the relative error increases, so a larger scatter in the results is expected.

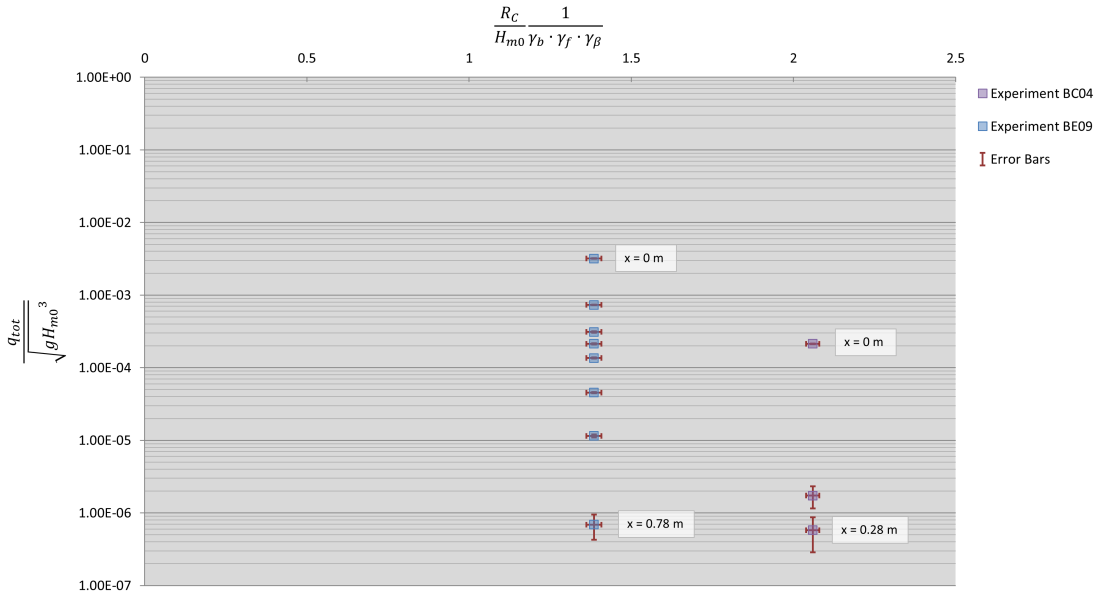


FIGURE 3.6-5: INDICATION OF THE MEASURING ERRORS

The error bars shown in Figure 3.6-5 indicate maximum and minimum values for the dimensionless numbers when all errors are combined.

*Note: these measuring errors do not contain possible effects of the backfill permeability and buffer capacity, as discussed in Chapter 6.*

## 3.7 EXPERIMENT OVERVIEW

During the experiment phase some modifications had to be made to the initial experiment programme. The wave generator sometimes was not able to deliver the desired wave height, other times overtopping discharges were so large tests had to be aborted. Despite these practical issues a good coverage of the area of interest was established with the experiments.

An overview of all parameters involved in the experiments is given in Table 3-12.

TABLE 3-12: OVERVIEW OF ALL PARAMETERS INVOLVED IN THE EXPERIMENTS

| Parameter | Symbol | Value | Unit |
|---|---|---|---|
| Breakwater configuration parameters | | | |
| slope angle | $\cot(\alpha)$ | 2 | [-] |
| armour freeboard | $A_C$ | 0.18 – 0.20 | [m] |
| crest width | $G_C$ | 0.18 | [-] |
| berm height | $d_B$ | -0.10 – 0.12 | [m] |
| berm width | $B$ | 0.00 – 0.60 | [m] |
| armour layer, nominal diameter | $D_{n50}$ | 0.062 | [m] |
| armour layer, grading | $D_{n85}/D_{n15}$ | 1.27 | [-] |
| armour layer, relative density | $\Delta$ | 1.678 | [-] |
| core, nominal diameter | $D_{n50}$ | 0.021 | [m] |
| core, relative density | $\Delta$ | 1.658 | [-] |
| Sea state parameters | | | |
| water level | $h$ | 0.50 – 0.52 | [m] |
| spectral wave height | $H_{m0}$ | 0.06 – 0.18 | [m] |
| wave period | $T_{m-1,0}$ | 1.18 – 3.06 | [s] |
| wave steepness | $s_{m-1,0}$ | 0.01 – 0.06 | [-] |
| number of waves | $N$ | 1000 | [-] |
| Wave-structure parameters | | | |
| Iribarren number | $\xi_{m-1,0}$ | 2.10 – 5.75 | [-] |
| total overtopping discharge | $q_{tot}$ | 9.17E-7 – 1.10E-3 | [m³/m/s] |

All wave conditions that were tested are plotted in Figure 3.7-1.

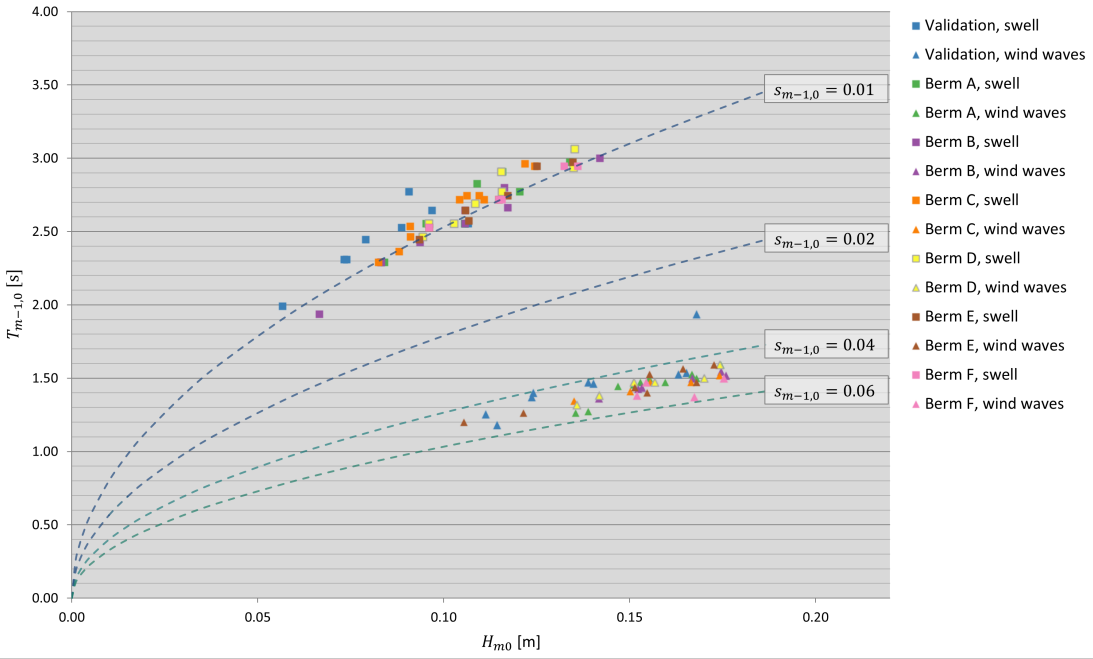


FIGURE 3.7-1: MEASURED WAVE CONDITIONS PER BREAKWATER CONFIGURATION

During the experiments the different berm configurations were marked “Berm A” to “Berm F”. The same notation is used in the graphs in Chapter 4 and Chapter 5.

Six breakwater configurations were tested, for an overview see Table 3-13. During the experiments two water depths were used. The berm height displayed in Table 3-13 is applicable for $h = 0.50$ m. For a water depth of $h = 0.52$ m $d_B$ is increased with 0.02 m.

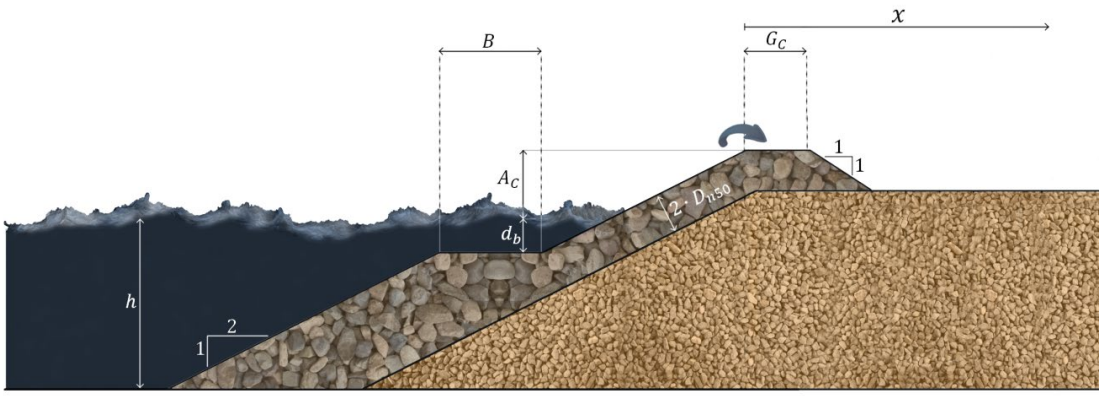


FIGURE 3.7-2: PARAMETERS OF THE BREAKWATER PROFILE

TABLE 3-13: BREAKWATER CONFIGURATIONS

| Configuration | Berm width, $B$ [m] | Berm height, $d_B$ [m] |
|---|---|---|
| Berm A | 0.3 | 0.1 |
| Berm B | 0.3 | 0 |
| Berm C | 0.3 | -0.1 |
| Berm D | 0.6 | 0.1 |
| Berm E | 0.6 | 0 |
| Berm F | 0.6 | -0.1 |

## 3.8 VALIDATION TESTS

At the start of the experiment phase results were compared with the findings of Lioutas (2010). In total 18 tests without a berm were run after which the total overtopping discharges were compared with Lioutas (2010), see Figure 3.8-1. It can be concluded that the total overtopping discharges of the validation tests are well comparable with Lioutas' experiments. Furthermore the Adjusted TAW method gives a good estimation of the overtopping discharge.

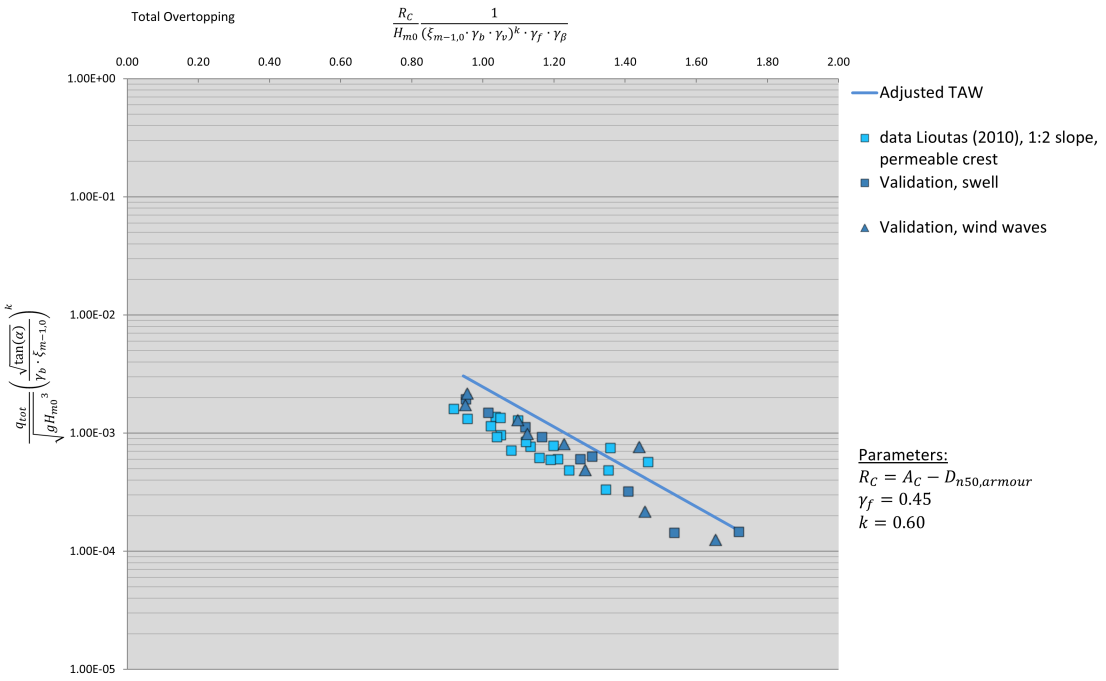


FIGURE 3.8-1: COMPARISON WITH DATA LIOUTAS (2010), $q_{tot}$

When the experiment phase was finished also the spatial distribution of the overtopping discharges in the two data sets was compared. When the overtopping directly behind the crest relative to the total overtopping is plotted against the total overtopping, a good indication is given about the amount of water that penetrates into the crest. It is expected that for large overtopping volumes the crest is fully saturated and more water will pass on to behind the crest.

In Figure 3.8-2 a comparison is drawn between the two data sets. Clearly both data sets follow the reasoning stated above; large overtopping volumes result in a higher fraction of $q_{bc}/q_{tot}$. While the nature of the trend is the same for both data sets, a very large difference exists in the position of the data clouds. In the current experiments more overtopping infiltrated into the core than in the experiments of Lioutas (2010). The supposed reason for this difference is the pump capacity used to drain the collection bins underneath the crest. In the current experiment setup the water falling velocity was equal for each collection bin, leading to presumably a larger drainage capacity in the crest, see also section 3.6.1.3.

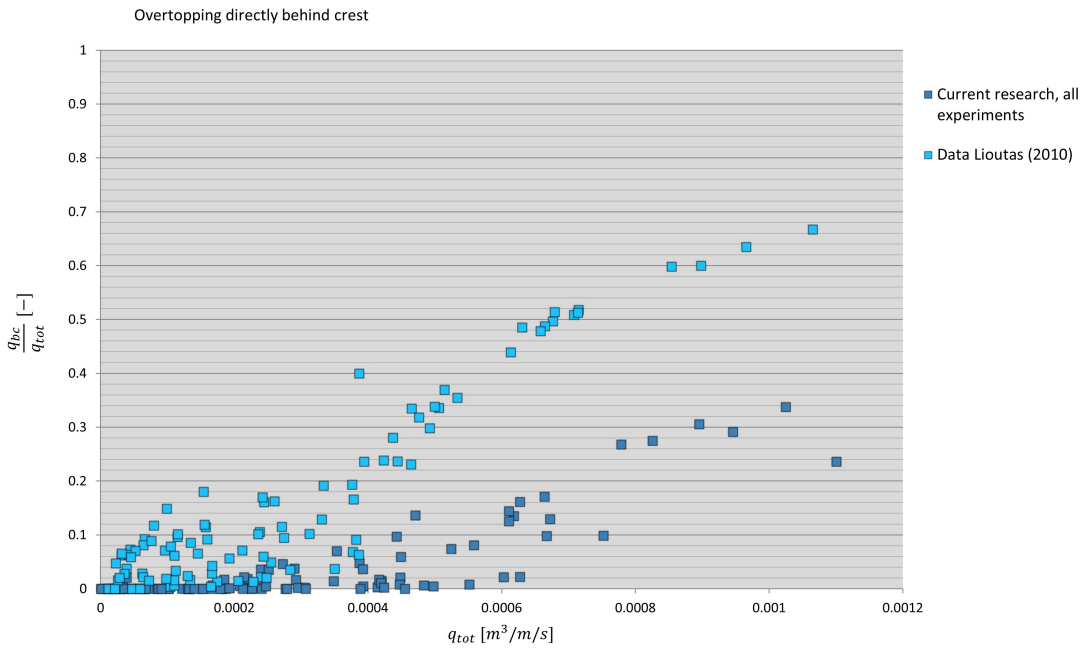


FIGURE 3.8-2: COMPARISON WITH DATA LIOUTAS (2010), $q_{bc}$

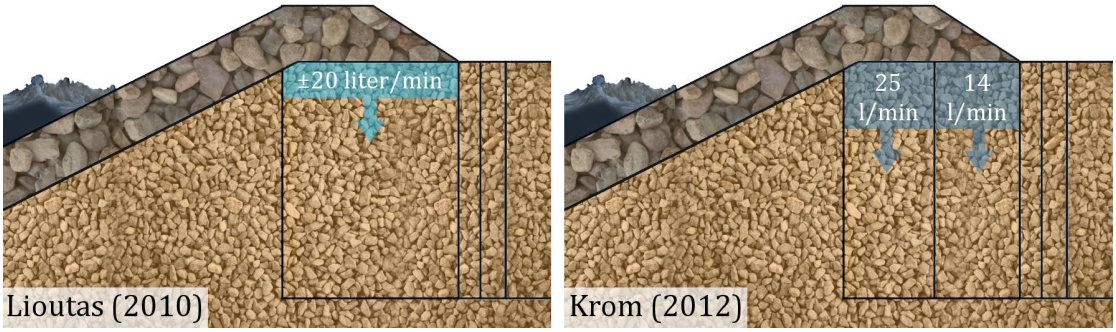


FIGURE 3.8-3: DIFFERENCE IN PUMP CAPACITIES

It can be concluded that for total overtopping discharges the two data sets are well comparable. For the spatial distribution of the overtopping discharges probably a large difference will exist.

# CHAPTER 4. TOTAL OVERTOPPING

The physical experiments as discussed in Chapter 3 resulted in a data set with overtopping discharges for 104 experiments. Different wave conditions and breakwater configurations were assessed. In this chapter the results will be interpreted for the total overtopping. First an introduction is given in section 4.1. Then existing prediction methods are compared with the experimental data in section 4.2. In section 4.3 a hypothesis is formed based on observations during the experiments and in section 4.2. A new expression to predict overtopping on breakwaters is presented in section 4.4. Finally section 4.5 provides conclusions that can be drawn from the analysis.

## 4.1 INTRODUCTION

### 4.1.1 METHOD OF COMPARISON

The test results of the data set are compared with the different prediction methods in a systematic manner.

Step 1 For each prediction method a graph is generated with such dimensionless axes that the prediction method can be represented with a smooth curve.

Step 2 For each experiment in the data set the two dimensionless numbers used in the prediction method are calculated. Each measurement is printed in the graph as one data point. Breakwater configuration and wave type are depicted in the graphs by marker shape and colour.

Step 3 The goodness-of-fit can be determined either visually or mathematically (see section 4.1.2). Much scatter in the data illustrates that the dimensionless numbers used in the prediction method do not account for every physical process that plays a role. Grouping in the data (for instance based on $\xi_{m-1,0}$, berm configuration or other parameters) can indicate in which direction improvement in the dimensionless numbers is possible.

Step 4 When no good fit with the data is established by the prediction method, the influence of the different parameters should be investigated. Ideally other dimensionless numbers can be formulated that lead to less scatter in the data.

### 4.1.2 GOODNESS-OF-FIT TEST

The goodness-of-fit of a prediction method with the experimental data can be determined either visually or mathematically. A mathematical method can provide benefits because it takes into account all considered experiment results and quantifies the goodness-of-fit. Still a mathematical method is not fully objective, a specific mathematical method can disregard a certain part of the data.

The test used in this research was selected based on two criteria; 1) relative errors rather than absolute errors should be used to determine the fit, and 2) large errors should be taken into account relatively stronger than small errors.

Experiments related to total overtopping commonly are assessed by plotting the dimensionless overtopping discharge on a logarithmic vertical axis. The vertical distance

between a data point and the prediction method then indicates the error that is made for that specific experiment. When absolute errors were to be calculated for this logarithmic vertical axis, the goodness-of-fit would primarily be determined by how good the prediction method predicts the large overtopping discharges. In the current research however overtopping discharges were examined ranging between roughly $10^{-6}$ m³/m/s and $10^{-3}$ m³/m/s (model scale). This whole range of data is relevant to design practice; it is desired to include all data in the goodness-of-fit method equally.

The chosen goodness-of-fit test is printed in Equation 4.1-1. It is a variant to the commonly used mean squared error. By calculating the difference between the measured and predicted logarithmic overtopping discharge, criterion 1 is fulfilled. The difference is squared, so that also criterion 2 is met.

$$G_{fit} = \frac{1}{n}\sum_{j=1}^{n}\left(\log(q_{meas,j}) - \log(q_{calc,j})\right)^2 \qquad \textit{Equation 4.1-1}$$

If all measured data falls exactly on the prediction method curve, a perfect fit is achieved and $G_{fit}$=0. A large value of $G_{fit}$ indicates the experimental data is not accurately predicted by the prediction method.

## 4.2 COMPARISON WITH EXISTING PREDICTION METHODS

### 4.2.1 INTRODUCTION

A variety of prediction methods exists to predict the amount of total overtopping for a specific combination of breakwater configuration and sea state. The most applicable methods discussed in section 2.2 will be compared with the experiment results. None of the existing methods leads to a good fit with the data. Therefore a new prediction method is proposed in section 4.4.

### 4.2.2 COMPARISON WITH THE TAW PREDICTION METHOD

In design practice of breakwaters the TAW formulae are often used. The prediction method is split into two formulae, one for breaking conditions and one for non-breaking conditions. The equation for breaking waves ($\gamma_b\xi_{m-1,0} \lesssim 2.0$) is reprinted in Equation 4.4-1.

$$\frac{q_{tot}}{\sqrt{g \cdot H_{m0}^3}} = \frac{\mathrm{A}}{\sqrt{\tan(\alpha)}} \cdot \gamma_b \cdot \xi_{m-1,0} \cdot \exp\left(-\mathrm{B} \cdot \frac{R_C}{H_{m0}} \frac{1}{\xi_{m-1,0} \cdot \gamma_b \cdot \gamma_f \cdot \gamma_\beta \cdot \gamma_v}\right) \qquad \textit{Equation 4.2-1}$$

The equation for non-breaking waves is reprinted in Equation 4.4-2. The overtopping discharge increases with increasing $\xi_{m-1,0}$ in the expression for breaking waves; this increase is stopped as soon as the expression for non-breaking waves is reached.

$$\frac{q_{tot}}{\sqrt{g \cdot H_{m0}^3}} = \mathrm{C} \cdot \exp\left(-\mathrm{D} \cdot \frac{R_C}{H_{m0}} \frac{1}{\gamma_f \cdot \gamma_\beta}\right) \qquad \textit{Equation 4.2-2}$$

The TAW prediction method was introduced after experiments on impermeable structures. For permeable structures it is mentioned the permeable crest should not be taken into account. In the following graphs the classic definition of crest freeboard is used, $R_C = A_C$. Hereby the scatter in the experimental data can be assessed.

Experiments with breaking waves (according to the criterion of the TAW formulae) are depicted in Figure 4.2-1.

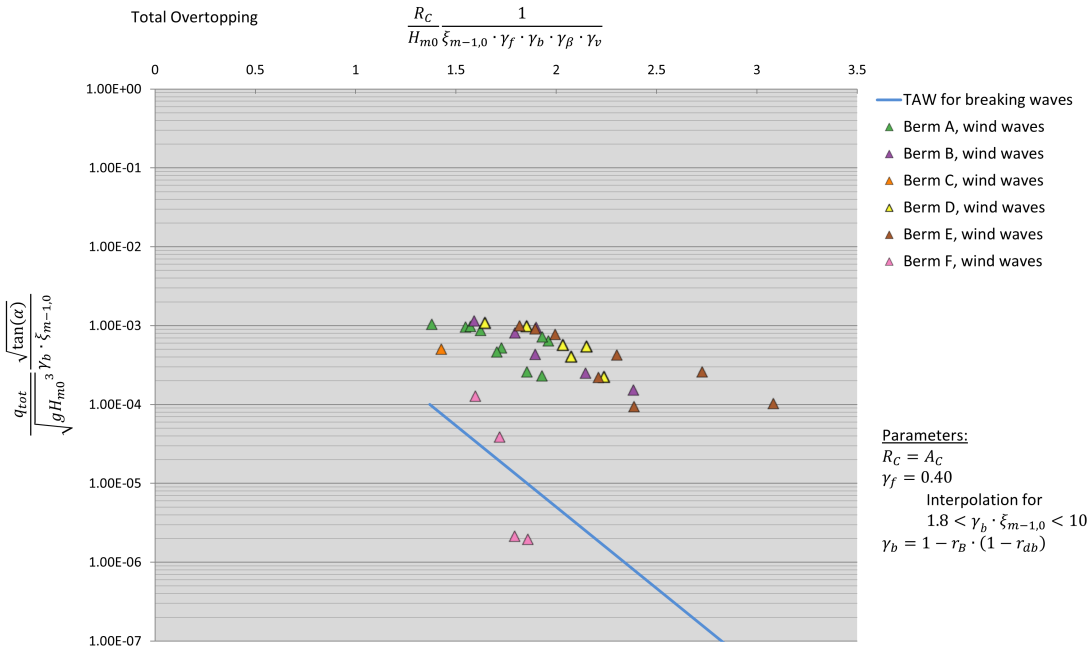


FIGURE 4.2-1: COMPARISON WITH TAW FOR BREAKING CONDITIONS

It can be concluded that for breaking conditions the chosen dimensionless numbers lead to considerable scatter in the experimental data. A trend per berm configuration can clearly be observed. This indicates the reduction factor that should account for the berm is not applicable to the permeable berms used in the current research.

Moreover a large part of the experimental data lies well above the prediction method. It is expected the main cause for this is the definition of the crest freeboard. A reduction should be made to account for the permeability of the crest.

The remaining experiments from the data set have non-breaking conditions. These are compared with the prediction method (Equation 4.2-2) in Figure 4.2-2.

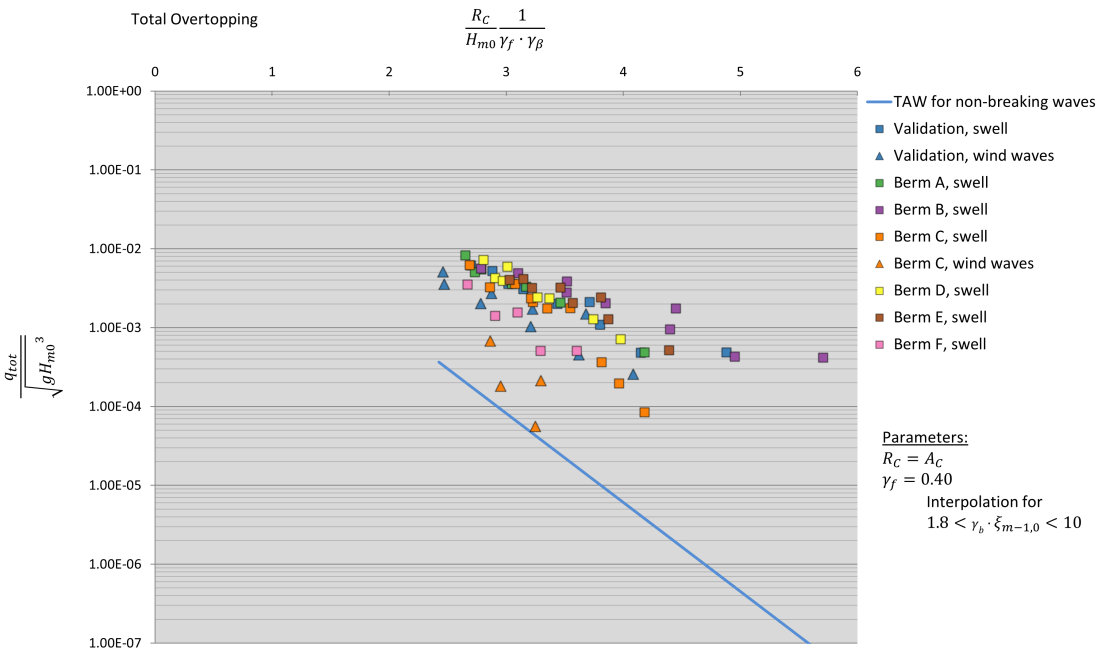


FIGURE 4.2-2: COMPARISON WITH TAW FOR NON-BREAKING CONDITIONS

For non-breaking conditions the same two phenomena can be observed. Data is grouped based on breakwater configuration. Apparently the berm does have a reducing effect, although the TAW formula for non-breaking waves does not contain a $\gamma_b$ reduction term. Overtopping discharges are underestimated by an order 10 on average, which is presumably caused by the crest freeboard definition.

To combine both graphs the dimensional overtopping discharges are plotted in Figure 4.2-3.

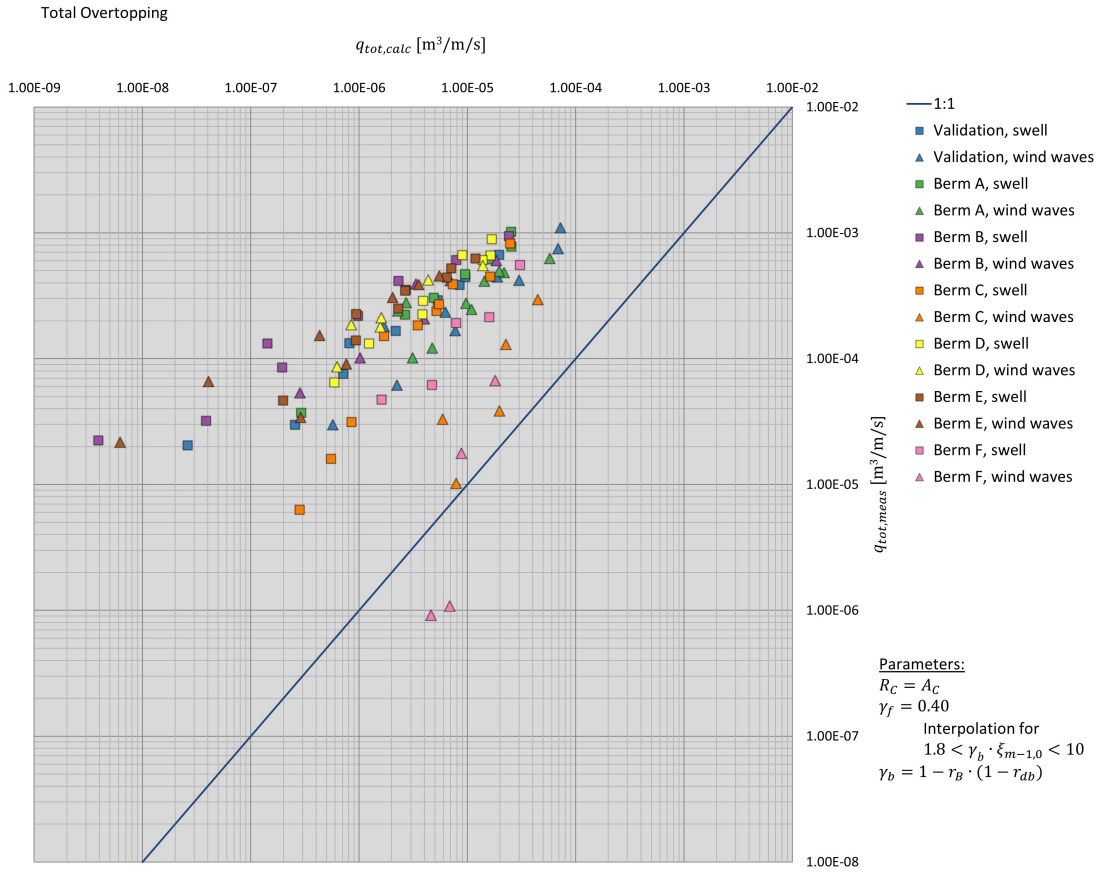


FIGURE 4.2-3: COMPARISON WITH TAW

It is clear that a reduction should be made to the crest freeboard, to make sure the average of the data falls well in line with the prediction method. This does however not solve the problem for the large amount of scatter.

For this method the goodness-of-fit $G_{fit}$=2.07. This is a rather high value, indicating that the prediction method predicts scarcely any experiments properly. A better fit will be obtained when the crest freeboard is lowered. More information on the goodness-of-fit test that is used in this thesis can be found in section 4.1.2.

### 4.2.3 COMPARISON WITH THE EUROTOP FORMULA

In 2007 the EurOtop manual was introduced as a replacement for among others the TAW manual. The EurOtop manual separately covers permeable structures whereas the TAW manual formally is only applicable to impermeable structures (sloping dikes). For the average overtopping on permeable structures the EurOtop manual suggests using the TAW expression for non-breaking waves, since breakwaters commonly are quite steep structures and theoretically only little wave breaking will occur. See Equation 4.2-3.

$$\frac{q_{tot}}{\sqrt{g \cdot H_{m0}^3}} = \mathrm{C} \cdot \exp\left(-\mathrm{D} \cdot \frac{R_C}{H_{m0}} \frac{1}{\gamma_f \cdot \gamma_\beta}\right)$$

*Equation 4.2-3*

According to EurOtop the permeable armour layer should not be taken into account for the overtopping calculation; $R_C = A_C - 2D_{n50,armour}$. Furthermore in the EurOtop manual two definitions for the roughness factor are introduced. Distinction is made between $\gamma_f$, which was experimentally found for $\gamma_b \cdot \xi_{m-1,0} < 1.8$, and $\gamma_{f,surging}$, which is an interpolation between $\gamma_f$ and 1 for $\gamma_b \cdot \xi_{m-1,0}$ between 1.8 and 10. It was argued longer waves encounter less friction from the armour layer than steep waves. In the EurOtop manual $\gamma_f$ is used in all expressions except the maximum for run-up.

Using $\gamma_f = 0.40$ (as is recommended for two layers of rock on a permeable core) and $R_C = A_C - 2D_{n50,armour}$ (neglecting any hydraulic resistance due to the armour layer) leads to Figure 4.2-4.

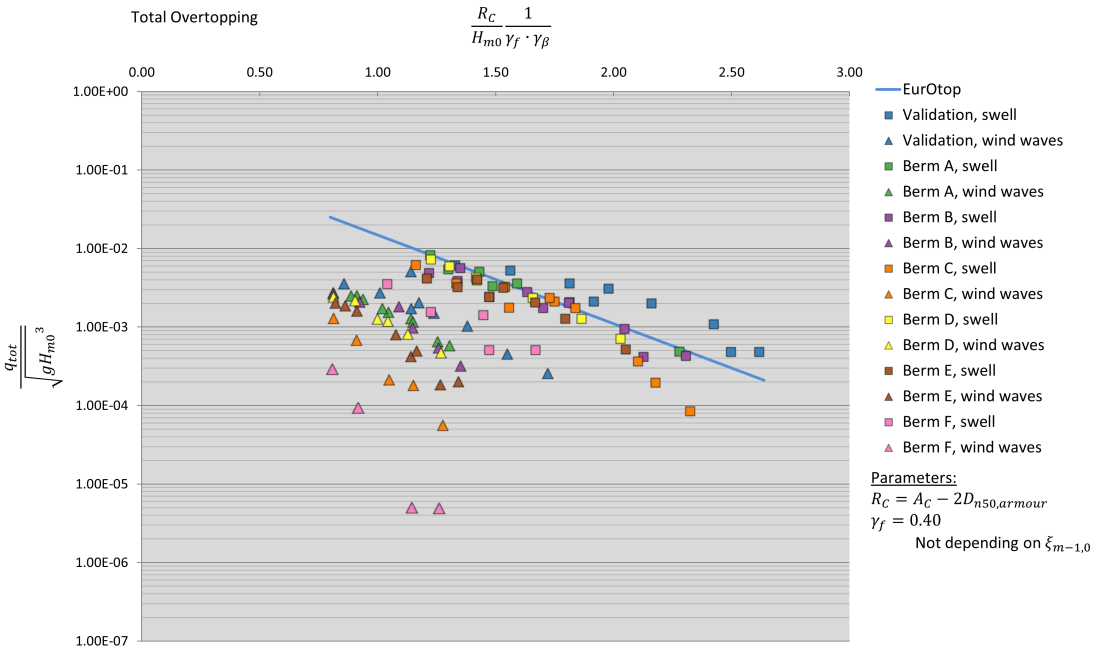


FIGURE 4.2-4: COMPARISON WITH EUROTOP

The prediction method for permeable structures in the EurOtop manual does not include any reduction factor accounting for a berm. In Figure 4.2-4 however it is clearly observable that there is an influence. For wind waves this influence is more pronounced than for swell.

The different types of waves can also clearly be distinguished. Although the formula assumes there are non-breaking conditions for all permeable structures, the wave steepness does influence the overtopping. During the conduction of the experiments it was observed that especially for wind waves the berm leads to breaking before the waves actually reached the main slope, thereby reducing overtopping.

A large amount of spreading exists around the prediction method. The method overestimates the majority of experiments.

For this method the goodness-of-fit $G_{fit}$=0.79. This indicates a better fit is obtained than with the TAW formulae. More information on the goodness-of-fit test that is used in this thesis can be found in section 4.1.2.

### 4.2.4 COMPARISON WITH THE "ADJUSTED TAW FORMULA"

Lioutas (2010) performed experiments using a similar experiment setup as the current research. He found that the TAW formula for non-breaking waves should be more dependent on the Iribarren number – just as the previous two analyses indicate. To overcome this problem a suggestion was made to interpolate between the two TAW formulae, since the expression for breaking waves does include the Iribarren number. The suggested expression is reprinted in Equation 4.2-4.

The factor $k$ determines which of the two formulae dominates. For $k = 0$ the Adjusted TAW expression is equal to the TAW formula for non-breaking waves. For $k = 1$ it is equal to the TAW formula for breaking waves.

$$\frac{q_{tot}}{\sqrt{g \cdot H_{m0}^3}} = (0.2 - 0.133 \cdot k)\left(\frac{\gamma_b \cdot \xi_{m-1,0}}{\sqrt{\tan(\alpha)}}\right)^k \cdot \exp\left[-(2.6 + 2.15 \cdot k) \cdot \frac{R_C}{H_{m0}} \frac{1}{(\xi_{m-1,0} \cdot \gamma_b \cdot \gamma_v)^k \cdot \gamma_f \cdot \gamma_\beta \cdot \gamma_c}\right] \qquad \textit{Equation 4.2-4}$$

Similar to the current experiments Lioutas found that the TAW prediction method underestimates the total overtopping discharge. Besides suggesting a new prediction method Lioutas therefore made a recommendation regarding the freeboard definition; $R_C = A_C - 0.9 \cdot D_{n50,armour}$. This definition roughly lies between the definitions of TAW and EurOtop. The prediction method is compared with the experimental data in Figure 4.2-5.

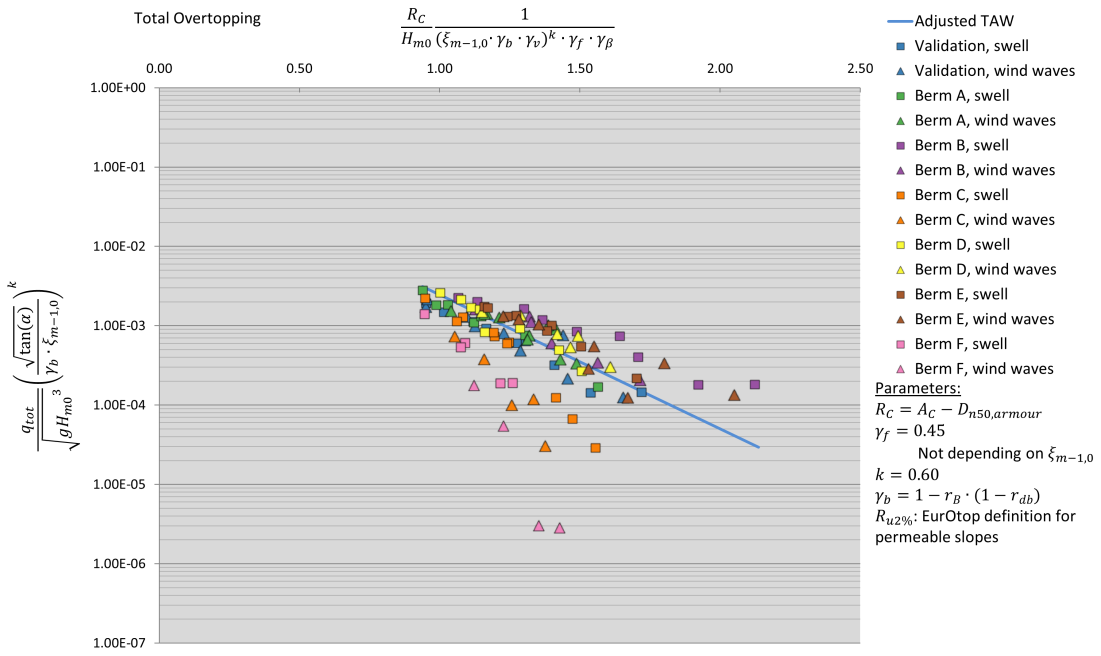


FIGURE 4.2-5: COMPARISON WITH ADJUSTED TAW, $\gamma_f$=0.45

Lioutas chose to use $\gamma_f = 0.45$ for his experiments whereas the EurOtop manual recommends $\gamma_f = 0.40$ for rocks with layer thickness $2D_{n50,armour}$ on top of a permeable core. Using $\gamma_f = 0.40$ results in a better fit with the validation test results (see Figure 4.2-6).

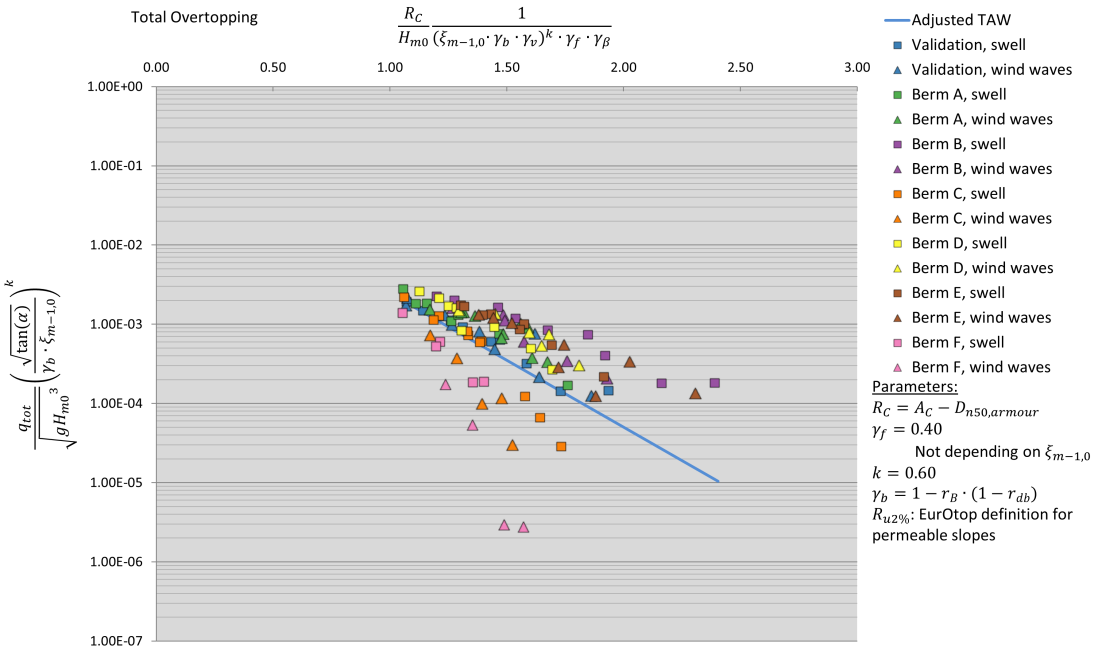


FIGURE 4.2-6: COMPARISON WITH ADJUSTED TAW, $\gamma_f$=0.40

The prediction method of Lioutas (2010) eliminates scatter based on wave steepness; the experiments per breakwater configuration now form a clear line. Furthermore the new definition for crest freeboard provides a good fit for the validation tests. For the breakwater configurations with a berm quite a good fit is established but still a clear grouping can be observed. For this method the goodness-of-fit $G_{fit}$=0.39.

## DEFINITION OF THE DIMENSIONLESS CREST FREEBOARD

To make a mathematically correct combination of both TAW formulae Lioutas raised $\gamma_b$ and $\gamma_v$ to the power $k$, while he applied neither a berm nor a vertical wall. Since in the current experiments berms were tested it can be concluded whether the factor $k$ indeed has a positive effect and leads to less scatter in the data. To investigate whether $\gamma_b$ or ${\gamma_b}^k$ should be used in the dimensionless crest freeboard, Figure 4.2-7 shows the results for dimensionless crest freeboard $R_C^* = \frac{R_C}{H_{m0}} \frac{1}{{\xi_{m-1,0}}^k \cdot \gamma_b \cdot \gamma_f \cdot \gamma_\beta \cdot \gamma_v}$.

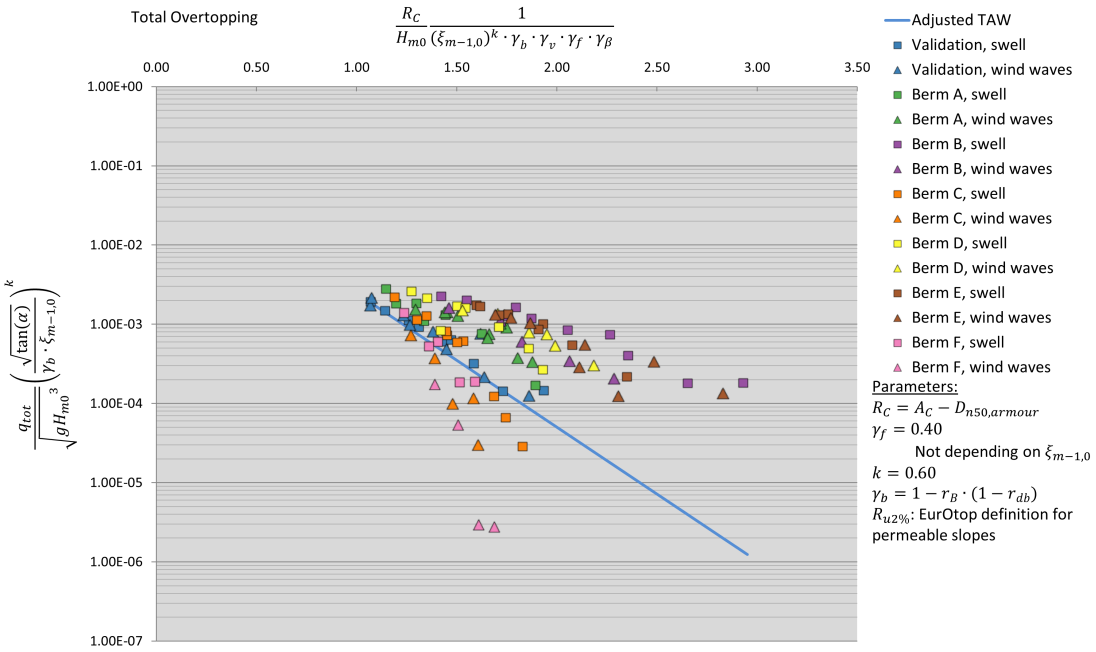


FIGURE 4.2-7: COMPARISON WITH ADJUSTED TAW, ALTERNATIVE $R_C^*$

For $R_C^* = \frac{R_C}{H_{m0}} \frac{1}{\xi_{m-1,0}{}^k \cdot \gamma_b \cdot \gamma_f \cdot \gamma_\beta \cdot \gamma_v}$ more reduction due to the berm is taken into account. For berms at SWL and below SWL this has a negative effect; the calculated effect is larger than what is actually measured. For berms above SWL a slightly better result is obtained while still the calculation method leads to too high overtopping discharges for these berms. It can be concluded that raising $\gamma_b$ and $\gamma_v$ to the power $k$ leads to less spreading in the data. Still a clear grouping can be discerned however.

## 4.3 HYPOTHESIS

In the previous section it was shown that existing prediction methods do not accurately predict the measured total overtopping discharges. Based on observations done during the experiments and in the comparison with existing prediction methods, it is expected a prediction method can be proposed that results in smaller scatter than was observed for existing prediction methods. The influence of each parameter is treated in a separate subsection.

### 4.3.1 CREST FREEBOARD DEFINITION

Existing literature either takes into account the full thickness of the permeable crest or disregards it completely. Based on observations during the conduction of the experiments and in the comparisons with existing prediction methods, it is expected a golden mean should be found. A significant part of the total overtopping propagates through the crest, but still the crest is an obstacle that leads to some resistance.

As Lioutas et al. (2012) illustrated reduction of the armour freeboard by a certain part of the armour layer thickness can lead to good results.

Based on the current experiments – where only permeable crest have been tested – theoretically it cannot be concluded that the crest freeboard definition should be adjusted. That would require additional experiments where solely the crest freeboard definition is investigated. Achieving a good fit with the experimental data however can at least suggest that a specific crest freeboard definition is applicable to the current experiments.

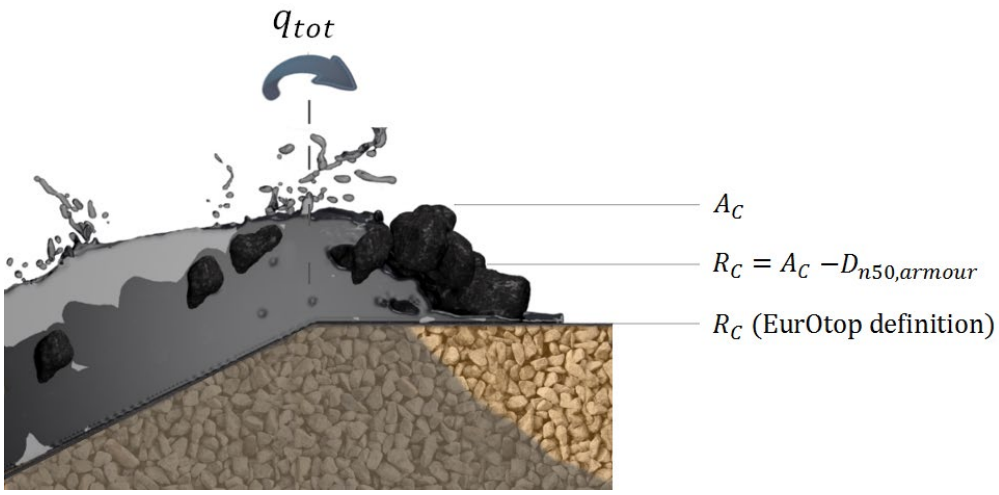


FIGURE 4.3-1: IMPRESSION OF OVERTOPPING FOR A PERMEABLE CREST

### 4.3.2 INFLUENCE OF $\xi_{m-1,0}$ ON $\gamma_f$

Both the TAW and the EurOtop prediction method lead to significant grouping of the data, based on the breaker parameter. One way to overcome this problem is to make a combination between the two TAW formulae. This leads to a very comprehensive expression and also introduces at least one new parameter that defines how the interpolation should be made. Lioutas (2010) used this approach to get a good fit with his data set.

It is expected that a more concise prediction method can be proposed that has the same effect as the approach stated above. The reduction factor to account for slope roughness, $\gamma_f$, was initially found to be applicable for $1.8 < \gamma_b \cdot \xi_{m-1,0}$. The TAW manual for instance recommends to interpolate $\gamma_f$ between $1.8 < \gamma_b \cdot \xi_{m-1,0} < 10$, see section 2.2.2.4. The physical meaning behind this interpolation is that for small Iribarren numbers the steep wave front leads to a violent clash with the armour layer, thus dissipating wave energy. High Iribarren numbers on the other hand represent waves that approach the structure gentler, leading to less energy dissipation. For very high values of the Iribarren number no slope roughness is encountered by the waves.

The following observations were done during the conduction of the experiments. In the wave breaking process of high wind waves the crest approaches the breakwater at quite a steep – almost perpendicular – angle. Consequently very turbulent behaviour takes place, leading to air entrainment and energy dissipation. High swell waves on the other hand also transform when moving towards the breakwater – forming steeper wave fronts – but here the wave crests approach the armour slope at a much smaller angle. Less turbulent behaviour was observed and less wave energy is dissipated.

In Figure 4.3-2 the observed differences in the experiments are indicated. Wind waves ($\xi_{m-1,0} \approx 2.4$ for a 1:2 slope) run up the slope while experiencing a lot of resistance, which results in the formation of air-water mixture. Apparently the friction between swell waves ($\xi_{m-1,0} \approx 5.0$ for a 1:2 slope) and the armour slope is smaller. Less air-water mixture was observed.

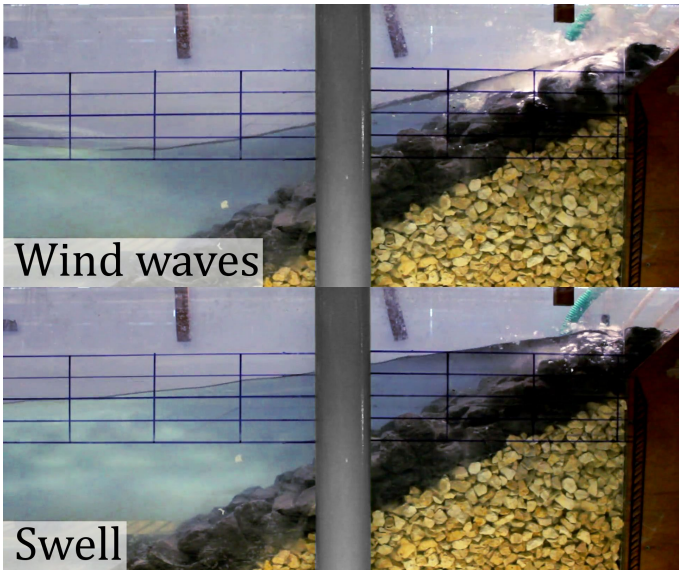


Wind wave breaking leads to much air entrainment

Swell running up the slope leads to less air entrainment.

FIGURE 4.3-2: INFLUENCE OF $\xi_{m-1,0}$ ON $\gamma_f$

### 4.3.3 FUNCTION OF A BERM

Within the TAW formulae the $\gamma_b$ term is supposed to account for the presence of a berm. When this reduction factor is applied the current data set is still grouped per breakwater configuration. For berms above SWL the overtopping is reduced more than for berms at SWL; in the TAW formulae this is exactly the opposite. It can be concluded that the TAW reduction factor does not accurately account for the permeable berm.

## GENERAL

Whenever waves are confronted with a decrease in water depth the wave energy gets redistributed. At a gently sloping beach the decrease in water depth is imposed slowly and shoaling takes place. The shoaling process can be described as follows. As waves move towards the coast, the water depth decreases gradually and so does the wave celerity. Wave energy however is conserved and gets concentrated in the available water depth, resulting in larger wave heights. Equation 4.3-1 shows the conservation of energy for two different cross sections. The shoaling factor – the ratio between the two subsequent wave amplitudes – is given by Equation 4.3-2. Larger waves in combination with a decreased water depth lead to wave breaking. For a more extensive discussion of shoaling refer to Holthuijsen (2007).

$$\frac{1}{2}\rho_w g a_1^2 c_{g,1} = \frac{1}{2}\rho_w g a_2^2 c_{g,2} \qquad \textit{Equation 4.3-1}$$

$$K_{sh} = \sqrt{c_{g,1}/c_{g,2}} \qquad \textit{Equation 4.3-2}$$

where:

| | | | |
|---|---|---|---|
| $a_1, a_2$ | = | wave amplitudes in cross-section 1 and 2 respectively | [m] |
| $c_{g,1}, c_{g,2}$ | = | wave group celerity in cross-section 1 and 2 respectively | [m/s] |
| $g$ | = | gravitational acceleration | [m/s$^2$] |
| $K_{sh}$ | = | shoaling factor, $a_2/a_1$ | [-] |
| $\rho_w$ | = | fluid density | [kg/m$^3$] |

Waves encounter the same decrease in water depth when approaching a breakwater, albeit less gradually. It can therefore be expected that part of the wave energy will reflect on the breakwater, but that still a large part gets concentrated in the remaining water depth.

When a berm is applied the location where wave steepening and wave breaking occurs moves offshore. Depending on the berm elevation and width energy dissipation will take place. Consequently the main slope – between the berm and the crest – is confronted with less severe wave attack and therefore also less overtopping will take place.

## INFLUENCE OF THE PERMEABILITY

In a fully impermeable berm no wave energy can protrude. Wave energy is either reflected or concentrated in the remaining water depth. For a permeable berm however waves can to a certain degree propagate through the berm. Therefore it can be expected less wave energy will reflect, and less concentration of wave energy takes place over the available water depth. Therefore the permeable berms can be expected to lead to less wave breaking before the main slope is reached than an impermeable berm. When it is assumed that the mechanism that causes a berm to have a reducing effect on overtopping is that waves are broken before the main slope is reached, permeable berms can be expected to have a lesser reducing effect than impermeable berms.

Furthermore the rough rubble mound material with which permeable berms generally are constructed leads to a very irregular surface. For flows with small water depths very turbulent behaviour and much energy dissipation can be expected. Especially for berms above SWL this can come into play.

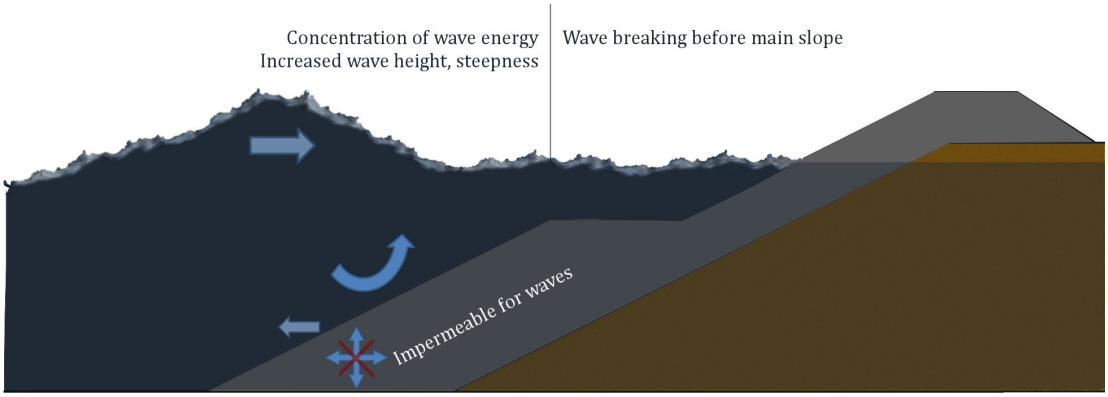


FIGURE 4.3-3: FUNCTION OF AN IMPERMEABLE BERM BELOW SWL

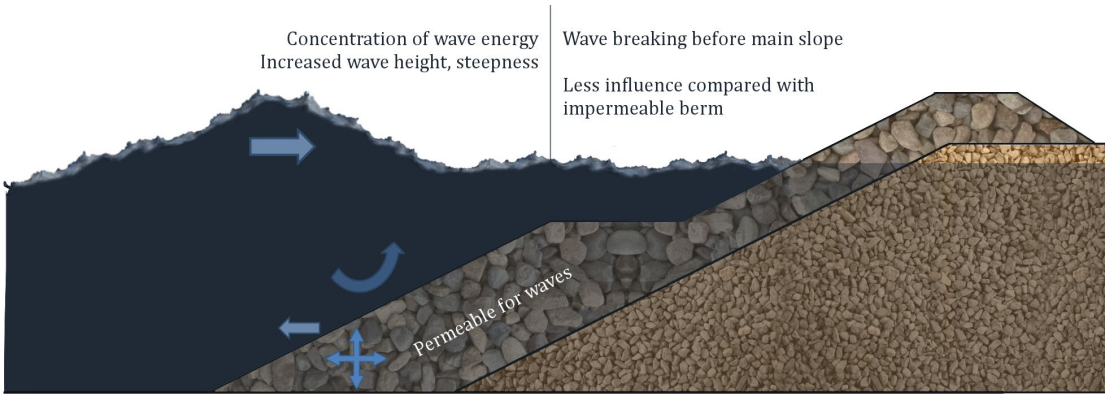


FIGURE 4.3-4: FUNCTION OF A PERMEABLE BERM BELOW SWL

During the conduction of the experiments a clear image was formed as to the manner in which a permeable berm reduces the amount of overtopping. A difference in behaviour was observed for on the one hand berms below and at SWL, and on the other hand berms above SWL. They will be treated separately below.

### PERMEABLE BERMS BELOW SWL

In the conducted experiment permeable berms below SWL were found to lead to reduction of overtopping, for both wind waves and swell conditions. As the waves are confronted with the berm, the wave front becomes steeper. Inside a wave the propagation velocity of the crest part is larger than the propagation velocity of the troughs. The difference in propagation velocity results in steepening of the wave front and eventually breaking behaviour is induced. For shallow water the propagation velocity of disturbances can be described with $c \approx \sqrt{gh}$, where $c$ is the propagation velocity and $h$ is the local water depth. Plunging breaking was demonstrated by the wind waves of the experiment set, see Figure 4.3-5.

FIGURE 4.3-5: BREAKING WIND WAVES ON A PERMEABLE BERM BELOW SWL (BERM D)

For most waves in swell conditions no breaking behaviour was observed. However some of the largest waves – being most important for wave overtopping – showed significant steepening of the wave front. This leads to a violent clash with the main slope and energy dissipation. See Figure 4.3-6.

FIGURE 4.3-6: SWELL ON A PERMEABLE BERM BELOW SWL (BERM D)

A more ideal prediction method should account for the reduction of overtopping as a result of a permeable berm. Based on the observations the reduction should be made for both wind waves and swell conditions. Compared with an impermeable berm however less reduction of overtopping is expected since wave propagation is to a certain degree still possible within the berm. The permeable berm does not block the wave propagation as strongly as an impermeable berm does and can be expected to lead to less wave breaking before the main slope is reached.

### PERMEABLE BERMS ABOVE SWL

During the experiments it was observed that berms above SWL act more as an extended crest than as a berm. The classic function of a berm is to dissipate wave energy before the waves break on the main slope. However, for berms above SWL the largest part of the wave breaking occurs on the slope in front of the berm. This observation strongly contrasts with the way influence of these berms is accounted for in the TAW prediction method.

Besides being more permeable the tested berms also have a more irregular, rougher surface than impermeable berms. Where for impermeable structures the run-up over the berm can travel onward with almost no hindrance, the run-up for permeable structures faces significant energy dissipation.

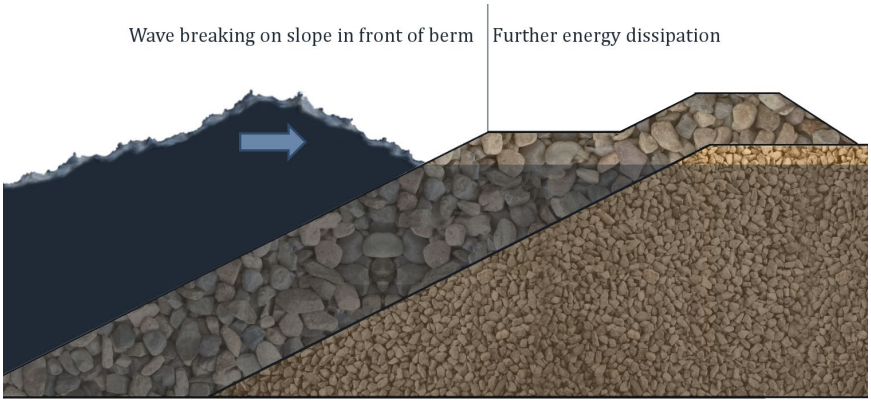


FIGURE 4.3-7: FUNCTION OF A PERMEABLE BERM ABOVE SWL

Wind waves in particular break fully on the slope in front of the berm. Only a marginal part of the wave travels onward and moves through the crest, see Figure 4.3-8. No complete sheets of water flowed over the berm, but rather air-water mixture that resulted from the breaking process.

FIGURE 4.3-8: BREAKING WIND WAVES ON A PERMEABLE BERM ABOVE SWL (BERM F)

For swell waves it was observed waves were able to propagate through the permeable berm. At times large sheets of water flowed over the berm, and thereafter through the crest, whereas for wind waves it was mainly air-water mixture that propagates over the berm. See also Figure 4.3-9.

FIGURE 4.3-9: SWELL ON A PERMEABLE BERM ABOVE SWL (BERM F)

To conclude the overtopping reducing effect of a permeable berm above SWL is expected to be stronger for wind waves than for swell conditions. Furthermore compared with a berm at or below SWL, a berm above SWL was observed to lead to more overtopping reduction for both swell and wind waves. This is quite remarkable since the TAW method accounts for less reduction for berms above SWL. Primarily the increased roughness of the berm is expected to be the cause for this difference.

## 4.4 PROPOSED EXPRESSION

None of the discussed prediction methods leads to a good fit with the experimental data. The best fit is obtained by using the Adjusted TAW formula that Lioutas et al. (2012) proposed but still a clear grouping can be observed per breakwater configuration.

Starting with very simple dimensionless axes the effect of each new parameter can be properly investigated. The EurOtop prediction for permeable slopes is taken as a starting point, see Figure 4.4-1. Here the crest freeboard is defined as $R_C = A_C - D_{n50,armour}$ since from earlier comparisons it was already shown this leads to better correlation with the measured data.

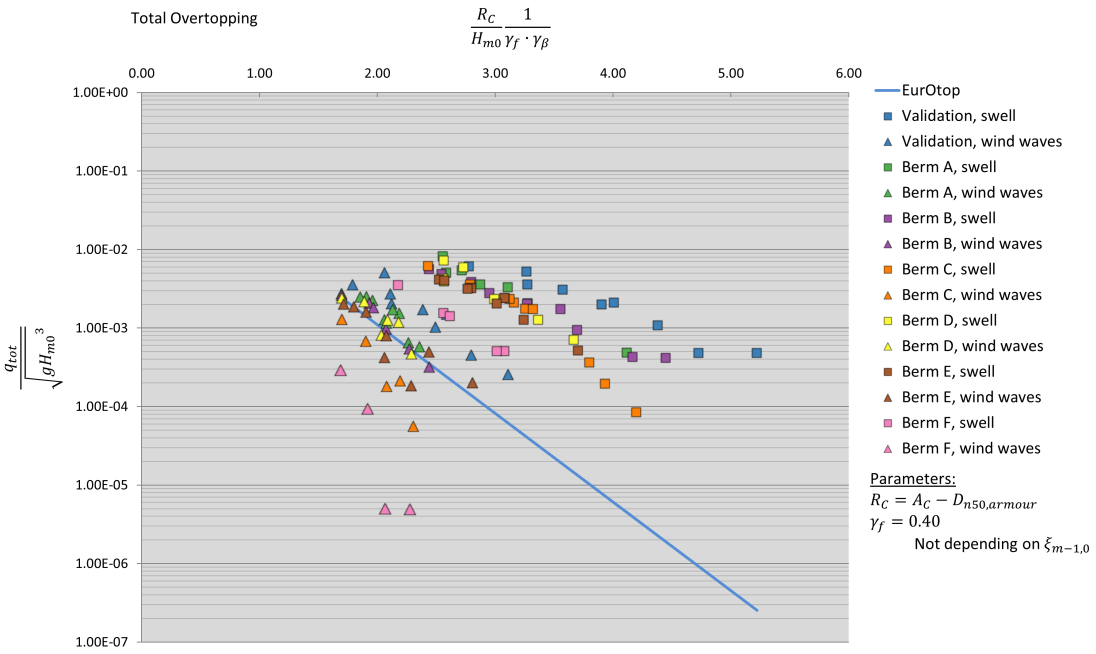


FIGURE 4.4-1: COMPARISON WITH EUROTOP

### 4.4.1 INFLUENCE OF THE BREAKER PARAMETER

Just as in the analysis of Lioutas (2010), also here a larger dependency of the dimensionless overtopping on the Iribarren number is needed. One way to achieve this is to make some kind of combination between the two TAW formulae - just as Lioutas did – thereby inserting the Iribarren number in the dimensionless crest freeboard. Another way to (implicitly) take the Iribarren number into account is to increase the roughness factor, $\gamma_f$, based on the Iribarren number. The TAW manual for instance recommends to interpolate $\gamma_f$ between $1.8 < \gamma_b \cdot \xi_{m-1,0} < 10$, see section 2.2.2.4.

In the current state the EurOtop formula does not reduce the effect of roughness for higher Iribarren numbers. When $\gamma_{f,surging}$ is used instead of $\gamma_f$, already smaller scatter of the data can be observed, see Figure 4.4-2. The expression for $\gamma_{f,surging}$ as recommended by TAW and EurOtop is printed in Equation 4.4-1.

$$\gamma_{f,surging} = \begin{cases} \gamma_f & \text{for } \gamma_b \cdot \xi_{m-1,0} < 1.8 \\ \gamma_f + \left(\gamma_b \cdot \xi_{m-1,0} - 1.8\right) \cdot \dfrac{1-\gamma_f}{8.2} & \text{for } 1.8 < \gamma_b \cdot \xi_{m-1,0} < 10 \\ 1.0 & \text{for } \gamma_b \cdot \xi_{m-1,0} > 10 \end{cases} \qquad \textit{Equation 4.4-1}$$

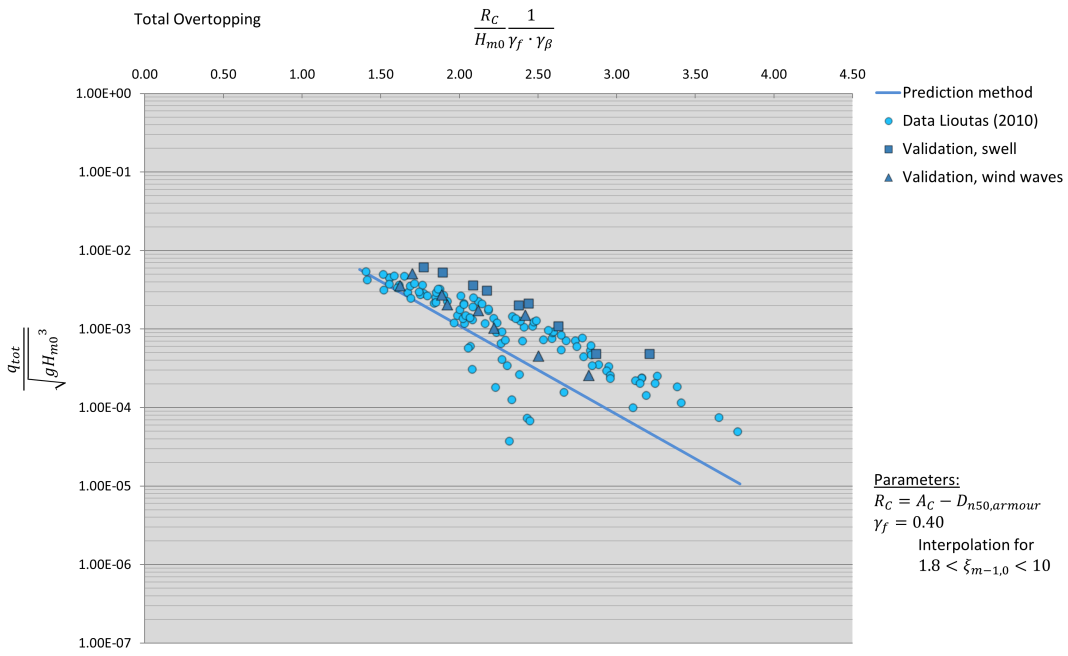


FIGURE 4.4-2: COMPARISON WITH ADAPTED PREDICTION METHOD

Still the data for wind waves and swell does not fall in line. However when the interpolation for $\gamma_{f,surging}$ is changed, the validation test results follow a clear line. Also the data of Lioutas (2010) shows less scatter. The adjustment made to the upper limit of $\xi_{m-1,0}$ is visualized in Figure 4.4-3. Using Equation 4.4-2 leads to Figure 4.4-4.

$$\gamma_{f,surging} = \begin{cases} \gamma_f & \text{for } \xi_{m-1,0} < 1.8 \\ \gamma_f + (\xi_{m-1,0} - 1.8) \cdot \dfrac{1-\gamma_f}{4.2} & \text{for } 1.8 < \xi_{m-1,0} < 6 \\ 1.0 & \text{for } \xi_{m-1,0} > 6 \end{cases} \qquad \textit{Equation 4.4-2}$$

*Note: Interpolation is based on $\xi_{m-1,0}$ rather than $\gamma_b \cdot \xi_{m-1,0}$ since for the berm breakwater tests analysis showed the latter led to even larger overestimation of overtopping for berms below SWL.*

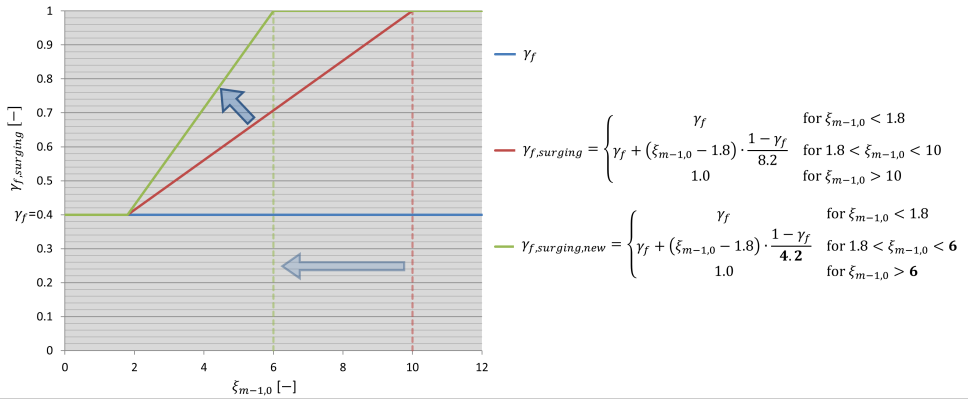


FIGURE 4.4-3: PROPOSED EXPRESSION FOR $\gamma_f$

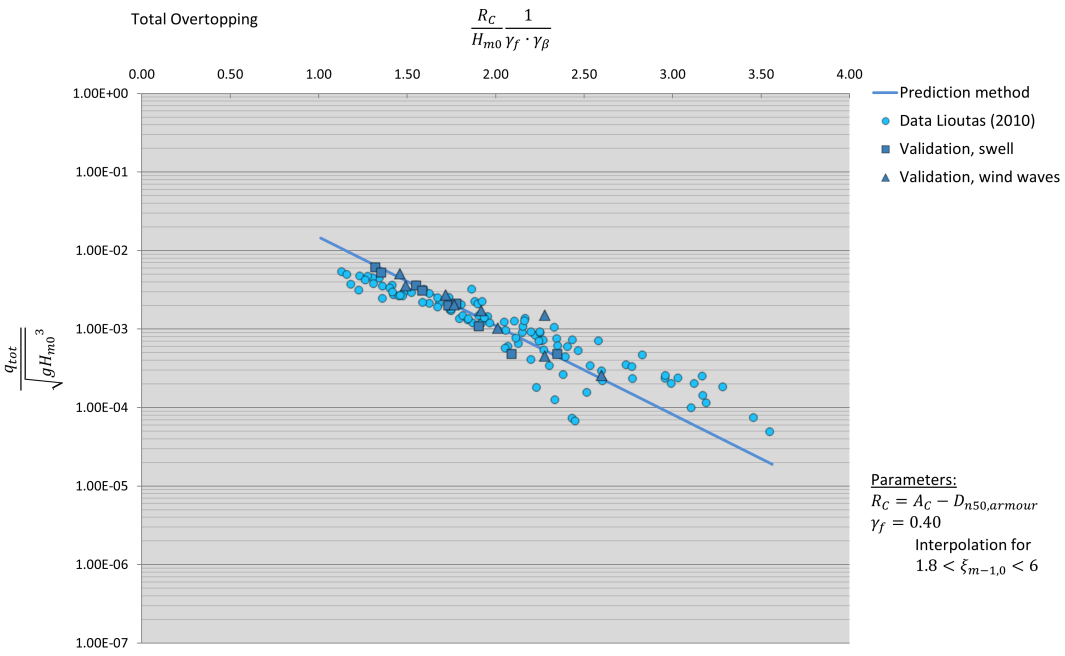


FIGURE 4.4-4: COMPARISON WITH ADAPTED PREDICTION METHOD

It can be observed that Lioutas' data exhibits more scatter than the validation tests, especially for lower overtopping discharges. Several reasons can be given. First of all Lioutas (2010) conducted experiments also with an "impermeable" crest (no drainage in the crest). It can be doubted if these experiments can reasonably be compared with the current experiments. Nevertheless they are included in the plot because these tests were not indicated in the data set. Furthermore measurement errors and practical problems during the experiments may have played a role, resulting in an increased scatter.

The goodness-of-fit was determined for both the dataset of Lioutas (2010) and the validation tests of the current research; see Table 4-1. Even though the proposed expression is much simpler than the Adjusted TAW prediction method, a better fit is obtained for both datasets.

TABLE 4-1: GOODNESS-OF-FIT VALUES FOR VALIDATION TESTS AND DATA SET OF LIOUTAS (2010)

| $G_{fit}$ | Adjusted TAW | Proposed expression |
|---|---|---|
| **Validation tests** | 0.03 | 0.02 |
| **Data Lioutas (2010)** | 0.11 | 0.10 |

Moreover it was observed that also for the breakwater configurations with a berm no spreading for Iribarren number exists any more. With the suggested adaption of $\gamma_f$ the proposed expression properly takes into account the Iribarren number.

### 4.4.2 INFLUENCE OF THE PERMEABLE BERM

Now the grouping based on wave steepness has been overcome the effect of a berm on the overtopping discharge should be properly taken into account. In its current form the EurOtop prediction method for permeable structures does not account for the existence of a berm. However Figure 4.2-4 indicated there is an influence. A first step is made by inserting the TAW expression for $\gamma_b$ in the prediction method. The result is depicted in Figure 4.4-5. The goodness-of-fit for this plot is $G_{fit}$=0.38.

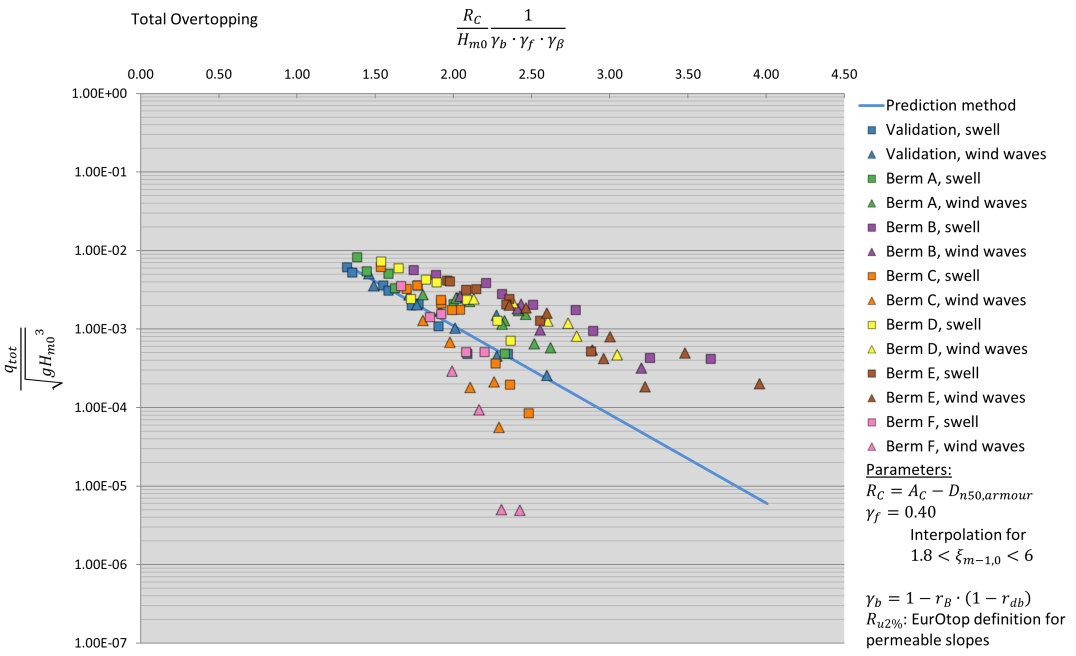


FIGURE 4.4-5: COMPARISON WITH ADAPTED PREDICTION METHOD

For berms at and below SWL, $\gamma_b$ leads to too much reduction whereas for berms above SWL too little reduction is calculated.

#### BERMS AT OR BELOW SWL

The reasoning of section 4.3.3 gives rise to the idea that for berms below SWL a permeable berm leads to less reduction of overtopping than an impermeable berm. Hereto a new expression for $\gamma_b$ is proposed with a parameter accounting for the permeability of the berm.

The following requirements were posed that the expression should meet:

1. For fully impermeable structures the berm factor should be equal to the one proposed by TAW.
2. For fully permeable structures no reduction due to a berm should be taken into account.
3. For $B \leq 0$ no reduction due to a berm should be taken into account.
4. $\lim_{B\to\infty}(\gamma_b) = 0$.
5. A good fit with the data should be established.

The current expression of $\gamma_b$, as recommended by TAW (2002), is printed below.

$$\gamma_b = 1 - r_B \cdot (1 - r_{db}) \text{ for } 0.6 \leq \gamma_b \leq 1.0 \qquad \textit{Equation 4.4-3}$$

$$r_B = \frac{B}{L_{Berm}} \qquad \textit{Equation 4.4-4}$$

$$r_{db} = 0.5 - 0.5 \cdot \cos\left(\pi \frac{d_B}{R_{u2\%}}\right) \quad \text{for a berm above SWL}$$
$$r_{db} = 0.5 - 0.5 \cdot \cos\left(\pi \frac{d_B}{2 \cdot H_{m0}}\right) \quad \text{for a berm below SWL} \qquad \textit{Equation 4.4-5}$$

In the calculation of $\gamma_b$ the overall effect of the berm can be reduced by inserting an additional factor $f_{dB\geq 0}$, see Equation 4.4-6. Where $f_{dB\geq 0}$ is a function of primarily berm material permeability but possibly also other material properties. Fully impermeable berms lead to maximum reduction of overtopping ($f_{dB\geq 0} = 1$) while fully permeable berms lead to no reduction of overtopping at all ($f_{dB\geq 0} = 0$). This is a theoretical case; a fully permeable berm would consist of sheer air.

Eventually the expression printed in Equation 4.4-6 is proposed which meets all requirements.

$$\gamma_b = 1 - f_{dB\geq 0} \cdot r_B \cdot (1 - r_{db}) \qquad \text{for } d_B \geq 0 \qquad \textit{Equation 4.4-6}$$

For the current research the berm material was not varied. Therefore $f_{dB\geq 0}$ cannot be given as a function of the berm permeability. For the data set a good fit is established when $f_{dB\geq 0} = 0.4$. The resulting graph is shown in Figure 4.4-6. For berms at and below SWL an excellent fit with the data is obtained.

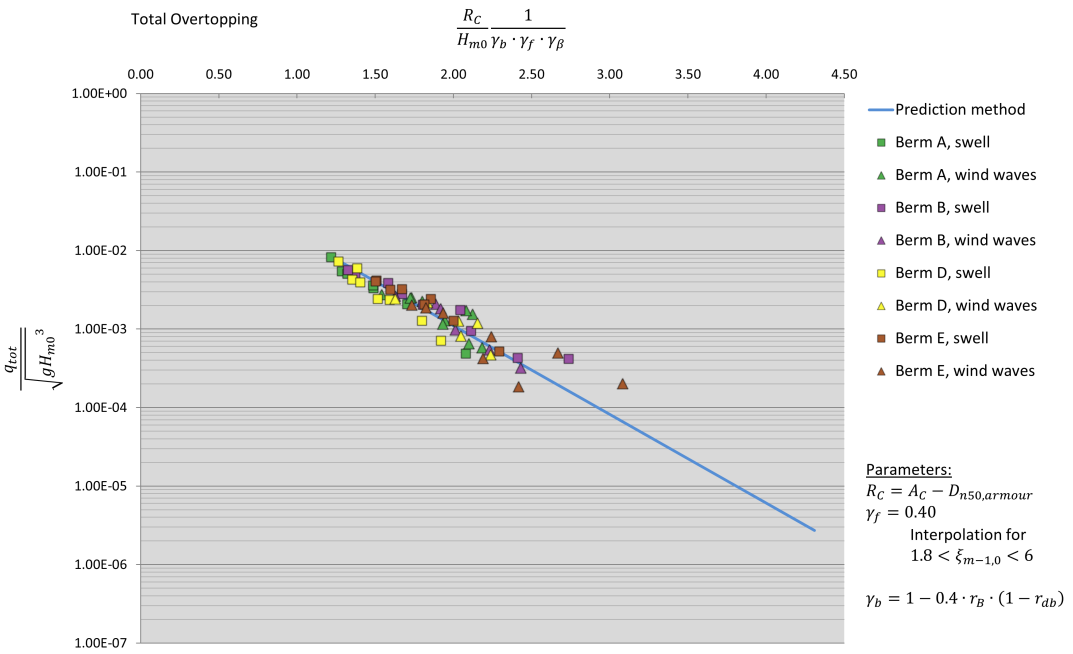


FIGURE 4.4-6: COMPARISON WITH ADAPTED PREDICTION METHOD

### BERMS ABOVE SWL

In the experiment phase of this research it was observed that berms above SWL act like an extended crest; the waves already break at the slope seaward of the berm. A different kind of expression for $\gamma_b$ is proposed that has the same character as many of the factors accounting for the decay of overtopping with spatial distance from the crest.

The following requirements were posed that the expression should meet:

1. For $B \leq 0$ no reduction due to a berm should be taken into account.
2. $\lim_{B\to\infty} \gamma_b = 0$.
3. A good fit with the data should be established.

Ideally also the following requirements are met:

4. A proper transition should be made for $d_B$=0 with Equation 4.4-6, the expression for $d_B \geq 0$.
5. A proper transition should be made for $d_B$=-$A_C$ with expressions accounting for the effect of an extended crest.

The expression printed in Equation 4.4-7 is proposed, which meets requirements 1-3. Requirements 4 and 5 are not fulfilled; mathematically a complicated interpolation of a linear relation and an exponential relation could be made, but there is not sufficient data to validate this.

$$\gamma_b = \exp\left(-f_{dB<0} \cdot \frac{B}{H_{m0} \cdot \xi_{m-1,0}}\right) \quad \text{for } d_B < 0 \qquad \textit{Equation 4.4-7}$$

The found dimensionless number $\frac{B}{H_{m0} \cdot \xi_{m-1,0}}$ leads to a good fit and no observable grouping of data. In Figure 4.4-7 for each experiment the optimal value for $\gamma_b$ is compared with the expression for $\gamma_b$. The optimal value for $\gamma_b$ can be calculated rather easily by rewriting the prediction method, see Equation 4.4-8.

$$\gamma_{b,optimal} = \frac{-2.6}{\ln\left(\frac{q_{tot,meas}}{\sqrt{g \cdot {H_{m0}}^3}} \cdot \frac{1}{0.2}\right)} \cdot \frac{R_C}{H_{m0} \cdot \gamma_f \cdot \gamma_\beta} \qquad \textit{Equation 4.4-8}$$

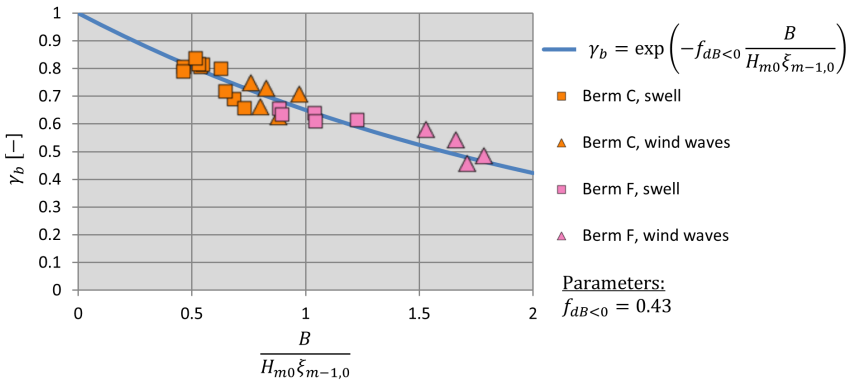


FIGURE 4.4-7: $\gamma_b$ FOR BERMS ABOVE SWL

For the total overtopping discharges this leads to Figure 4.4-8.

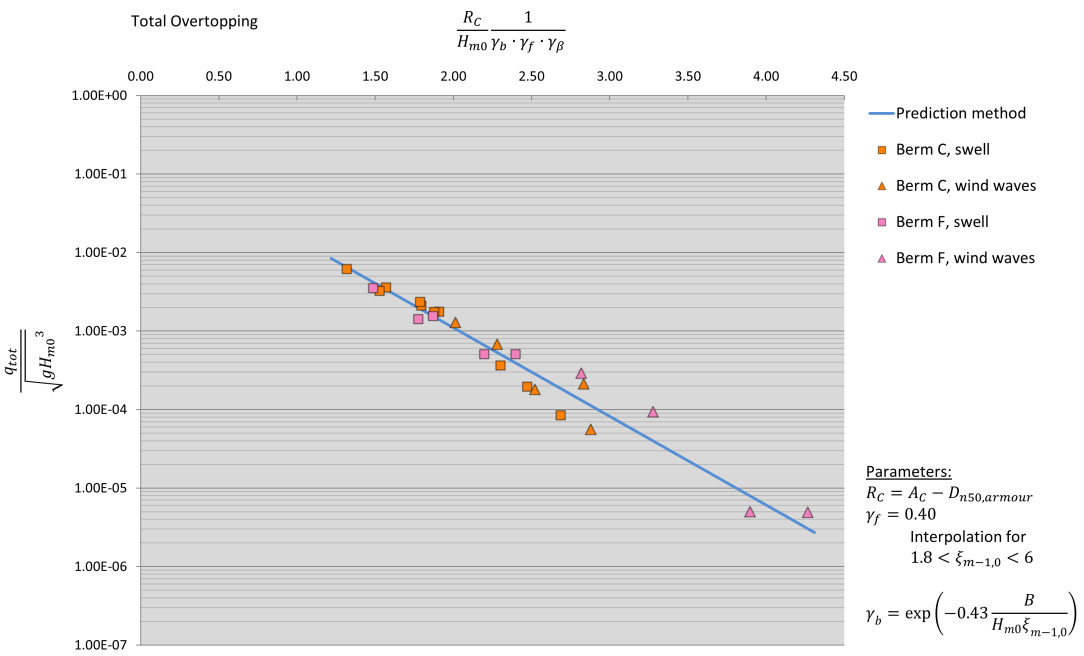


FIGURE 4.4-8: COMPARISON WITH ADAPTED PREDICTION METHOD

It should be stressed that in the current experiments only one berm elevation above SWL was tested. Therefore the berm elevation is not included in $\gamma_b$. It is advised to conduct more experiments to investigate the influence of the berm elevation for berms above SWL. Possibly then an expression can be proposed such that also requirements 4 and 5 are met.

### CONCLUSION FOR $\gamma_b$

The permeable berms that were used in the current research are adequately described with an adapted expression for $\gamma_b$. The expression is split into one part for berms at or below SWL and one part for berms above SWL. The suggested expression is printed in Equation 4.4-9.

$$\gamma_b = \begin{cases} 1 - f_{dB\geq 0} \cdot r_B \cdot (1 - r_{db}) & \text{for } d_B \geq 0 \\ \exp\left(-f_{dB<0} \cdot \dfrac{B}{H_{m0} \cdot \xi_{m-1,0}}\right) & \text{for } \dfrac{d_B}{A_c} \approx -0.5 \end{cases} \qquad \textit{Equation 4.4-9}$$

For berms above SWL a different dimensionless berm width is applicable that is more similar to terms accounting for spatial decay of overtopping. Due to this difference in dimensionless number, the influence of the berm elevation cannot be illustrated in a universal chart. Instead two graphs are drawn in Appendix A for representative conditions.

For the material used in the current experiments $f_{dB\geq 0} = 0.4$ and $f_{dB<0} = 0.43$. The value of these parameters is expected to be a function of the material properties of the berm. It should be stressed that during the experiments only one berm elevation above SWL was tested. Until further experiments are conducted it is advised to interpolate linearly between the two provided expressions in cases where $-0.5 < \frac{d_B}{A_C} < 0$. The proposed expression is compared with experimental data in Figure 4.4-9.

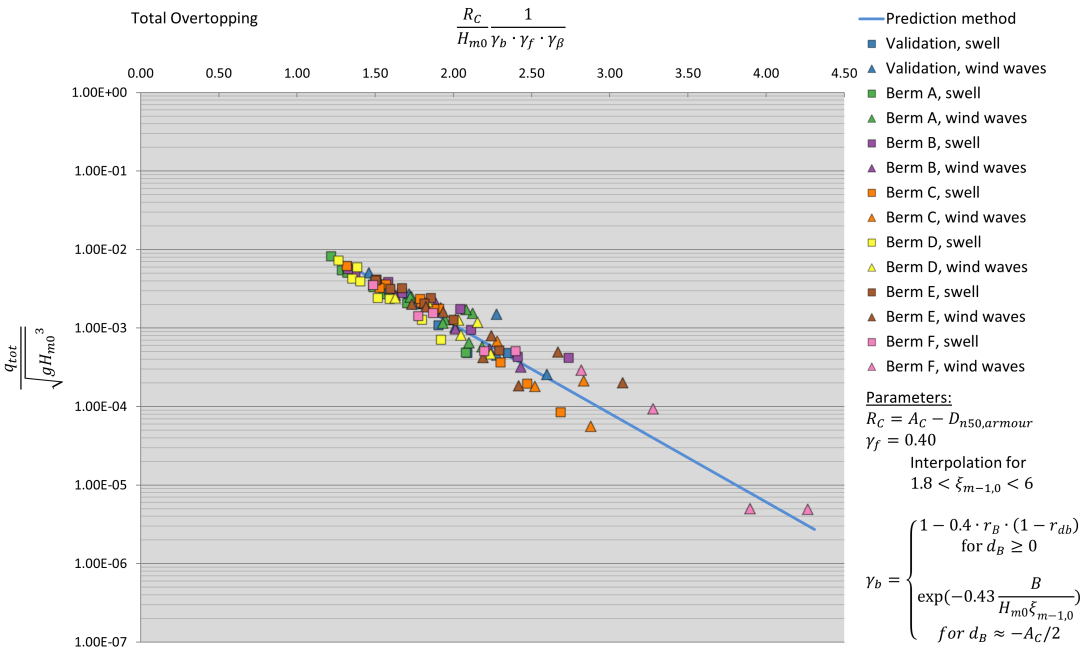


FIGURE 4.4-9: COMPARISON WITH PROPOSED EXPRESSION

For each berm configuration the goodness-of-fit of the prediction method is provided in Table 4-2. It can be concluded a very good fit is achieved for every berm configuration.

TABLE 4-2: GOODNESS-OF-FIT VALUES FOR BERM BREAKWATER TESTS

| $G_{fit}$ | Proposed expression |
|---|---|
| **Berm A** | 0.02 |
| **Berm B** | 0.02 |
| **Berm C** | 0.03 |
| **Berm D** | 0.02 |
| **Berm E** | 0.04 |
| **Berm F** | 0.04 |

### 4.4.3 RELIABILITY OF THE PREDICTION METHOD

In the proposed prediction method the empirical coefficients C and D govern the relationship between the dimensionless overtopping discharge and the dimensionless crest freeboard, see Equation 4.4-10.

$$q_{tot}^* = \mathrm{C}\cdot\exp(-\mathrm{D}\cdot R_C^*) \qquad \textit{Equation 4.4-10}$$

The empirical coefficient D was determined for several confidence levels. For instance, for a 95% confidence level the values of C and D result in an expression that is conservative for 95% of the data set.

TABLE 4-3: CONFIDENCE LEVELS FOR THE PROPOSED EXPRESSION

| Confidence level | C | D |
|---|---|---|
| **5%** | 0.2 | 2.25 |
| **10%** | 0.2 | 2.31 |
| **50%** | 0.2 | 2.60 |
| **90%** | 0.2 | 2.95 |
| **95%** | 0.2 | 3.10 |

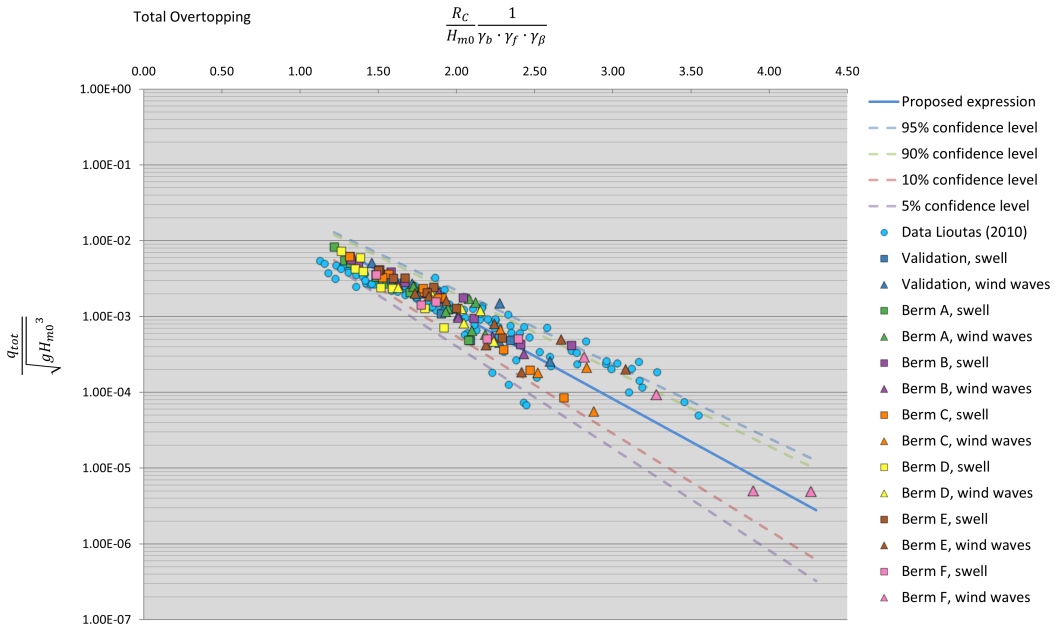


FIGURE 4.4-10: COMPARISON WITH PROPOSED EXPRESSION

For a deterministic prediction method the 95% confidence level can be used.

### 4.4.4 DISCUSSION

The Adjusted TAW formula was found after extensive data analysis. A physical explanation of the found interpolation of the two existing TAW formulae was that, because irregular waves were used, the distinction between breaking and non-breaking waves cannot be made so strictly. In every wave spectrum there are both breaking and non-breaking waves. Therefore it was argued that also in the prediction method no strict separation should be made.

The current research argues that the slope roughness up-rushing waves encounter should be reduced for longer waves. Observations during the experiments agree with this reasoning. The result is a more concise expression and a better fit with the data.

Because of the complexity with which the overtopping process is associated no analytical grounds could be found to base a prediction method on. The quality of a prediction method can solely be based on the goodness-of-fit with experimental data.

When the proposed expression for $\gamma_b$ is applied to the Adjusted TAW formula this results in a reduction of the amount of scatter, see Appendix B. Still the expression proposed in this thesis leads to a better fit with the experimental data.

It does make sense that a wave spectrum always contains both breaking and non-breaking waves, but apparently it is possible to make a strict distinction, based on the parameter $\xi_{m-1,0}$.

## 4.5 CONCLUSIONS FOR TOTAL OVERTOPPING

Experiments were conducted where the total amount of overtopping was collected. In this chapter the main observations were discussed and a prediction method was proposed that leads to reduction of scatter and a good fit with the experimental data. Restriction of time led to a selection of representative conditions to be tested. Based on this experimental data the following conclusions can be made.

1. Existing prediction formulae do not accurately predict the overtopping discharges measured in the experiments. Grouping on breaker parameter and berm configuration could be observed.
2. Based on the experimental data, the crest freeboard should be adjusted to account for the permeability of the crest. The hypothesis can be confirmed on this point. A good fit is achieved when the crest freeboard is defined as $R_C = A_C - D_{n50,armour}$.On the one hand more water can penetrate when compared with an impermeable crest, while on the other hand the armour elements lead to a combination of physical obstruction and increased hydraulic resistance due to turbulence. Further research specifically on the crest freeboard definition is required to give a more definite answer.
3. The recommendation of Lioutas (2010) to use $\gamma_f = 0.45$ instead of $\gamma_f = 0.40$ was not found to be applicable for these experiments.
4. The Adjusted TAW prediction formula as suggested by Lioutas et al. (2012) accurately predicts the overtopping discharge of the validation tests of the current research experiment programme. The expression effectively removes any data grouping based on the breaker parameter. Breakwaters with a berm were not properly predicted.
5. A new expression for total overtopping is proposed. Being a variation on the Adjusted TAW, this new prediction method removes the grouping on breaker parameter by adapting the $\gamma_f$ reduction factor. For long waves the roughness of the armour slope does not lead to reduction of overtopping. The hypothesis can be confirmed on this point. The upper limit of $\gamma_f$ for $\xi_{m-1,0} = 10$ is changed to $\xi_{m-1,0} = 6$. See Equation 4.5-1.

$$\frac{q_{tot}}{\sqrt{g \cdot H_{m0}^3}} = \mathrm{C} \cdot \exp\left(-\mathrm{D} \cdot \frac{R_C}{H_{m0}} \frac{1}{\gamma_b \cdot \gamma_{f,surging} \cdot \gamma_\beta}\right) \qquad \textit{Equation 4.5-1}$$

where:

$$R_C = A_C - D_{n50,armour} \qquad \textit{Equation 4.5-2}$$

$$\gamma_{f,surging} = \begin{cases} \gamma_f & \text{for } \xi_{m-1,0} < 1.8 \\ \gamma_f + \left(\xi_{m-1,0} - 1.8\right) \cdot \dfrac{1 - \gamma_f}{4.2} & \text{for } 1.8 < \xi_{m-1,0} < 6 \\ 1.0 & \text{for } \xi_{m-1,0} > 6 \end{cases} \qquad \textit{Equation 4.5-3}$$

6. In the current experiments the effect of a permeable berm on total overtopping is found to be remarkably different from the effect of impermeable berms as calculated by TAW (2002). Below SWL a permeable berm leads to less reduction of overtopping than an impermeable berm. In spite of the rough character of a permeable berm overtopping is reduced less effectively; presumably because wave propagation within the berm is to a certain extent possible. Berms above SWL lead to wave breaking on the slope in front of the berm, and act more as an extended crest. Contrarily to impermeable berms above SWL, a permeable berm above SWL leads to significant energy dissipation of run-up. This is consistent with the hypothesis.
7. In the experimental data grouping based on berm dimensions was removed by applying a new expression for $\gamma_b$. The proposed expression is printed in Equation 4.5-4.

$$\gamma_b = \begin{cases} 1 - f_{dB\geq 0} \cdot r_B \cdot (1 - r_{db}) & \text{for } d_B \geq 0 \\ \exp\left(\dfrac{-f_{dB<0} \cdot B}{H_{m0} \cdot \xi_{m-1,0}}\right) & \text{for } \dfrac{d_B}{A_c} \approx -0.5 \end{cases} \qquad \textit{Equation 4.5-4}$$

8. In the current research a very permeable berm was used, constructed from armour stones. For this configuration $f_{dB\geq 0} = 0.4$ and $f_{dB<0} = 0.43$ lead to an excellent fit. It is definitely recommended to conduct experiments where the berm is constructed partly with smaller rock material, just as in reality. It is expected that – due to the decreased permeability – these berms will have a stronger overtopping reducing effect.
9. When the proposed expression for $\gamma_b$ (Equation 4.5-4) is used in the Adjusted TAW formula this leads to a significantly better fit than when the expression as formulated by TAW (2002) is used. Still the proposed expression printed in Equation 4.5-1 performs better.
10. Only one berm elevation above SWL was tested during the current research. Until further experiments are conducted it is advised to interpolate linearly between the two provided expressions in cases where $-0.5 < \frac{d_B}{A_c} < 0$.
11. The influence of the different parameters as stated in the hypothesis (section 4.3) was confirmed in the data analysis. Underlying physical processes should be studied separately to provide an increased insight.

# CHAPTER 5. SPATIAL DISTRIBUTION OF OVERTOPPING

The physical experiments as discussed in Chapter 3 resulted in a data set with overtopping discharges for 104 experiments. For each experiment the overtopping discharge was determined at 8 horizontal distances from the crest. Different wave conditions and breakwater configurations were assessed. In this chapter the results will be interpreted for the spatial distribution of overtopping. First an introduction is given in section 5.1. The overtopping directly behind the crest is discussed in section 5.2. In section 5.3 the spatial distribution of overtopping is treated. Conclusions are stated per section.

## 5.1 INTRODUCTION

Overtopping behind the crest is subdivided into the whole amount of overtopping behind the crest and the spatial distribution of overtopping behind the crest, $q_{bc}$ and $q(x)$ respectively.

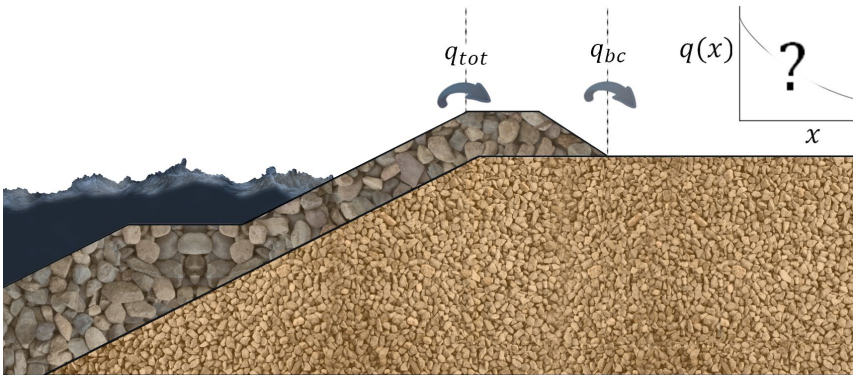


FIGURE 5.1-1: OVERTOPPING DEFINITIONS

Generally two calculation methods are used to estimate the amount of overtopping. Either a reduction factor is used in the dimensionless crest freeboard (e.g. $\gamma_c$ in Lioutas et al. (2012)) or the total overtopping is multiplied with a factor $C_r$ (e.g. Steenaard (2002), Van Kester (2009)). The influence of $\gamma_c$ is not a fixed ratio of the total overtopping discharge. Instead, the influence depends on the value of total overtopping. In Appendix C the mathematical difference is illustrated.

During the experiments quite often collection bins contained little or no water at all. A minimum water volume of 100 ml was chosen; overtopped volumes smaller than 100 ml cannot accurately be measured in the experiment setup. In graphs where the dimensionless overtopping is on a logarithmic axis, volumes lower than the minimum value are plotted at the very bottom of the graph. See for instance Figure 5.2-3.

Concluding, it is noted that the measured values of $q_{bc}$ may to a greater or lesser extent be influenced by the experiment setup. The influence of the experiment setup is discussed in Chapter 6.

## 5.2 OVERTOPPING DIRECTLY BEHIND THE CREST

The measured values of $q_{bc}$ will be plotted against four prediction methods. The method of Steenaard (2002) and the method of Van Kester (2009) use a reduction factor $C_r$. The Adjusted TAW formula that was suggested by Lioutas et al. (2012) uses $\gamma_c$ to increase the dimensionless crest freeboard. Furthermore the curve fitting formula of Lykke Andersen (2006) is compared with the experimental data, as this formula was recommended after experiments where the overtopping volumes were collected behind the crest.

### 5.2.1 COMPARISON WITH STEENAARD (2002)

The expression of Steenaard, as discussed in section 2.3.1.2, is reprinted below.

$$\frac{q_{bc}}{q_{tot}} = \begin{cases} \dfrac{Q_{tot}^* - Q_d^*}{Q_{tot}^* + 7.0 \cdot 10^{-2}} & Q_{tot}^* > Q_d^* \\ 0 & Q_{tot}^* \leq Q_d^* \end{cases} \qquad \textit{Equation 5.2-1}$$

with:

$$Q_{tot}^* = \frac{q_{tot}}{\sqrt{g \cdot {G_C}^3}} \qquad \textit{Equation 5.2-2}$$

In Figure 5.2-1 the experimental data is compared with this prediction method. First of all it can be concluded that the prediction method does not correlate with the data. The measured total overtopping discharges are too small to even surpass the threshold value Steenaard introduced. It appears that the ratio between $q_{bc}$ and $q_{tot}$ depends on the amount of total overtopping. During the experiments it was observed that overtopping splashed primarily through the crest, rather than over it. Collection bins in the crest first needed to be filled entirely before overtopped water would flow to bins down the flume. This seems to be well in line with Figure 5.2-1. The influence of the experiment setup is discussed in Chapter 6.

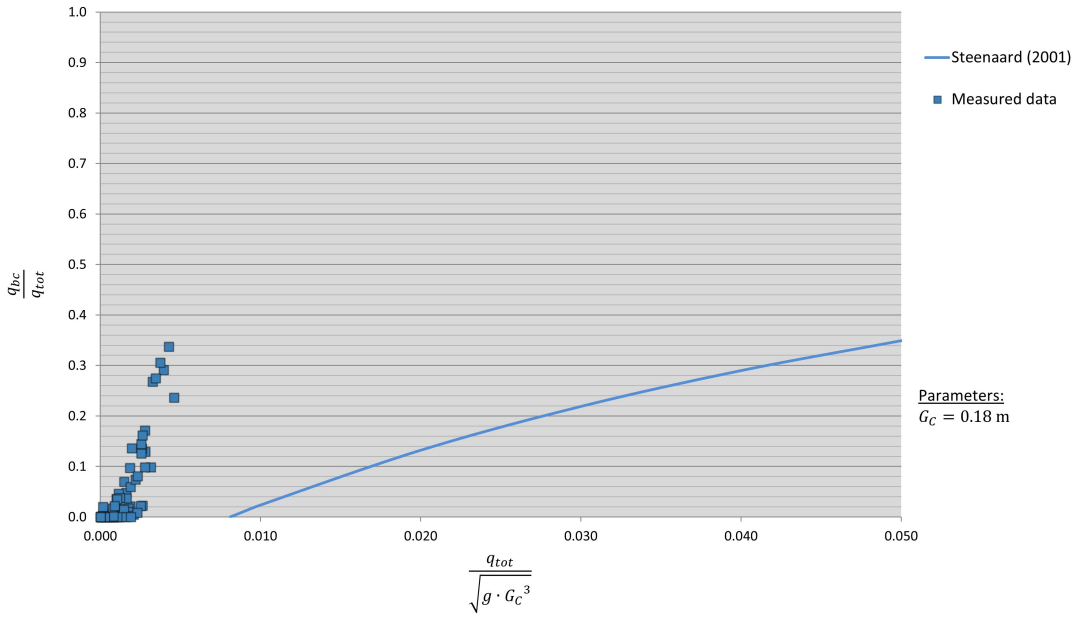


FIGURE 5.2-1: COMPARISON WITH STEENAARD

*Note: For this prediction method no goodness-of-fit is provided since only a reduction factor is calculated and no overtopping discharge.*

### 5.2.2 COMPARISON WITH VAN KESTER (2009)

Van Kester tested regular waves and measured one overtopping discharge at a time. Based on his test results he recommended using the expression below. Here the wave height, wave length, crest width and crest freeboard all influence the ratio between $q_{bc}/q_{tot}$.

$$\frac{q_{bc}}{q_{tot}} = \begin{cases} \left(\frac{H^* - H_d^*}{H^* - 15}\right)^2 & H^* > H_d^* \\ 0 & H^* \leq H_d^* \end{cases} \qquad \textit{Equation 5.2-3}$$

with:

$$H^* = \frac{H \cdot L}{G_C \cdot R_C} \qquad \textit{Equation 5.2-4}$$

In Figure 5.2-2 the experimental data from the current research is compared with this prediction method.

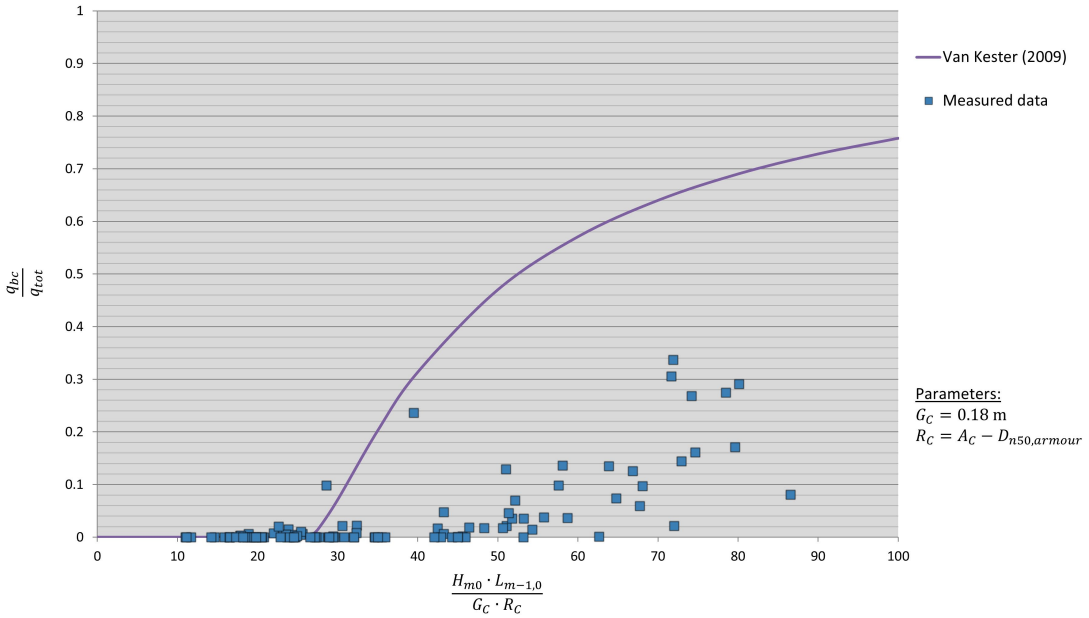


FIGURE 5.2-2: COMPARISON WITH VAN KESTER

Here hardly any relation can be distilled from the measurement points alone. The threshold value used in the relation of Van Kester cannot be justified based on these data. The prediction method does not have a good fit with the data.

*Note: For this prediction method no goodness-of-fit is provided since only a reduction factor is calculated and no overtopping discharge.*

### 5.2.3 COMPARISON WITH LIOUTAS ET AL. (2012)

Lioutas et al. (2012) introduced a parameter $\gamma_c$ in the dimensionless freeboard to account for the spatial decay, see Equation 5.2-5 and Equation 5.2-6.

$$\frac{R_C}{H_{m0}} \frac{1}{(\xi_{m-1,0} \cdot \gamma_b \cdot \gamma_v)^k \cdot \gamma_f \cdot \gamma_\beta \cdot \gamma_c} \qquad \textit{Equation 5.2-5}$$

with:

$$\gamma_c = -0.142 \cdot \frac{x}{G_C} + 0.577 \qquad \textit{Equation 5.2-6}$$

For the overtopping directly behind the crest Lioutas used $x = 0$, so $\gamma_c = 0.577$. In the current experiments the same crest width was used as Lioutas (2010) used. Therefore any influence of crest width could not be determined based on the current experimental data set.

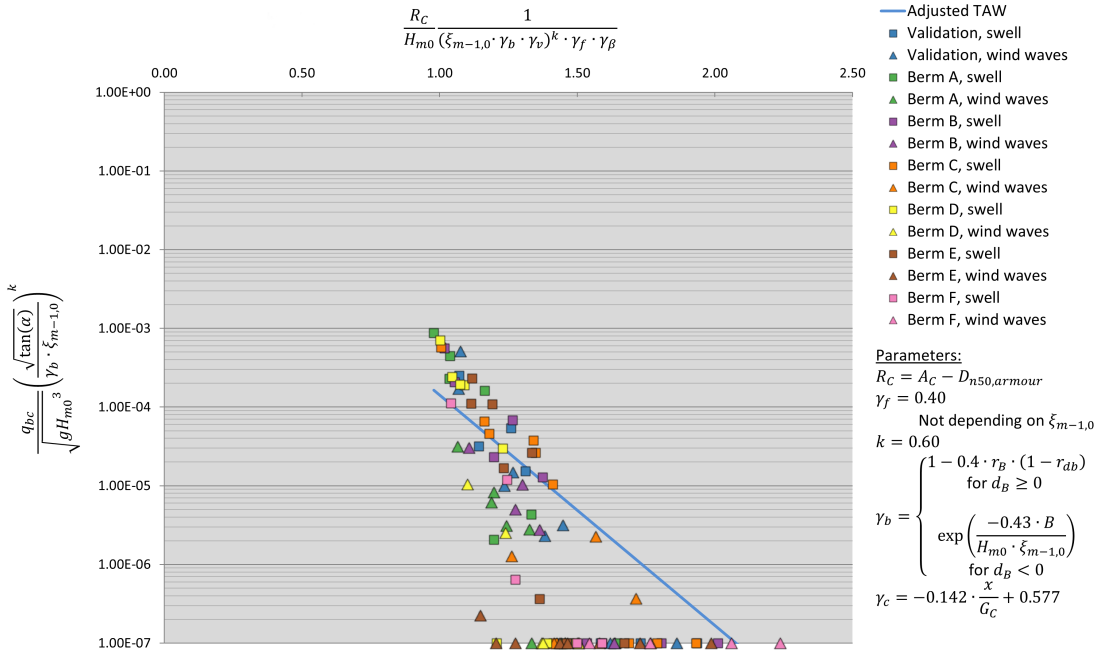


FIGURE 5.2-3: COMPARISON WITH LIOUTAS

The Adjusted TAW formula moves through the average of the measurement data, but there is much scatter. Already for the total overtopping the data was quite heavily scattered. The same trend is observed as for Lioutas' own experimental data; large values of $q_{bc}$ are underestimated and small values of $q_{bc}$ are overestimated.

Overtopping volumes that could not be measured (< 100 ml) are indicated by markers on the very bottom of the graph. For these values the prediction method presumably overestimates $q_{bc}$ significantly. It is expected the trend for the rest of the data is extended for smaller overtopping discharges. The data cloud has a larger inclination than the prediction method so for small values $q_{bc}$ a larger error is expected.

When all overtopped volumes lower than 100 ml are set to 100 ml, the goodness-of-fit for this prediction method is $G_{fit}$=1.00. The here used goodness-of-fit test should not be confused with the $R^2$ coefficient of determination. For the current method low values indicate small errors.

### 5.2.4 COMPARISON WITH LYKKE ANDERSEN (2006)

The prediction method of Lykke Andersen was suggested after extensive physical model tests for berm breakwaters, among which breakwaters with a non-reshaping berm. Overtopping was measured at the end of the crest.

After a curve fitting routine a very comprehensive expression was proposed, as reprinted in Equation 5.2-7.

$$q_* = 1.79 \cdot 10^{-5} \cdot (f_{H0}^{1.34} + 9.22) \cdot s_{0p}^{-2.52} \cdot \exp[-5.63 \cdot R_*^{0.92} - 0.61 \cdot G_*^{1.39} - 0.55 \cdot h_{b*}^{1.48} \cdot B_*^{1.39}] \qquad \textit{Equation 5.2-7}$$

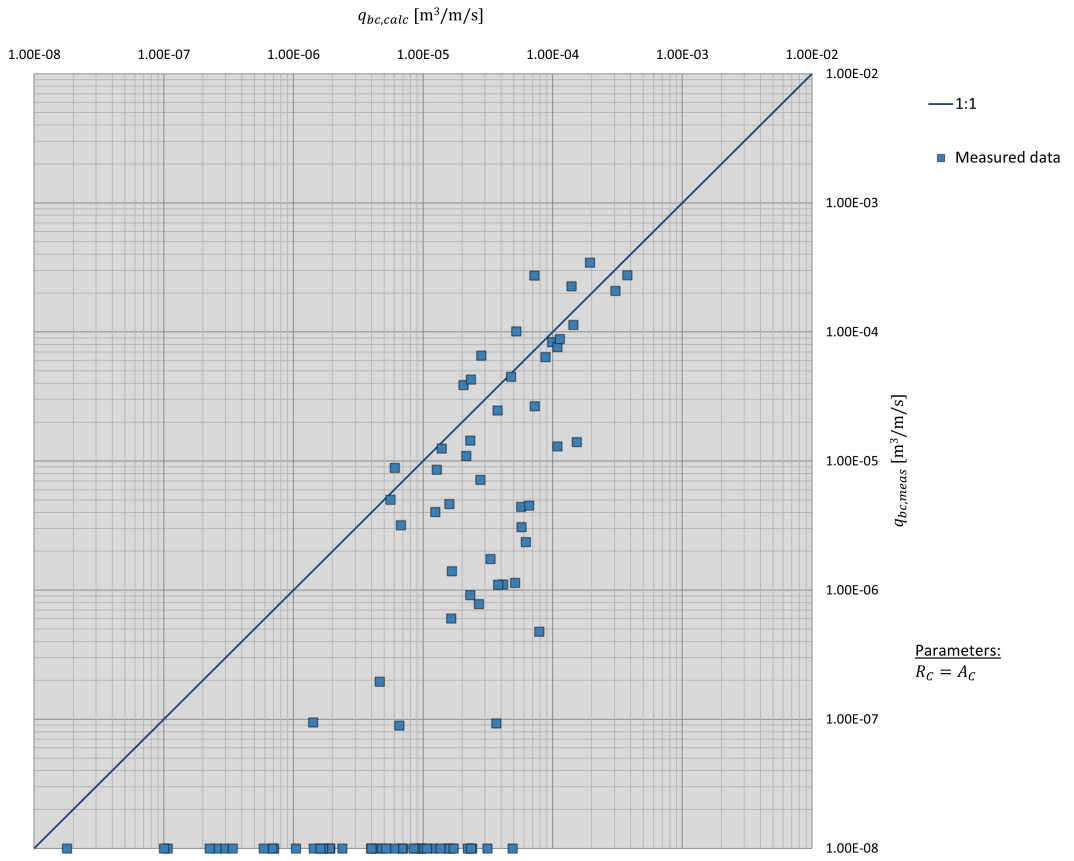


FIGURE 5.2-4: COMPARISON WITH LYKKE ANDERSEN

Some of the experiments with quite large values of $q_{bc}$ are predicted accurately. However for the majority of the experiments the overtopping is overestimated significantly.

When all overtopped volumes lower than 100 ml are set to 100 ml, the goodness-of-fit for this prediction method is $G_{fit}$=4.1. There are very large deviations between measurement results and predicted values.

### 5.2.5 CONCLUSIONS FOR $q_{bc}$

Comparison of the experimental data of the current research and that of Lioutas (2010) learned that the overtopping behind the crest is presumably strongly influenced by the used experiment setup. This influence is discussed separately in Chapter 6.

For the conditions as simulated during the experiments, the following conclusions can be drawn.

1. The ratio between $q_{bc}$ and $q_{tot}$ tends to increase for higher values of $q_{tot}$.
2. The parameter of Steenaard (2002) leads to such a data cloud that a rough trend can be discerned. However the expression proposed by Steenaard (2002) does not properly describe the measured data.
3. The dimensionless parameter proposed by Van Kester (2009) does not lead to reduction of scatter. The threshold value of the prediction method Van Kester (2009) introduced cannot be confirmed.
4. The prediction method of Lioutas et al. (2012) leads to quite a good fit with the data. For this method it is observed that large values of $q_{bc}$ are underestimated and small values of $q_{bc}$ are overestimated.
5. The method recommended by Lykke Andersen (2006) proves not to be valid for the current experimental data.

## 5.3 OVERTOPPING DISTRIBUTION BEHIND THE CREST

During the experiments the average overtopping discharge was determined for 8 horizontal positions in total, 6 of which were positioned behind the crest. The spatial distribution of overtopping for each experiment conducted will be investigated.

A comparison will be drawn with 3 existing prediction methods, being 1) Juul Jensen (1984), 2) Van Kester (2009), and 3) Lioutas et al. (2012).

In Figure 5.3-1 the measured spatial distribution of overtopping is depicted. The aim for each prediction method for $C_r$ is to adjust the horizontal position of a data point on a dimensionless horizontal axis such that clustering of the data is achieved.

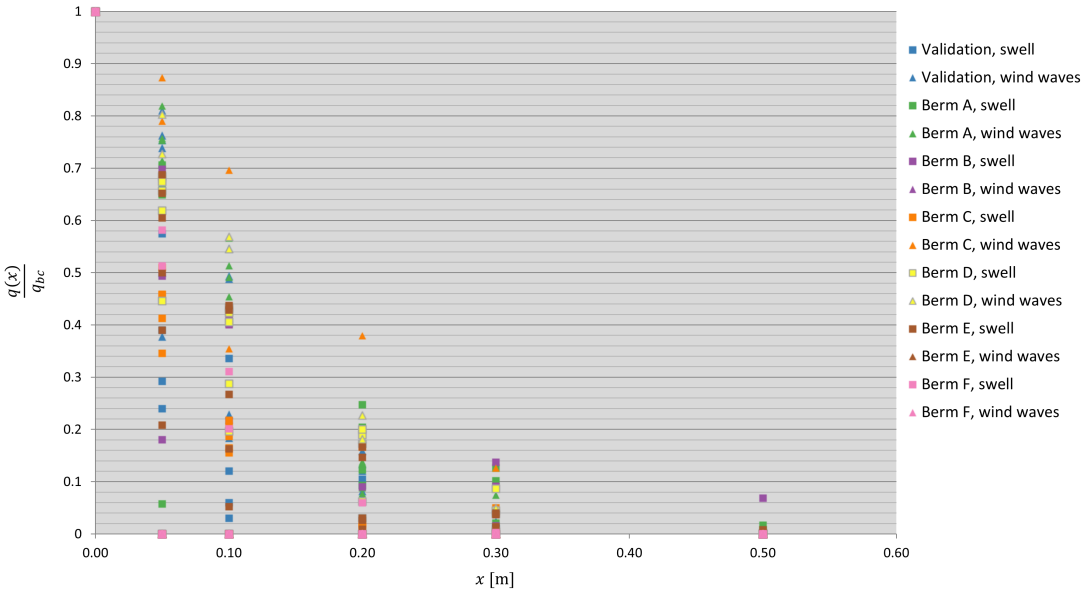


FIGURE 5.3-1: SPATIAL DISTRIBUTION OF OVERTOPPING IN THE EXPERIMENTS

In Figure 5.3-1 the horizontal position is depicted in consistence with Lioutas et al. (2012), i.e. $x$ = 0 at the landward end of the crest.

### 5.3.1 COMPARISON WITH JUUL JENSEN (1984)

Juul Jensen chose to describe the spatial decay of overtopping with an exponential function. The method that was recommended can be written as a reduction factor $C_r$, see Equation 5.3-1.

$$C_r = 10^{-\frac{x}{\beta}} \qquad \textit{Equation 5.3-1}$$

In Figure 5.3-2 a comparison is drawn between the method of Juul Jensen and the measured values of $C_r$. The measured value of $C_r$ was calculated as $\frac{q(x)_{meas}}{q_{bc,meas}}$. $x$ is the horizontal distance from the end of the crest.

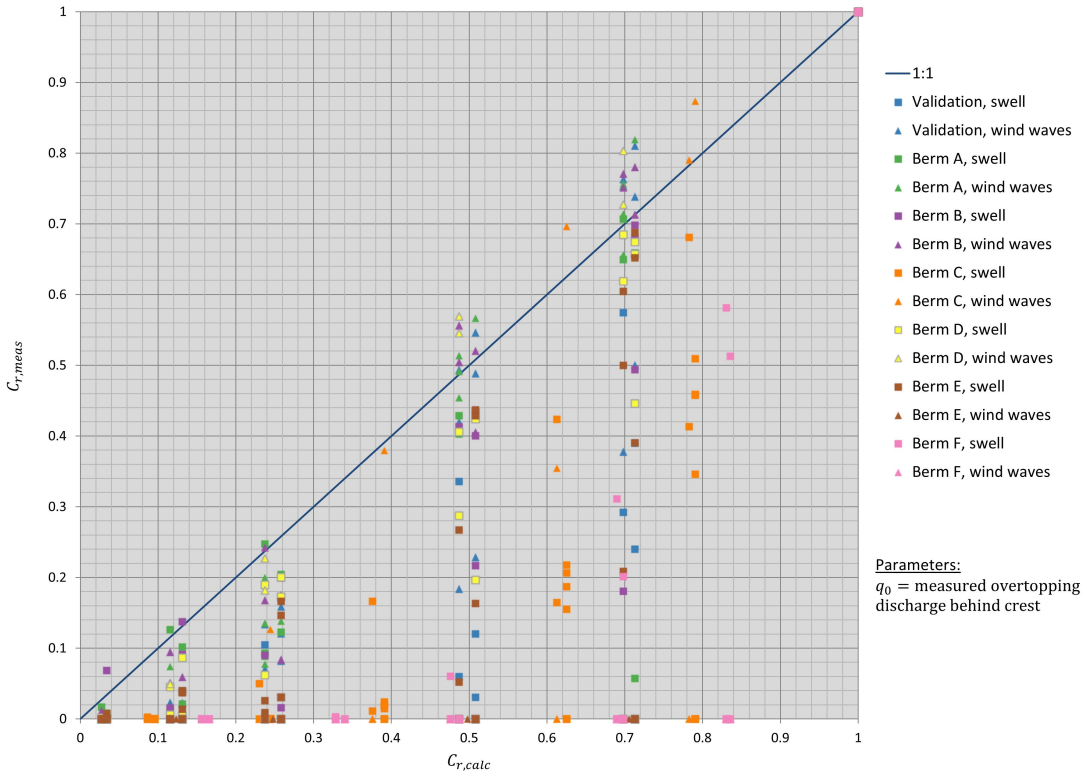


FIGURE 5.3-2: COMPARISON WITH JUUL JENSEN

The prediction method seems adequate to provide an upper limit. There's a large amount of scatter however. It is quite clear that other parameters play a major role. Apparently not solely the horizontal distance from the end of the crest is important for the distribution of the overtopping discharge.

*Note: For this prediction method no goodness-of-fit is provided since only a reduction factor is calculated and no overtopping discharge.*

### 5.3.2 COMPARISON WITH VAN KESTER (2009)

Van Kester introduced a reduction factor for the total overtopping based on the wave energy flux.

$$C_r = \frac{q(x)}{q_{bc}} = \exp\left(-1.64 \cdot 10^5 \cdot \frac{x}{H_{m0}} \cdot \frac{1}{(H^*T^*)^3}\right) \qquad \textit{Equation 5.3-2}$$

Here $H^*T^*$ is supposed to be a dimensionless form of the wave energy flux. The horizontal position from the end of the crest, $x$, is made dimensionless as shown in Equation 5.3-4.

$$H^*T^* = \frac{H_{m0}}{R_C} \cdot T \cdot \sqrt{\frac{g}{R_C}} \qquad \textit{Equation 5.3-3}$$

$$x^* = \frac{x}{H_{m0}} \cdot \frac{1}{(H^*T^*)^n} \qquad \textit{Equation 5.3-4}$$

The prediction method is compared with the measured data in Figure 5.3-3.

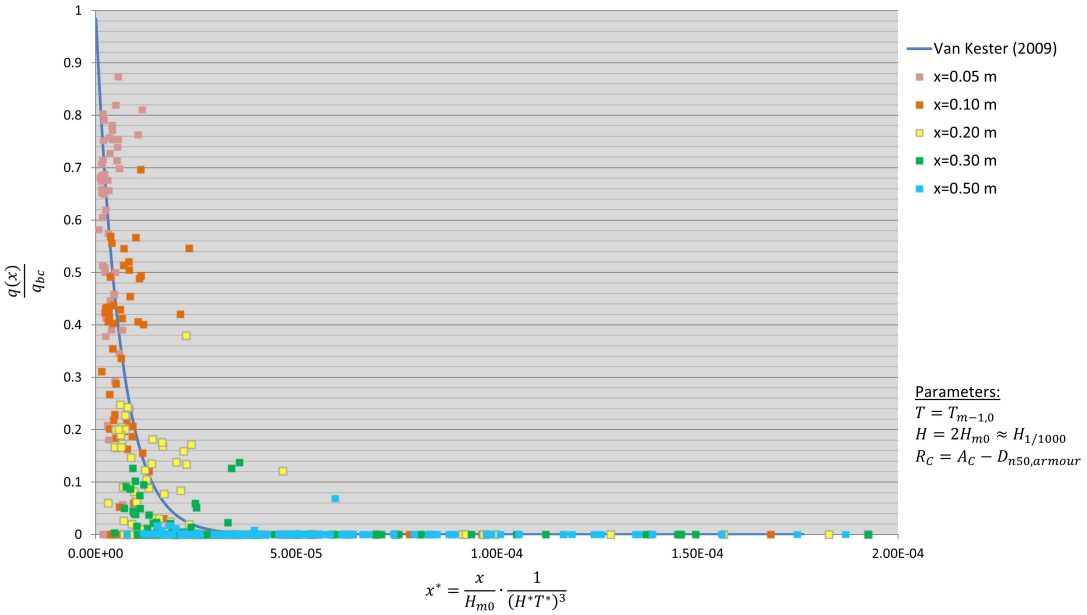


FIGURE 5.3-3: COMPARISON WITH VAN KESTER

The prediction method does not have a good fit with the measured data. This corresponds with Van Kester's own remark that irregular waves lead to considerably larger values of $x^*$. Moreover the dimensionless parameter $x^*$ does not lead to reduction of scatter in the data. A rough trend can be discerned; larger values of $x^*$ lead to a lower value of $\frac{q(x)}{q_{bc}}$.

Figure 5.3-4 presents a similar graph as was made for the prediction method of Juul Jensen. This graph shows that the prediction method of Van Kester underestimates the overtopping discharge for quite a few experiments. Furthermore the chosen method leads to very much scatter in the data.

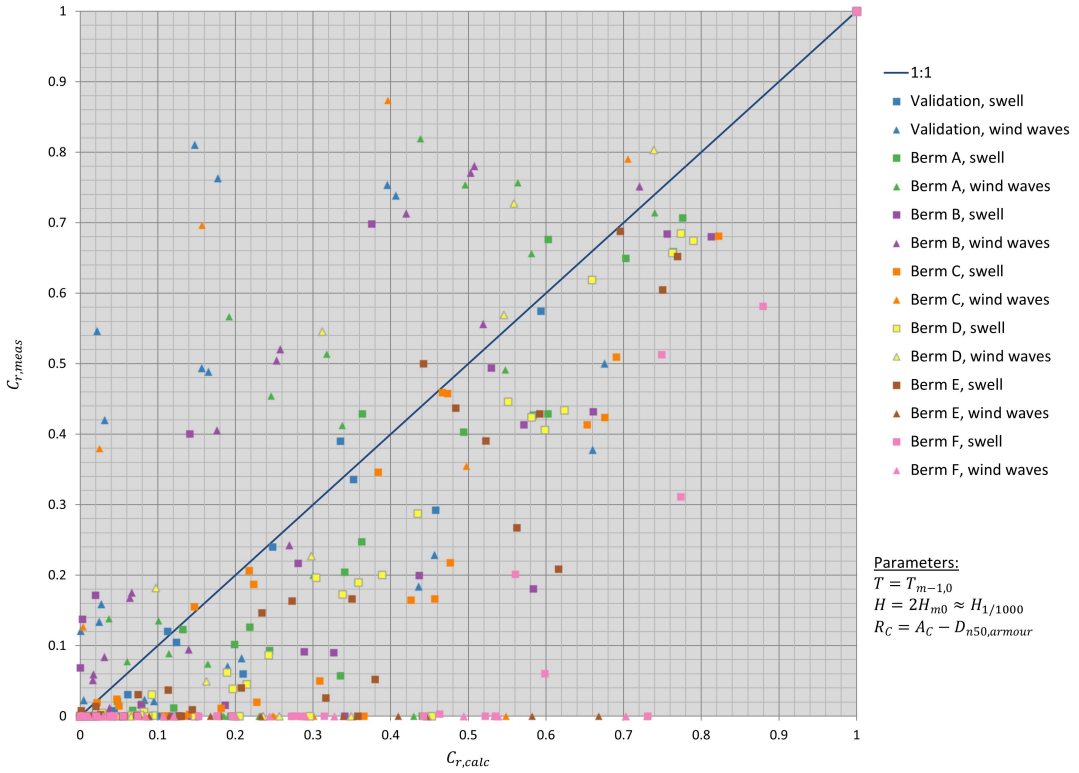


FIGURE 5.3-4: COMPARISON WITH VAN KESTER

*Note: For this prediction method no goodness-of-fit is provided since only a reduction factor is calculated and no overtopping discharge.*

### 5.3.3 COMPARISON WITH LIOUTAS ET AL. (2012)

Here the found expression for total overtopping is taken as a starting point. The $\gamma_c$ term as introduced by Lioutas is applied to the proposed expression.

$$\gamma_c = -0.142 \cdot \frac{x}{G_C} + 0.577 \qquad \textit{Equation 5.3-5}$$

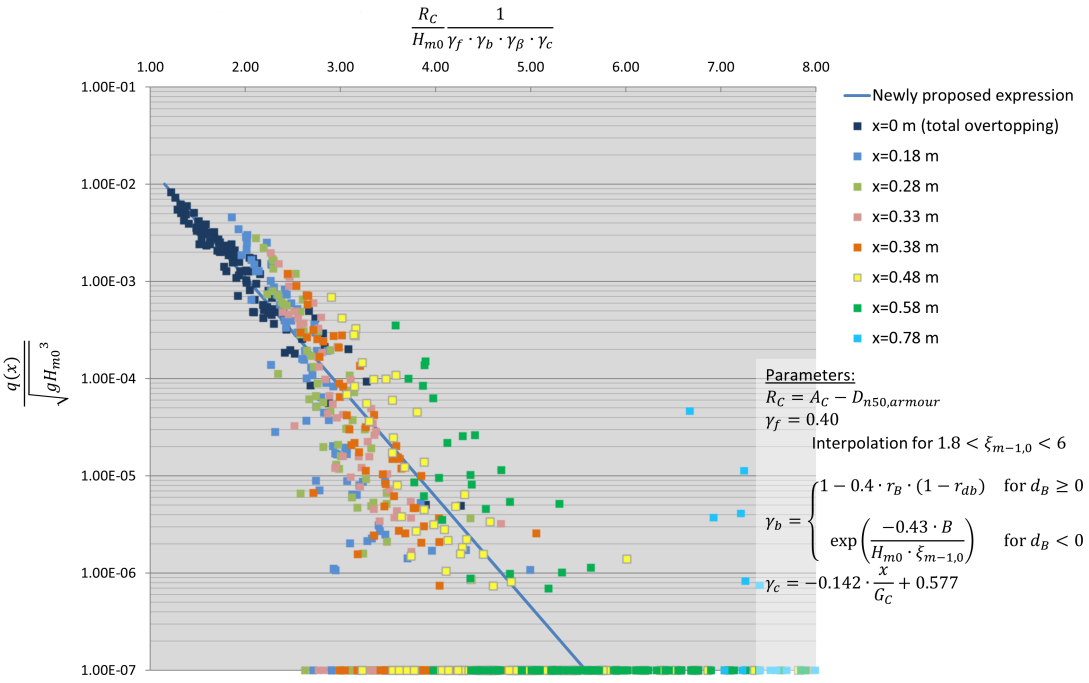


FIGURE 5.3-5: COMPARISON WITH LIOUTAS

The chosen $\gamma_c$ results in clear grouping of the experimental data based on location. Measurements that were taken at a location quite far from the crest are considerably underestimated by the prediction method.

### 5.3.4 OVERALL SPATIAL DISTRIBUTION OF OVERTOPPING

None of the above mentioned prediction methods adequately predicts the measurements done during the experiments. Therefore a new expression was sought for the spatial distribution of overtopping, which uses the same approach as Lioutas et al. (2012) chose. A parameter $\gamma_c$ is introduced to enlarge the dimensionless freeboard and thus make the prediction for the dimensionless overtopping discharge lower.

The following requirements were posed that the expression should meet:

1. For $x \leq 0$ no reduction should be taken into account.
2. $\lim_{x\to\infty} \gamma_c = 0$.
3. A good fit with the data should be established, especially for the larger overtopping discharges. The data cloud should not show any grouping based on horizontal position.

After data analysis an expression was found that makes use of a dimensionless number $x/H_{m0}$, see Equation 5.3-6. To facilitate design, the reference point $x = 0$ is now placed at the seaward edge of the crest. Theoretically there should be a difference in the spatial decay over the armour layer and over the backfill. However this difference could not be discerned from the data.

$$\gamma_c = \exp\left(-0.14 \cdot \frac{x}{H_{m0}}\right) \qquad \textit{Equation 5.3-6}$$

This expression leads to some reduction of scatter in the data. No grouping based on distance from the crest could be discerned. Furthermore the expression results in either a good fit with the data, for large overtopping discharges, or overestimation of overtopping, i.e. conservative design. The expression was found after data analysis and is entirely based on curve fitting; it does not have a theoretical basis.

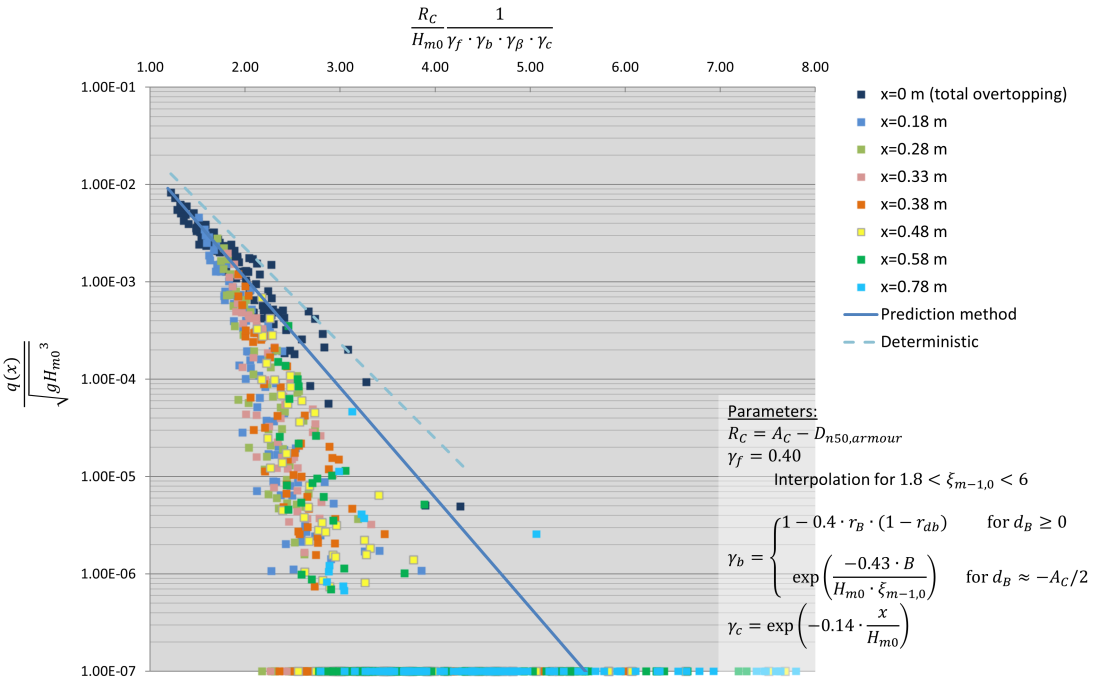


FIGURE 5.3-6: COMPARISON WITH PREDICTION METHOD

The plotted prediction method is printed below.

$$\frac{q(x)}{\sqrt{g \cdot H_{m0}^3}} = 0.2 \cdot \exp\left(-2.6 \cdot \frac{R_C}{H_{m0}} \frac{1}{\gamma_b \cdot \gamma_{f,surging} \cdot \gamma_\beta \cdot \gamma_c}\right) \qquad \textit{Equation 5.3-7}$$

$$\gamma_b = \begin{cases} 1 - 0.4 \cdot r_B \cdot (1 - r_{db}) & \text{for } d_B \geq 0 \\ \exp\left(\frac{-0.43 \cdot B}{H_{m0} \cdot \xi_{m-1,0}}\right) & \text{for } \frac{d_B}{A_c} \approx -0.5 \end{cases} \qquad \textit{Equation 5.3-8}$$

$$\gamma_{f,surging} = \begin{cases} \gamma_f & \text{for } \xi_{m-1,0} < 1.8 \\ \gamma_f + (\xi_{m-1,0} - 1.8) \cdot \frac{1 - \gamma_f}{4.2} & \text{for } 1.8 < \xi_{m-1,0} < 6 \\ 1.0 & \text{for } \xi_{m-1,0} > 6 \end{cases} \qquad \textit{Equation 5.3-9}$$

$$\gamma_c = \exp\left(-0.14 \cdot \frac{x}{H_{m0}}\right) \qquad \textit{Equation 5.3-10}$$

For deterministic design Equation 5.3-11 can be used.

$$\frac{q(x)}{\sqrt{g \cdot H_{m0}^3}} = 0.2 \cdot \exp\left(-2.25 \cdot \frac{R_C}{H_{m0}} \frac{1}{\gamma_b \cdot \gamma_{f,surging} \cdot \gamma_\beta \cdot \gamma_c}\right) \qquad \textit{Equation 5.3-11}$$

A large difference exists between the term found by Lioutas et al. (2012) and the term applicable to the current data set, see Figure 5.3-7. Rather than an improvement to Lioutas et al. (2012), the here presented expression serves as an illustration of the influence of the experiment setup. A particular peculiarity is that – in spite of an increased drainage capacity of the backfill – the $\gamma_c$ term of Lioutas et al. (2012) does not lead to conservative design. One would expect the overtopping discharge to decay more quickly with horizontal position.

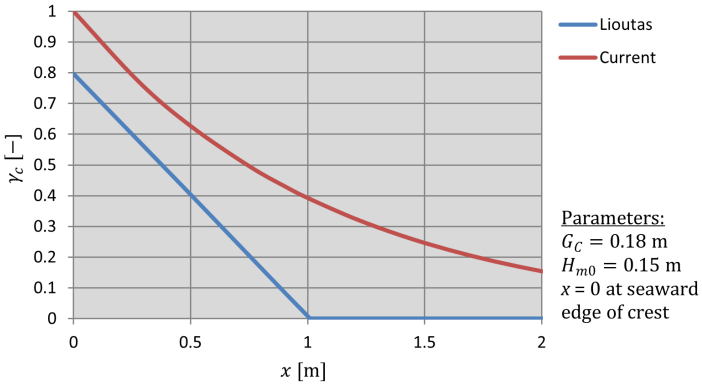


FIGURE 5.3-7: COMPARISON CURRENT $\gamma_c$ AND THE $\gamma_c$ TERM PROPOSED BY LIOUTAS ET AL. (2012)

Further research – using an alternative experiment setup – will be required to provide a more accurate picture of the spatial distribution of overtopping for irregular waves. The experiment setup is discussed extensively in Chapter 6.

### 5.3.5 CONCLUSIONS FOR $q(x)$

Comparison of the experimental data of the current research and that of Lioutas (2010) learned that the spatial distribution of overtopping is presumably strongly influenced by the used experiment setup. This influence is discussed separately in Chapter 6.

For the conditions as simulated during the experiments, the following conclusions can be drawn.

1. The spatial distribution of overtopping is associated with quite a lot of seemingly random behaviour.
2. The method of Juul Jensen (1984) does not accurately predict the experimental data. However the method can be used as an upper limit, i.e. conservative design.
3. The method of Van Kester (2009) does not accurately predict the experimental data. The chosen dimensionless parameter does not lead to reduction of scatter in the data.
4. The $\gamma_c$ term of Lioutas et al. (2012) leads to considerable grouping in the data based on horizontal position. The method is not conservative for the experimental data of the current research.
5. A different $\gamma_c$ term is presented, see Equation 5.3-12. This expression does result in reduction of scatter in the data and is conservative for the current data set.

$$\gamma_c = \exp\left(-0.14 \cdot \frac{x}{H_{m0}}\right) \qquad \textit{Equation 5.3-12}$$

6. The difference between the $\gamma_c$ term of Lioutas et al. (2012) and Equation 5.3-12 is thought to originate from the difference in experiment setup.

# CHAPTER 6. EXPERIMENT SETUP DISCUSSION

During the conduction of the experiments it became clear that the current experiment setup may deviate from the prototype on some important points. These possible flaws only concern the spatial distribution of overtopping; no errors are induced for the total overtopping.

First possible deficiencies in the current test setup are discussed in section 6.1. Subsequently in section 6.2 an experiment program is presented to investigate the impact on the experiment outcome. Section 6.3 discusses improvements that can be made to the experiment setup.

## 6.1 POSSIBLE FLAWS IN THE CURRENT TEST SETUP

The spatial distribution of overtopping depends strongly on the infiltration of the overtopped water in the collection bins. Two model effects can be distinguished in the current experiment setup.

### 6.1.1 INTERNAL WATER LEVEL

The internal water level inside a breakwater fluctuates as a result of wave attack. Waves running up the slope lead to infiltration of water and elevation of the phreatic level. During downwash water flows out of the slope. Averaged over time the phreatic level lies just above SWL (Abbott & Price, 1994). Refer to Figure 6.1-1.

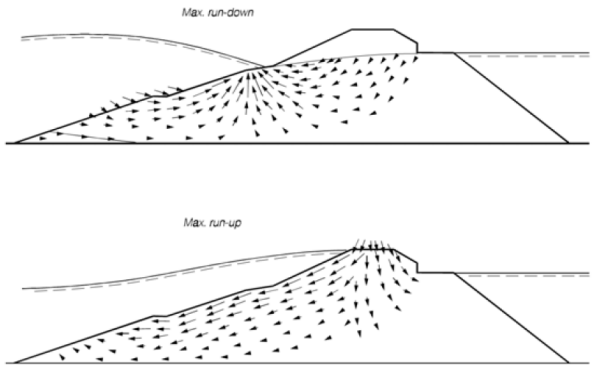


FIGURE 6.1-1: PHREATIC LEVEL IN A BREAKWATER (ABBOTT & PRICE, 1994)

In the experiment setup as used in both Lioutas (2010) and the current research, the water level in the collection bins was significantly lower than SWL, see Figure 6.1-3. At the start of each experiment the collection bins were completely empty. Therefore in the experiment setup more water could be stored per linear meter than would be the case in reality. Figure 6.1-2 and Figure 6.1-3 illustrate the difference.

FIGURE 6.1-2: IMPRESSION OF THE INTERNAL WATER LEVEL IN REALITY

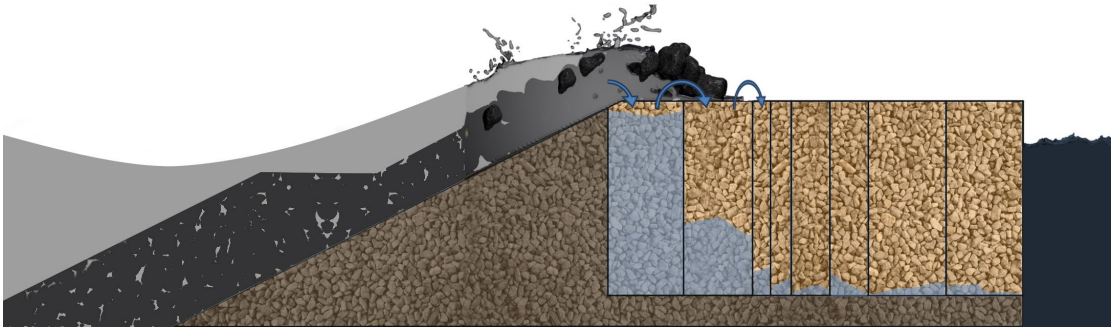

FIGURE 6.1-3: IMPRESSION OF THE INTERNAL WATER LEVEL IN THE EXPERIMENT SETUP

### 6.1.2 INFILTRATION VELOCITY

As discussed in section 3.6.1.3 in the current research the infiltration velocity was set equal for each collection bin. This was already an improvement made to the setup used by Lioutas (2010). Now the infiltration velocity of the water was at least quantifiable.

However in reality the infiltration process of overtopped water is very complex. The movement of water falling on a porous medium first should be described with a model for unsaturated flow. Then, when the internal water table has risen, the flow can be described with a model for saturated flow in porous media, e.g. can be described with a model for saturated flow in porous media, e.g. the Extended Forchheimer equation. The infiltration speed of the water is a variable in the differential equations and needs to be solved in combination with other parameters such as the layer depth of the overflowing water and the height of the internal water table.

Therefore it is likely the drainage capacity as it was modelled in the experiments differs from the prototype situation. The drainage capacity of the backfill material determines how much water is removed from a collection bin in the time between two waves. Consequently the amount of water of a wave that can be stored at the seaward end of the breakwater is determined by the drainage capacity, and thereby the spatial distribution of overtopping is affected.

## 6.2 DETERMINATION OF INFLUENCE ON SPATIAL DISTRIBUTION

The influence of both deficiencies should be quantified to determine to what extent the data sets of Lioutas (2010) and the current research have been affected. It is advised to conduct a small number of additional experiments. A minimum of four experiments would have to be repeated for different configurations of pump capacity and extraction depth. No berm needs to be applied in the scale model.

### 6.2.1 EXPERIMENT PROGRAM

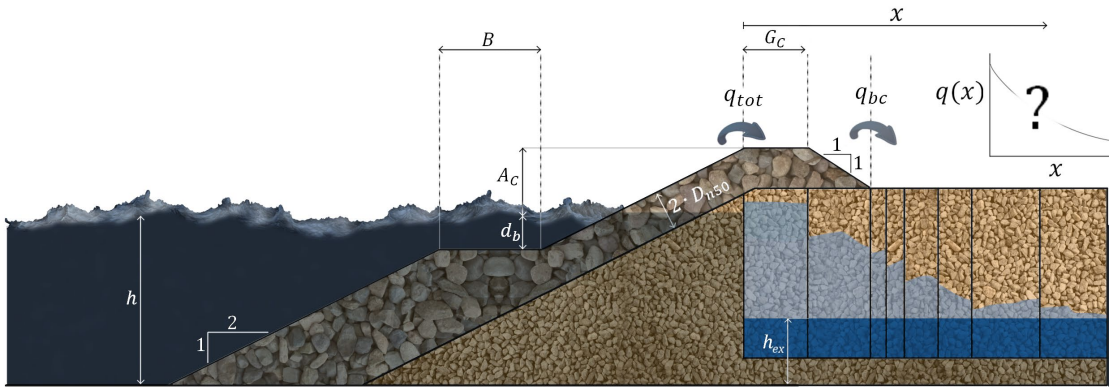


FIGURE 6.2-1: EXPERIMENT SETUP TO INVESTIGATE DRAINAGE INFLUENCE

In the experiments displacement pumps are used to extract water from the collection bins. The level at which the water is extracted defines the minimum water level inside the collection bin. The combination of extraction depth and pump discharge determines how much water can be stored in a collection bin when a wave overtops the structure.

Running the experiments for different values of the water extraction depth $h_{ex}$ and the pump capacity $u_{drain}$ can determine whether these parameters significantly influence the spatial distribution of overtopping that is found.

The following experiment program is suggested.

TABLE 6-1: EXPERIMENT PROGRAM: FIXED PARAMETERS

| $h$ [m] | slope $\tan(\alpha)$ | $A_C$ [m] |
|---|---|---|
| 0.52 | 1/2 | 0.18 |

TABLE 6-2: EXPERIMENT PROGRAM: WAVE CONDITION PARAMETERS

| Experiment code | $H_{m0}$ [m] | $s_{m-1,0}$ [−] |
|---|---|---|
| V01 | 0.10 | 0.01 |
| V14 | 0.06 | 0.01 |
| V03 | 0.16 | 0.05 |
| V02 | 0.12 | 0.05 |

TABLE 6-3: EXPERIMENT PROGRAM: PARAMETERS RELATED TO DRAINAGE CAPACITY

| $h_{ex}$ [m] | $u_{drain}$ [$m^3/m^2/s$] |
|---|---|
| 0.15 | 0.0025 |
| 0.52 | 0.0015 |

The extraction depth $h_{ex}$ [m] is here defined as the vertical distance between the bottom of the flume and the lowest elevation in the collection bins from which water can be extracted. In the current experiments PVC-tubes were attached to the walls of the collection bins, through which the displacement pumps could transport the overtopped water. $h_{ex} = 0.15$ m in the current experiments.

The falling velocity $u_{drain}$ indicates the average drainage capacity per bin. In the current experiments $u_{drain}$ = 0.0025 m³/m²/s was used. In prototype scale this would amount to a time-average falling velocity in the backfill material of 1 cm/s, which seems to be in the right order of magnitude. The required pump discharge per collection bin can be calculated by multiplying $u_{drain}$ with the length and width of the collection bin. Experiments should be carried out again for a falling velocity in the same order of magnitude, but significantly different from what was used in the current research. $u_{drain}$ = 0.0015 m³/m²/s is suggested.

It is advised to carry out additional experiments as described Table 6-1 to Table 6-3. Four different wave conditions should be tested. Also four variations should be made for the backfill infiltration properties.

An amount of $2 * 2 * 4 = 16$ experiments would suffice to give an impression of the influence of the drainage capacity on the spatial distribution of overtopping.

### 6.2.2 ASSESSMENT OF INFLUENCE

To assess the influence of the experiment setup some very elementary graphs should be plotted, similar to Figure 6.2-2.

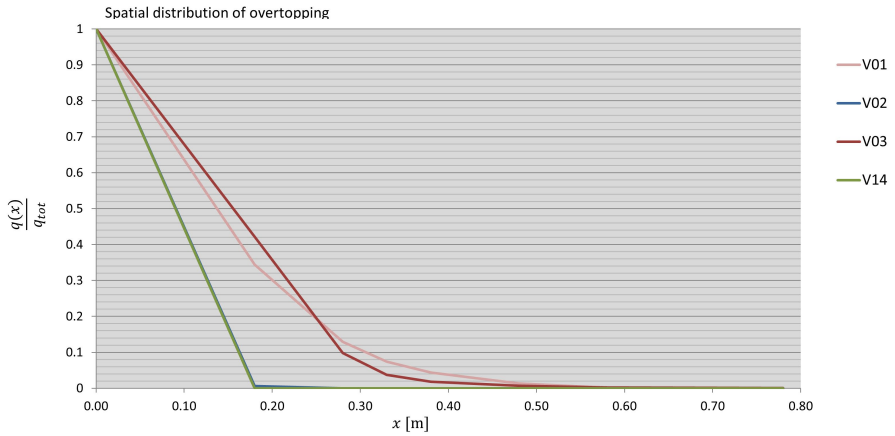


FIGURE 6.2-2: SPATIAL DISTRIBUTION OF OVERTOPPING PER EXPERIMENT

The sole purpose of these tests would be to determine whether there is a significant influence of the drainage capacity in the collection bins. It is expected the spatial decay of overtopping will be gentler for smaller drainage capacities in the bins. In the graphs this would be expressed as curves declining more slowly.

## 6.3 IMPROVEMENTS IN THE EXPERIMENT SETUP

Ideally a physical experiment setup is made where infiltration of overtopped water into the backfill is correctly modelled from the prototype situation. Furthermore wave propagation should not be hindered by constructions inside the scale model. Then for different horizontal positions vertical cross-sections can be defined where the water discharge should be measured without disruption of the water.

There are two options to determine the overtopping discharge at a particular location. One method is to continuously measure velocity and water depth of the water flow above the backfill. The flow over the backfill consists for a large part of air-water mixture so that also the fluid density should somehow be measured. With these measurements one would be able to calculate the mean overtopping discharge. However to the best of my knowledge no equipment is available that can accurately measure these quantities.

A second method is to collect overtopped water that passes the location of interest. This method is commonly chosen in research that focuses on overtopping. Also in the current research this method was applied. When the overtopping discharge at one location in the scale model is required no problems arise. However when overtopping discharges need to be determined for multiple locations in the same experiment the overtopped water cannot simply be collected in collection bins. The drainage capacity in those bins would have to depend on all influencing parameters to correctly simulate the infiltration of overtopped water in the backfill material. Water pressures in the collection bins would have to be measured, a computer should in real-time calculate the infiltration speed and the discharge of the displacement pumps should be computer-controlled. It can be concluded that this results in quite a complicated and not too feasible scale model.

One could also opt for a numerical approach, simulating the water motion computationally. Then all quantities required to calculate the overtopping discharge can be computed at the same time-step. Computationally combining the Navier-Stokes equations for external water motion, the Extended Forchheimer equation for internal water motion and adding a model for unsaturated flow theoretically could lead offer a solution. However, let alone the computational challenges, the results still would have to be validated with a physical model.

### RECOMMENDED EXPERIMENT SETUP

A physical model is desired where overtopped water is collected and where the infiltration behaviour of overtopped water is correctly simulated. This can be established by physically dividing the model into two parts. At one side the overtopped water directly behind the crest is collected, while on the other side the overtopping at a certain distance from the end of the crest can be stored. As any method also this experiment setup has some drawbacks. Investigating the spatial distribution of overtopping for one specific wave spectrum will require multiple tests to be run. Therefore less wave conditions can be tested per value of time compared to the current experiment setup. Furthermore wave conditions as generated by the wave generator will never be exactly the same. However, because quantities are made dimensionless, it is expected this will bring about only small errors.

The recommended experiment setup is visualized in Figure 6.3-1. A vertical plane physically separates the two sides of the flume. The plane should run to the very bottom

of the flume tank as to prevent exchange of water inside the breakwater. In Appendix L the recommended experiment setup is illustrated more extensively.

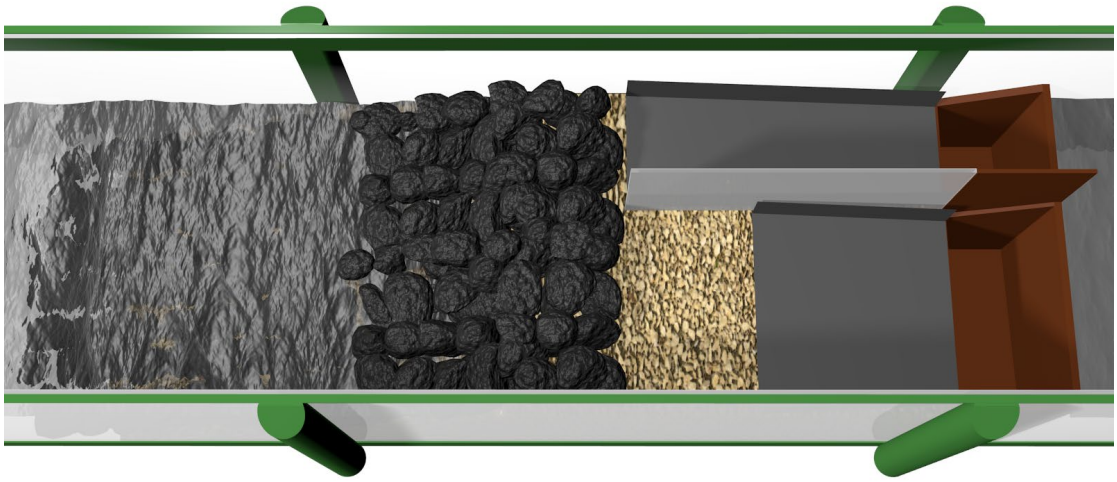

FIGURE 6.3-1: IMPRESSION OF THE RECOMMENDED EXPERIMENT SETUP

It is advised to run experiments for 5 different horizontal positions behind the crest. In the current experiments at 0.60 m behind the crest scarcely any overtopped water was collected. Therefore this point is recommended as the farthest distance at which the overtopping discharge should be measured.

Per wave condition 4 experiments should be run. Refer to Table 6-4.

TABLE 6-4: EXPERIMENT PROGRAM: DISTANCES BEHIND END OF CREST

| Experiment number | Position chute 1 [m] | Position chute 2 [m] |
|---|---|---|
| 1 | 0.00 | 0.15 |
| 2 | 0.00 | 0.30 |
| 3 | 0.00 | 0.45 |
| 4 | 0.00 | 0.60 |

By measuring the overtopping discharge directly behind the crest for each experiment, a check can be performed if overtopping conditions are sufficiently similar. For these 4 experiments it is desired to simulate exactly the same overtopping conditions such that the spatial distribution of overtopping can be determined properly.

Construction drawings and some other recommendations are presented in Appendix L.

### POINTS OF CONSIDERATION

In Figure 6.3-1 two chutes are visible that collect overtopped water. Still displacement pumps are needed to pump the water from the chutes to floating tanks, as to prevent lowering of the water table. The pump capacity of these pumps must be sufficiently large, such that the chutes will never overflow.

Correct simulation of the infiltration of overtopping requires a correct scaling of the permeability of the backfill material. The method described in Burcharth et al. (1999) can be taken as a starting point. However it should be investigated if the flow inside the breakwater may still be regarded as one-dimensional flow.

Furthermore the boundary conditions at the landward end of the breakwater should be selected. In the recommended experiment setup the landward end of the breakwater is separated from the water behind the breakwater by means of an impermeable sheet of wood. Outflow of water at the landward end of the breakwater is not possible in this setup. This choice depends on the prototype that needs to be modelled. In the setup backfill material underneath the chutes can still be used to store overtopped water. This is a model effect and needs to be minimized.

Plastic pipelines at the bottom of the tank should ensure both sides of the flume are hydraulically connected and water can be exchanged. In that way the water level in front of the breakwater remains constant.

# CHAPTER 7. CONCLUSIONS AND RECOMMENDATIONS

This chapter discusses the main results from the present study. A comparison is drawn with the research objectives as discussed in section 1.3. First conclusions are drawn in section 7.1. Then recommendations for further research are given in section 7.2.

## 7.1 CONCLUSIONS

The research objectives were stated as follows in section 1.3.

> *To provide insight in the overtopping phenomenon for breakwaters with a non-reshaping berm. When existing prediction methods do not accurately describe the relations found, it is the intention to recommend a method that properly describe the experimental data. In the end the aim is to provide more accurate guidance in the design practice of breakwaters. Both total overtopping and the spatial distribution of overtopping will be investigated.*

The findings of this research are separately presented for total overtopping and the spatial distribution of overtopping.

### TOTAL OVERTOPPING

1.1. Existing prediction formulae do not accurately predict the overtopping discharges measured in the experiments. Grouping based on breaker parameter and berm configuration was observed.

1.2. Based on the experimental data, the crest freeboard should be adjusted to account for the permeability of the crest. A good fit is achieved when the crest freeboard is defined as $R_C = A_C - D_{n50,armour}$.

1.3. The recommendation of Lioutas (2010) to use $\gamma_f = 0.45$ instead of $\gamma_f = 0.40$ was not found to be applicable for the current experimental data.

1.4. The Adjusted TAW prediction formula as suggested by Lioutas et al. (2012) accurately predicts the overtopping discharge of the validation tests of the current research experiment programme. The expression effectively removes any data grouping based on the breaker parameter. Overtopping for breakwaters with a berm was not properly predicted.

1.5. A new expression for total overtopping is proposed. Being a variation on the Adjusted TAW, this new prediction method removes the grouping on breaker parameter by adapting the $\gamma_f$ reduction factor. For long waves the roughness of the armour slope does not lead to reduction of overtopping. The upper limit of $\gamma_f$ for $\xi_{m-1,0} = 10$ is changed to $\xi_{m-1,0} = 6$. See Equation 7.1-3.

$$\frac{q_{tot}}{\sqrt{g \cdot H_{m0}^3}} = \mathrm{C} \cdot \exp\left(-\mathrm{D} \cdot \frac{R_C}{H_{m0}} \frac{1}{\gamma_b \cdot \gamma_{f,surging} \cdot \gamma_\beta}\right) \qquad \textit{Equation 7.1-1}$$

where:

$$R_C = A_C - D_{n50,armour} \qquad \textit{Equation 7.1-2}$$

$$\gamma_{f,surging} = \begin{cases} \gamma_f & \text{for } \xi_{m-1,0} < 1.8 \\ \gamma_f + \left(\xi_{m-1,0} - 1.8\right) \cdot \dfrac{1 - \gamma_f}{4.2} & \text{for } 1.8 < \xi_{m-1,0} < 6 \\ 1.0 & \text{for } \xi_{m-1,0} > 6 \end{cases} \qquad \textit{Equation 7.1-3}$$

1.6. In the current experiments the effect of a permeable berm on total overtopping is found to be remarkably different from the effect of impermeable berms as calculated by TAW (2002). Below SWL a permeable berm leads to less reduction of overtopping than an impermeable berm. In spite of the rough character of a permeable berm overtopping is reduced less effectively; presumably because wave propagation within the berm is to a certain extent possible. Berms above SWL lead to wave breaking on the slope in front of the berm, and act more as an extended crest. Contrarily to impermeable berms above SWL, a permeable berm above SWL leads to significant energy dissipation of run-up.

1.7. In the experimental data grouping based on berm dimensions was removed by applying a new expression for $\gamma_b$, see Equation 7.1-4. In the current research a very permeable berm was used, constructed from armour stones. For this configuration $f_{dB\geq 0} = 0.4$ and $f_{dB<0} = 0.43$ lead to an excellent fit.

$$\gamma_b = \begin{cases} 1 - f_{dB\geq 0} \cdot r_B \cdot (1 - r_{db}) & \text{for } d_B \geq 0 \\ \exp\left(\dfrac{-f_{dB<0} \cdot B}{H_{m0} \cdot \xi_{m-1,0}}\right) & \text{for } \dfrac{d_B}{A_c} \approx -0.5 \end{cases} \qquad \textit{Equation 7.1-4}$$

1.8. When the proposed expression for $\gamma_b$ is used in the Adjusted TAW formula this leads to a significantly better fit. Still the proposed expression printed in Equation 7.1-1 performs better.

1.9. Only one berm elevation above SWL was tested during the current research. Until further experiments are conducted it is advised to interpolate linearly between the two provided expressions in cases where $-0.5 < \frac{d_B}{A_c} < 0$.

### LANDWARD SPATIAL DISTRIBUTION OF OVERTOPPING

Comparison of the experimental data of the current research and that of Lioutas (2010) learned that the spatial distribution of overtopping is presumably strongly influenced by the used experiment setup.

For the conditions as simulated during the experiments, the following conclusions can be drawn.

2.1. The spatial distribution of overtopping is associated with quite a lot of seemingly random behaviour.

2.2. The method of Juul Jensen (1984) does not accurately predict the experimental data. However the method can be used as an upper limit, i.e. conservative design.

2.3. The method of Van Kester (2009) does not accurately predict the experimental data. The chosen dimensionless parameter does not lead to reduction of scatter in the data.

2.4. The $\gamma_c$ term of Lioutas et al. (2012) leads to considerable grouping in the data based on horizontal position. The method is not conservative for the experimental data of the current research.

2.5. A different $\gamma_c$ term is presented, see Equation 7.1-5. This expression does result in reduction of scatter in the data and is conservative for the current data set.

$$\gamma_c = \exp\left(-0.14 \cdot \frac{x}{H_{m0}}\right) \qquad \textit{Equation 7.1-5}$$

2.6. The difference between the $\gamma_c$ term of Lioutas et al. (2012) and Equation 7.1-5 is thought to originate from the difference in experiment setup.

## 7.2 RECOMMENDATIONS

Recommendations that can be stated as a result of this thesis are listed below.

### VALIDATION OF THE PROPOSED EXPRESSION

For the experimental data sets of Lioutas (2010) and the current research the proposed expression as printed in Equation 7.1-1 leads to an excellent fit. These data sets contain a variety of seaward slopes, water depths, wave heights, wave periods, berm elevations and berm widths. It is advised to compare other data sets for total overtopping with the proposed expression. Special attention should be paid to the way overtopped water is collected in the experiments from which the data originates. In the current research also water propagating through the crest was labelled as total overtopping. When in an experiment overtopping is collected with a chute positioned at $A_C$ it is clear the crest freeboard definition found in this thesis is not applicable.

### CREST FREEBOARD DEFINITION

Based on the current experiments – where only permeable crest have been tested – theoretically it cannot be concluded that the crest freeboard definition should be adjusted. It is recommended to conduct experiments where solely the crest freeboard definition is investigated. In these tests the crest permeability should be varied and overtopped water should be collected at the seaward edge of the crest, at the underside of the armour layer.

### INFLUENCING PARAMETERS

The most important parameters were included in the current experiments. This experimental data was accurately predicted by the proposed prediction method. However there are several other factors that influence the overtopping discharge, which have not been tested. It is recommended to study the influence of the following parameters. Per parameter it is indicated for the influence can be investigated.

- Hydraulic conditions
  - Oblique waves. A physical model can be tested in a 3D wave basin to investigate this effect.
  - Wind action. Wave spray created by the interaction between waves and breakwater can be carried over the crest by wind. An upper limit can be determined using a physical model in a wave flume. Above the area of wave breaking a structure – e.g. a paddle wheel – can be made to transport all wave spray to a collection bin. However the formation of droplets is not scaled correctly in a Froude model. Being strongly influenced by surface tension effects, the production of wave spray should be scaled such that the Weber number remains constant. A large scale model is recommended to decrease model effects.
- Physical dimensions
  - Crest width. A physical model as recommended in section 6.3 can be used in a wave flume. Several crest widths should be tested.
  - Presence of an under layer. In the current research a simplified breakwater configuration was used. A more veracious scale model is recommended which can be tested in a wave flume. Internal water flow inside the breakwater should be scaled correctly. Generally this results in non-geometric scaling (see Burcharth et al. (1999)).

### PERMEABLE BERMS

The berm dimensions covered in the current experiments were taken properly into account by a new expression for $\gamma_b$. Berms above SWL were accounted for by means of a reduction factor with an exponential function. The proposed function does however not contain the berm elevation, as only one berm elevation above SWL was tested. For $-1 < \frac{d_B}{A_C} < 0$ more experiments are advised as to improve the found relation.

Furthermore the berms used in this research were entirely constructed with armour material. In reality part of the berm is constructed with core material as to deliver a more economical design. This leads to a lower permeability of the berm. It is recommended to investigate this more veracious setting.

Permeable berms were found to have a lesser overtopping reducing effect than calculated by TAW (2002) for impermeable berms. In section 4.3 a qualitative reasoning was given, but no thorough insight exists on the processes that cause this effect. It is recommended to study the propagation of wave energy in the vicinity of a berm. Tests should be run for both permeable and impermeable berms. As a first step regular waves can be used.

### EXPERIMENT SETUP

As discussed in Chapter 6 the current experiment setup may give rise to a larger drainage capacity of the backfill than would be the case in reality. It is advised to investigate the influence of the experiment setup as described in section 6.2. A more veracious experiment setup is presented in section 6.3. It is recommended not to use collection bins inside the breakwater as to not disturb the internal water flow. Instead it is recommended to repeat tests and collect overtopped water at a different position for each experiment. Moreover the backfill should be split longitudinally, so that for each experiment also the overtopping directly behind the crest can be collected. In that way the fraction $q(x)/q_{bc}$ can be determined, disregarding small differences in overtopping behaviour that may exist between the different experiments.

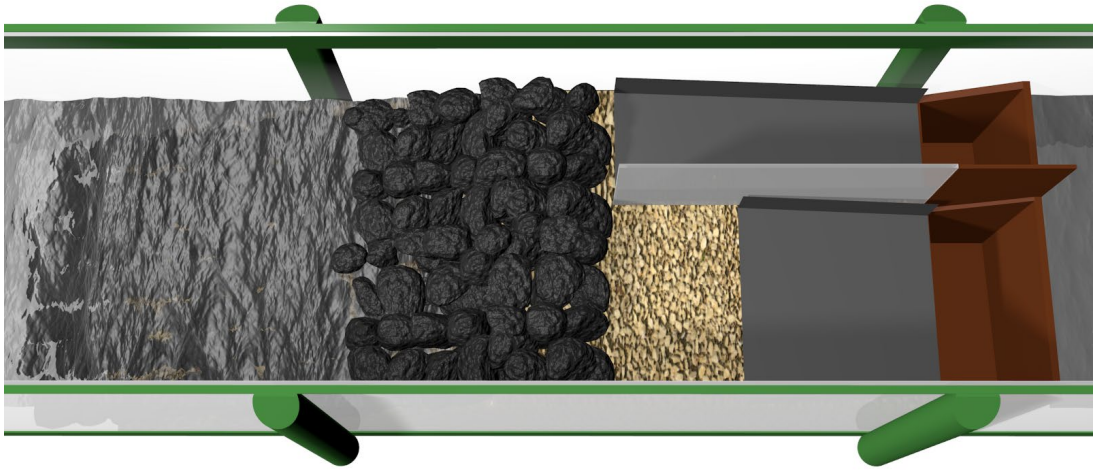

FIGURE 7.2-1: IMPRESSION OF THE RECOMMENDED EXPERIMENT SETUP

# BIBLIOGRAPHY


Abbott, M. B., & Price, W. A. (1994). *Coastal, estuarial, and harbour engineers' reference book*. London: Chapman & Hall.

Allsop, N. W. H., Franco, L., Bellotti, G., Bruce, T., & Geeraerts, J. (2005). *Hazards to people and property from wave overtopping at coastal structures.* Paper presented at the International conference on coastlines, structures and breakwaters 2005, London, UK.

Besley, P. (1999). Wave overtopping of seawalls - design and assessment manual *R&D Technical Report W178*: HR Wallingford.

Bruce, T., Van der Meer, J. W., Franco, L., & Pearson, J. M. (2009). Overtopping performance of different armour units for rubble mound breakwaters. *Coastal Engineering, 56*, 166-179.

Burcharth, H. F., Liu, Z., & Troch, P. (1999). *Scaling of Core Material in Rubble Mound Breakwater Model Tests.* Paper presented at the COPEDEC V, Cape Town, South Africa.

De Waal, J. P., & Van der Meer, J. W. (1992). *Wave runup and overtopping on coastal structures.* Paper presented at the 23rd ICCE, Venice, Italy.

EurOtop. (2007). Wave overtopping of sea defences and related structures: assessment manual. Heide i. Holstein: EA-Environmental Agency, UK; ENW-Expertise Netwerk Waterkeren, NL; KFKI-Kuratorium für Forschung im Küsteningenieurwesen, DE.

Forchheimer, P. (1901). Wasserbewegung durch boden. *Zeitschrift verein Deutscher Ingenieure, 45*, 1782-1788.

Goda, Y. (1985). *Random seas and design of maritime structures*: University of Tokio Press.

Hawkes, P. J., Coates, T. T., & Jones, R. J. (1998). Impact of bi-modal seas on beaches and control structures (pp. 6-13). Wallingford: HR Wallingford.

Holthuijsen, L. H. (2007). *Waves in Oceanic And Coastal Waters*. Cambridge: Cambridge University Press.

Hughes, S. A. (1993). *Physical Models and Laboratory Techniques in Coastal Engineering*: Coastal Engineering Research Center, Waterways Experiment Station, USA.

Juul Jensen, O. (1984). *A monograph on rubble mound breakwaters*. Hørsholm, Denmark: Danish Hydraulic Institute.

Kennisbank Waterbouw. (2012). International Breakwater Directory, from http://www.kennisbank-waterbouw.nl/breakwaters/details.php?id=143

Lioutas, A. C. (2010). *Experimental research on Spatial Distribution of Overtopping.* (M.Sc.), Delft University of Technology, Delft. Retrieved from http://repository.tudelft.nl/assets/uuid:0122fe2e-0260-489f-b258-6e167fa9a621/Final_report_-_A.Lioutas-1.pdf

Lioutas, A. C., Smith, G. M., & Verhagen, H. J. (2012). *Spatial Distribution of Overtopping*. Paper presented at the 33rd ICCE, Santander, Spain.

Lykke Andersen, T. (2006). *Hydraulic Response of Rubble Mound Breakwaters: scale effect - berm breakwaters.* (PhD.), Aalborg University. (Series Paper; 27)

Lykke Andersen, T., & Burcharth, H. F. (2004). D24 Report on additional tests: Aalborg University.

Lykke Andersen, T., & Burcharth, H. F. (2006). *Landward distribution of wave overtopping for rubble mound breakwaters.* Paper presented at the first international conference on the application of physical modelling to port and coastal protection, Porto, Portugal.

Owen, M. W. (1980). Design of seawalls allowing for wave overtopping: HR Wallingford.

Pearson, J. M., Bruce, T., Franco, L., Van der Meer, J. W., Falzacappa, M., & Molino, R. (2004). Roughness factor *CLASH report EVK3-CT-2001-00058*.

Peng, Z., & Zou, Q.-P. (2011). Spatial distribution of wave overtopping water behind coastal structures. *Coastal Engineering, 58*, 489-498.

PIANC. (2003). State-of-the-art of designing and constructing berm breakwaters. Brussels: MarCom WG22.

Rock Manual. (2007). The Use of Rock in Hydraulic Engineering: CIRIA-CUR-CETMEF.

Schiereck, G. J. (2001). *Introduction to bed, bank and shore protection*. Delft: Delft University Press.

Shi-igai, H., & Kono, T. (1970). *Analytical approach on wave overtopping on levees.* Paper presented at the 12th Conference on Coastal Engineering, Washington, D.C.

Sigurdarson, S., Jacobsen, A., Smarason, O. B., Bjørdal, S., Viggosson, G., Urrang, C., & Tørum, A. (2003). Sirevåg Berm Breakwater, design, construction and experience after design storm *Coastal Structures 2003* (pp. 1212-1224). Portland, Oregon: ASCE.

Steenaard, J. (2002). *Verdeling van overslaand water over een golfbreker.* (M.Sc.), Delft University of Technology, Delft. Retrieved from http://repository.tudelft.nl/assets/uuid:5f6f0f6f-9001-40a6-9724-b61b0696e7a4/2002Steenaard.pdf

TAW. (1974). Wave run-up and overtopping: Technical Advisory Committee on Water Defences in The Netherlands. .

TAW. (2002). Technical report on wave run-up and wave overtopping at dikes: Technical Advisory Committee on Water Defences, The Netherlands.

Van der Meer, J. W. (1988). *Rock slopes and gravel beaches under wave attack.* (PhD), Delft University of Technology, Delft.

Van Gent, M. R. A., Smith, G. M., & Van der Werf, I. M. (2012). *Stability of Rubble Mound Breakwaters with a Berm: the Upper Slope.* Paper presented at the 33rd ICCE, Santander, Spain.

Van Kester, D. C. P. (2009). *Spatial distribution of wave overtopping.* (M.Sc.), Delft University of Technology. Retrieved from http://repository.tudelft.nl/assets/uuid:5e91b150-3d62-462e-83f0-0efe570df822/Final_report.pdf

Verhagen, H. J., d'Angremond, K., & Roode, F. v. (2009). *Breakwaters and closure dams*. Delft: VSSD.

Warnock, J. E. (1950). Hydraulic similitude. *Engineering Hydraulics*, 136-176.

Zelt, J. A., & Skjelbreia, J. E. (1992). *Estimating incident and reflected wave fields using an arbitrary number of wave gauges.* Paper presented at the 23rd ICCE, Venice, Italy.

# APPENDICES

## APPENDIX A. REDUCTION FACTOR TO ACCOUNT FOR A BERM

The $\gamma_b$ factor that is recommended in the proposed expression contains multiple important adjustments compared with the term that is used in the TAW formulae. The reduction factor is split into two parts; one for berms at or below SWL and one term for berms above SWL. See Equation A-1.

$$\gamma_b = \begin{cases} 1 - f_{dB\geq 0} \cdot r_B \cdot (1 - r_{db}) & \text{for } d_B \geq 0 \\ \exp\left(-f_{dB<0} \cdot \dfrac{B}{H_{m0} \cdot \xi_{m-1,0}}\right) & \text{for } d_B < 0 \end{cases} \qquad \textit{Equation A-1}$$

For the current experiment setup $f_{dB\geq 0} = 0.4$ and $f_{dB<0} = 0.43$ were found applicable.

The experimental data indicated that in the two terms a different dimensionless berm width should be used; using the same dimensionless number would result in grouping based on Iribarren number. $\gamma_b$ for $d_B \geq 0$ traditionally uses $\frac{B}{L_{Berm}}$, but for $d_B < 0$ $\frac{B}{H_{m0} \cdot \xi_{m-1,0}}$ was found.

This creates a problem when the influence of the berm elevation should be presented. There is no possibility to present a universal graph indicating the influence of the berm elevation. Instead the influence of the berm elevation is indicated for a few specific configurations. See Figure A-1 and Figure A-2.

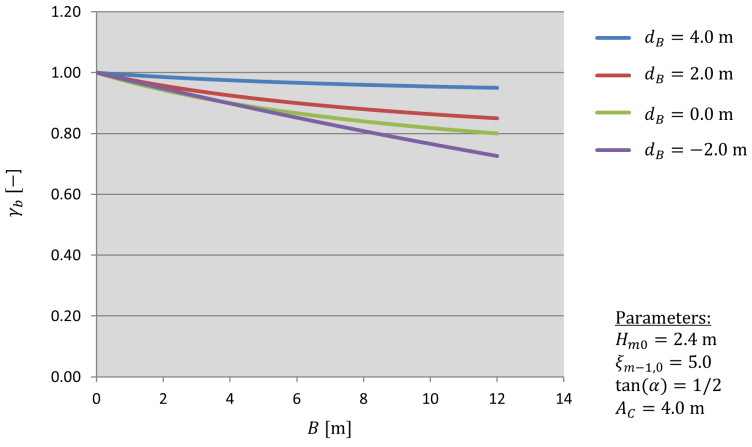


FIGURE A-1: INFLUENCE OF BERM ELEVATION FOR TYPICAL SWELL CONDITIONS

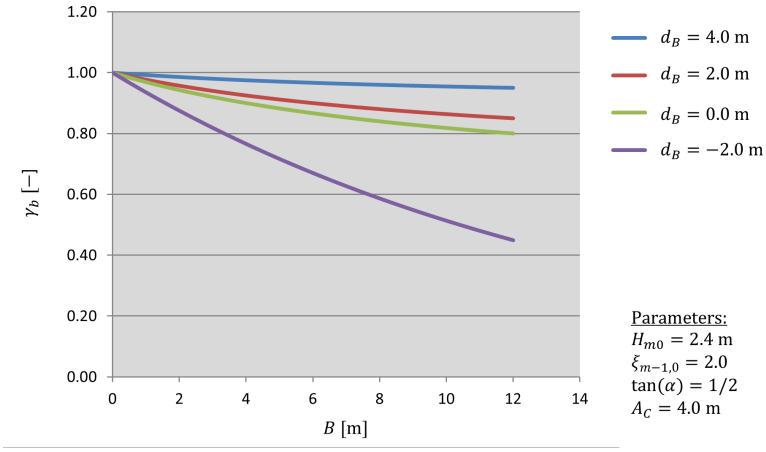


FIGURE A-2: INFLUENCE OF BERM ELEVATION FOR TYPICAL WIND WAVE CONDITIONS

TABLE A-1: EXPRESSIONS PER BERM ELEVATION

| Berm elevation | Expression |
|---|---|
| $d_B = 4.0$ m | $\gamma_b = 1 - f_{dB\geq 0} \cdot r_B \cdot (1 - r_{db})$ |
| $d_B = 2.0$ m | |
| $d_B = 0.0$ m | |
| $d_B = -2.0$ m | $\gamma_b = \exp\left(-f_{dB<0} \cdot \frac{B}{H_{m0} \cdot \xi_{m-1,0}}\right)$ |

Because the water depth was varied for berm configurations C and F, two different berms elevations were tested, albeit with only 2 cm difference. When a best fit is determined for both berm elevations, the already observed – higher berms lead to more reduction – is confirmed, see Figure A-3. For $d_B$=-0.08 m $f_{dB<0} = 0.39$ was found, and for $d_B$=-0.10 m $f_{dB<0} = 0.47$.

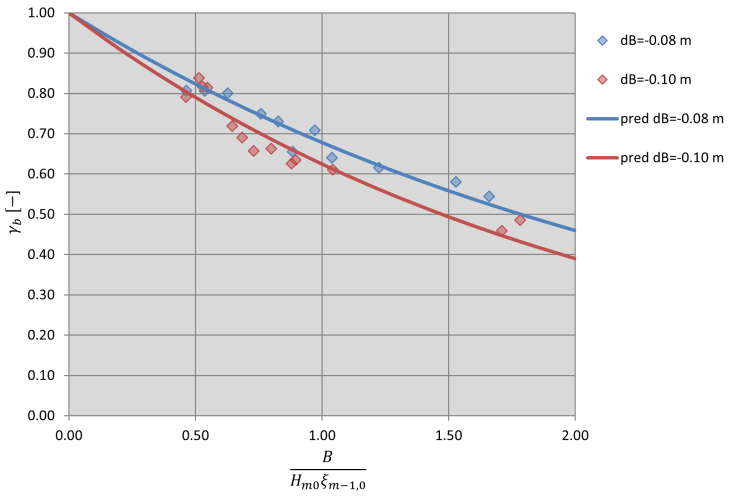


FIGURE A-3: INFLUENCE OF BERM ELEVATION ON OVERTOPPING REDUCTION

## APPENDIX B. NEW EXPRESSION FOR $\gamma_b$ APPLIED TO ADJUSTED TAW

For the proposed expression grouping of the data based on breakwater configuration was neutralized by means of an adapted $\gamma_b$-factor. To make a proper comparison between the proposed expression and the Adjusted TAW formula, the new $\gamma_b$ factor should also be applied to the Adjusted TAW method.

Figure B-1 illustrates that also for this prediction method, the new expression for $\gamma_b$ is able to remove grouping of the data based on berm dimensions.

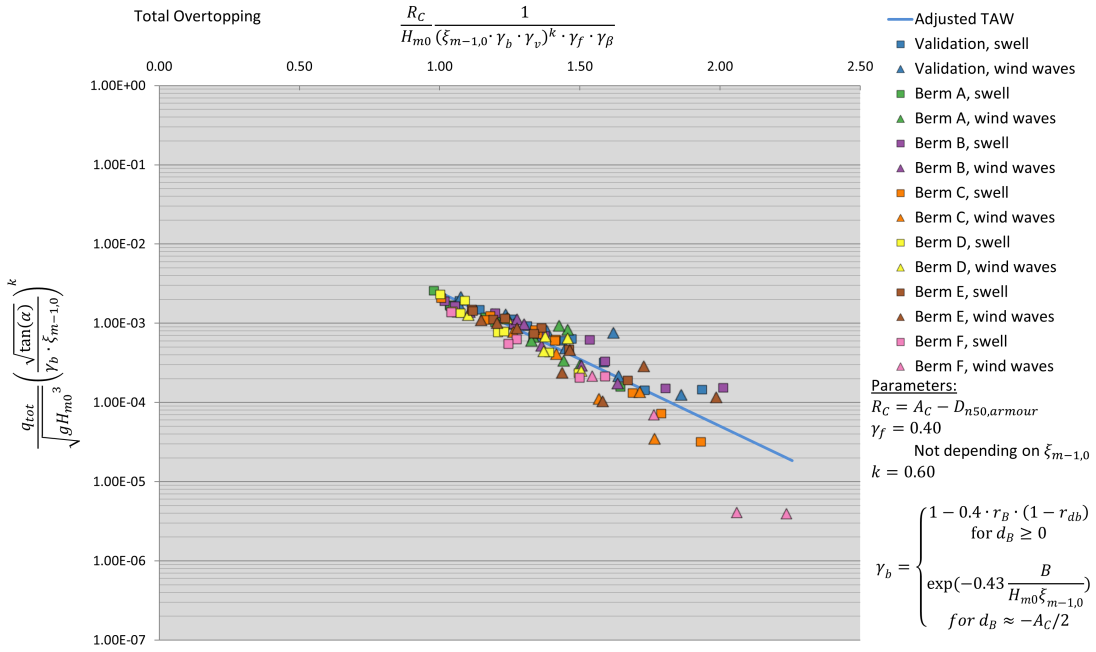


FIGURE B-1: COMPARISON WITH ADJUSTED TAW

With this modification also the Adjusted TAW prediction method accurately predicts the experimental data. The goodness-of-fit per berm configuration is tabulated in Table B-1.

TABLE B-1: GOODNESS-OF-FIT VALUES FOR BERM BREAKWATER TESTS

| $G_{fit}$ | **Adjusted TAW new $\gamma_b$ definition** |
|---|---|
| **Berm A** | 0.02 |
| **Berm B** | 0.03 |
| **Berm C** | 0.06 |
| **Berm D** | 0.02 |
| **Berm E** | 0.03 |
| **Berm F** | 0.26 |

A comparison with the goodness-of-fit values of the proposed expression (Table 4-2) learns that still the proposed expression results in a better fit.

# APPENDIX C. OVERTOPPING REDUCTION FACTOR

The overtopping at a certain distance from the crest can either be calculated by multiplying the total overtopping $q_{tot}$ by a factor $C_r$ or by increasing the dimensionless crest freeboard, dividing by a reduction factor $\gamma_c$. In this appendix it is shown how the calculation methods relate to each other.

Let's assume one overtopping discharge is a fraction $C_r$ from another overtopping discharge, and calculate what the dimensionless freeboard should be to arrive at the same fraction.

$$q_1^* = \mathrm{C} \cdot \exp\left(-\mathrm{D} \cdot R_{C,1}^*\right) \qquad \textit{Equation C-1}$$

$$q_2^* = \mathrm{C} \cdot \exp\left(-\mathrm{D} \cdot R_{C,2}^*\right) \qquad \textit{Equation C-2}$$

$$R_{C,1}^* = \frac{R_C}{H_{m0}} \cdot \frac{1}{\gamma_b \cdot \gamma_f \cdot \gamma_\beta} \qquad \textit{Equation C-3}$$

$$C_r \cdot q_1^* = q_2^* \qquad \textit{Equation C-4}$$

Re-writing Equation C-2 leads to Equation C-5.

$$R_{C,2}^* = -\frac{1}{\mathrm{D}} \ln\left(\frac{q_2^*}{\mathrm{C}}\right) \qquad \textit{Equation C-5}$$

Substituting Equation C-4 into Equation C-5 leads to Equation C-6.

$$R_{C,2}^* = -\frac{1}{\mathrm{D}} \ln\left(\frac{C_r \cdot q_1^*}{\mathrm{C}}\right) \qquad \textit{Equation C-6}$$

Substituting Equation C-1 into Equation C-6 leads to Equation C-7.

$$R_{C,2}^* = -\frac{1}{\mathrm{D}} \ln\left(C_r \cdot \exp\left(-\mathrm{D} \cdot R_{C,1}^*\right)\right) \qquad \textit{Equation C-7}$$

Re-writing Equation C-7 leads to Equation C-8.

$$R_{C,2}^* = -\frac{1}{\mathrm{D}}\left(\ln(C_r) + \mathrm{D} \cdot R_{C,1}^*\right) = R_{C,1}^* - \frac{\ln(C_r)}{\mathrm{D}} \qquad \textit{Equation C-8}$$

$$q_2^* = \mathrm{C} \cdot \exp\left(-\mathrm{D} \cdot R_{C,1}^* + \ln(C_r)\right) \qquad \textit{Equation C-9}$$

Now the reduction factor for the crest freeboard $\gamma_c$ is written as a reduction factor $C_r$.

$$q_1^* = \mathrm{C} \cdot \exp\left(-\mathrm{D} \cdot R_{C,1}^*\right) \qquad \textit{Equation C-10}$$

$$q_2^* = \mathrm{C} \cdot \exp\left(-\mathrm{D} \cdot R_{C,2}^*\right) \qquad \textit{Equation C-11}$$

$$R_{C,1}^* = \frac{R_C}{H_{m0}} \cdot \frac{1}{\gamma_b \cdot \gamma_f \cdot \gamma_\beta \cdot \gamma_c} \qquad \textit{Equation C-12}$$

$$R_{C,2}^* = \frac{R_C}{H_{m0}} \cdot \frac{1}{\gamma_b \cdot \gamma_f \cdot \gamma_\beta} \qquad \textit{Equation C-13}$$

$$q_1^* = \mathrm{C} \cdot \exp\left(-\mathrm{D} \cdot R_{C,2}^*\right)^{\frac{1}{\gamma_c}} = \left(q_2^*\right)^{\frac{1}{\gamma_c}} \qquad \textit{Equation C-14}$$

$$C_r = \frac{q_1^*}{q_2^*} = \left(q_2^*\right)^{\frac{1}{\gamma_c}-1} \qquad \textit{Equation C-15}$$

The reducing effect of $C_r$ is a fixed ratio of $q_{tot}$. The reduction factor $\gamma_c$ leads to reduction of the overtopping discharge by a ratio that depends on the other terms in the dimensionless crest freeboard.

# APPENDIX D. TIME SCHEDULE EXPERIMENT PHASE

The laboratory experiments were carried out over a time span of approximately 2 months. The duration of each phase is indicated in Table D-1, primarily to facilitate planning of future experiments.

TABLE D-1: DURATION PER EXPERIMENT PHASE

| Phase | Activity | Duration |
|---|---|---|
| Preparation | Manual selection of armour stones<br>Rinsing of armour, core material | 5 days |
| | Placement of collection bins structure in wave flume<br>Construction of breakwater | 1 day |
| | Acquiring displacement pumps<br>Instalment pumps, tubes | 5 days |
| Experiments | Running of 104 experiments in total<br>Including adjustments to the breakwater profile | 30 days |
| Finalisation | Recording a 5 minute side view of each breakwater configuration for swell and wind wave conditions | 1 day |
| | Removal of the experiment setup | 1 day |
| **Total** | | **43 working days** |

# APPENDIX E. CONSTRUCTION DRAWINGS FOR THE COLLECTION BIN

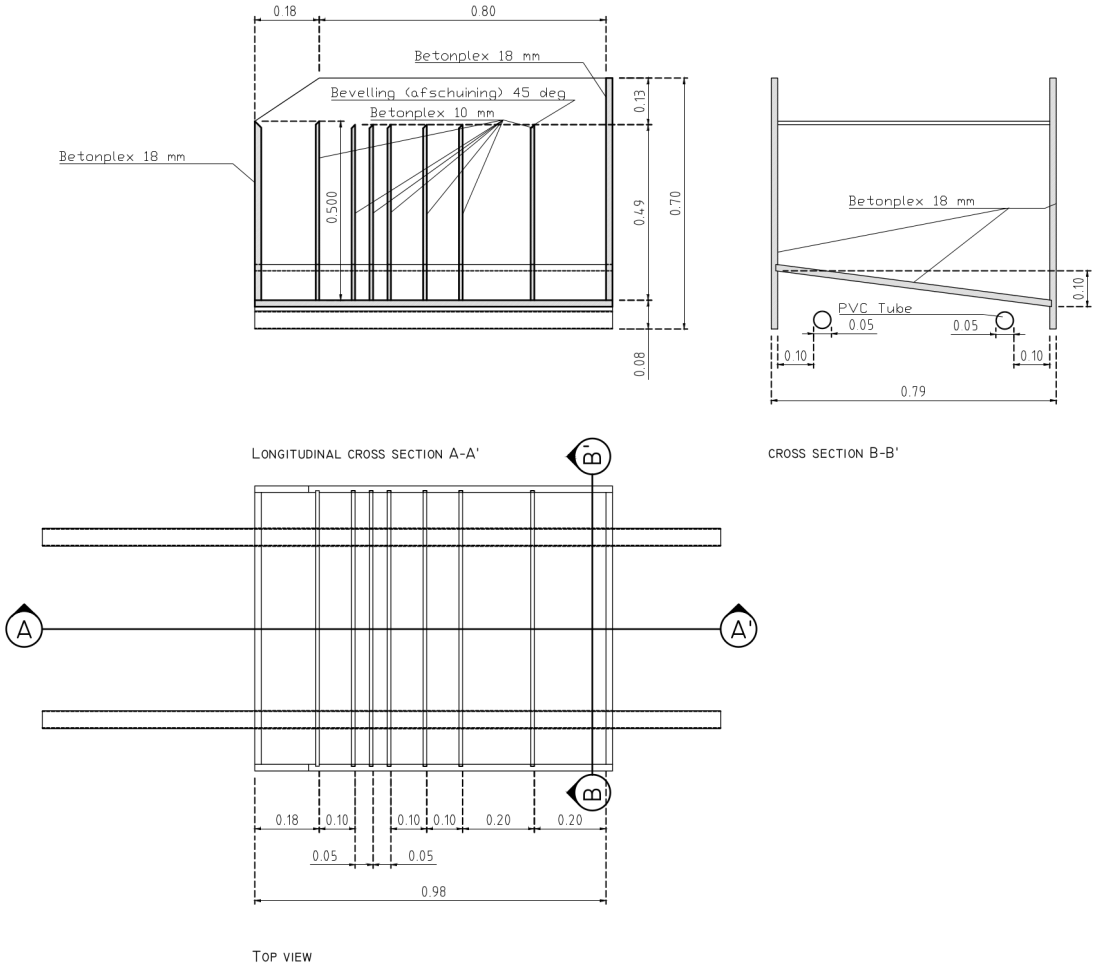


FIGURE E-1: CONSTRUCTION DRAWINGS FOR THE COLLECTION BIN

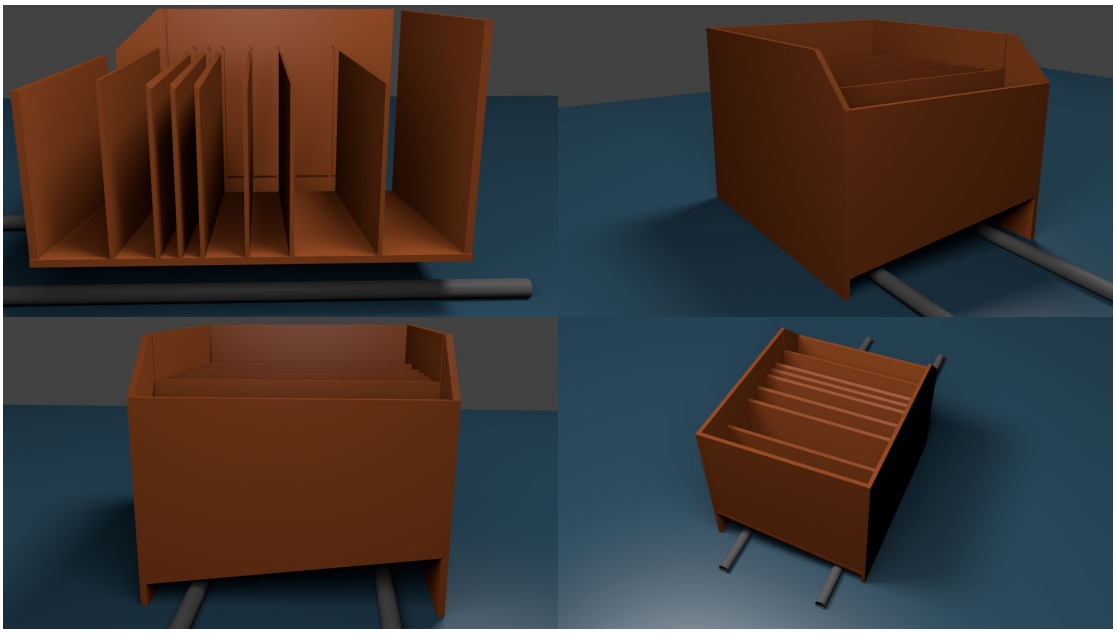

FIGURE E-2: IMPRESSION OF THE COLLECTION BIN. MODELLED AND RENDERED IN BLENDER3D

# APPENDIX F. PICTURES OF THE SCALE MODEL

Below a selection of photographs is presented to illustrate the work done in the laboratory.

FIGURE F-1: OVERVIEW OF THE FLUME; WAVE GAUGES JUST IN FRONT OF THE SCALE MODEL

FIGURE F-2: OVERVIEW OF THE FLUME; SCALE MODEL

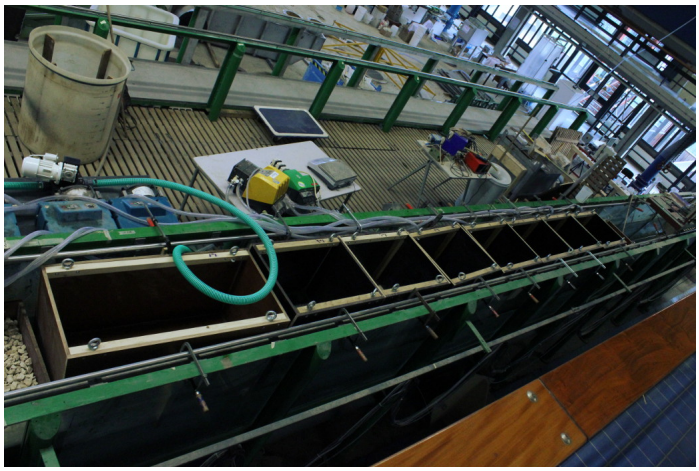

FIGURE F-3: OVERVIEW OF THE FLUME; FLOATING TANKS BEHIND THE SCALE MODEL

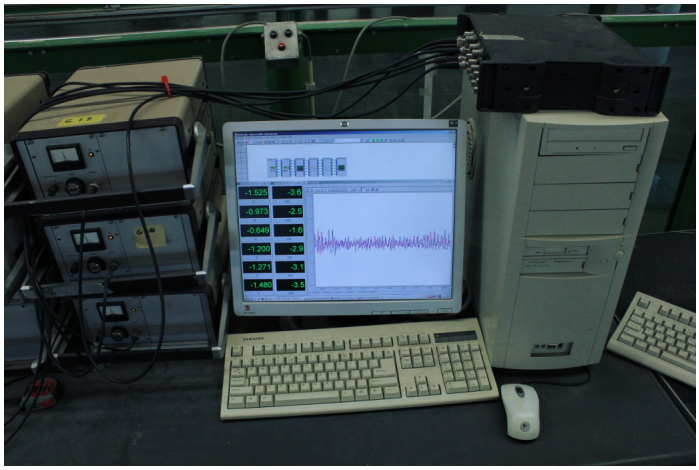

FIGURE F-4: PC RUNNING DASYLAB V9.0. WAVE GAUGE REGISTRATION

FIGURE F-5: PC RUNNING WAVEGENERATOR CONTROL.

# APPENDIX G. WAVE GENERATOR INPUT FILES

For each experiment a wave input file was made to correctly drive the wave generator. This file was then to be processed by a MS-DOS script called “MakeWave.bat” to generate a drive file that could be read by the software driving the wave generator. Beneath an example of a wave input file is printed, specifying all relevant wave conditions. This wave input file was used for test BA01.

```
** invoerfile voor ONregelmatige golven, data file: E-ireg
** Aangepast voor Elektronische Golfmachine sep 2004

debug
facility,e-wave.pos
signal,generation
data,BA01,delete
depth,0.52
second-order,yes
reflection-compensation,yes

WAVETYPE,JONSWAP-SPECTRUM
  Hm0,.10
  PEAK,tp=2.78
  sigma,.07,.09
  gamma,9
  precision,.99
  duration,0:43:0
  longcrested
  random,type=phase,seed=-1
END:WAVETYPE
```

## APPENDIX H. WAVE GENERATOR RESPONSE

During the experiment phase in the Hydraulic Laboratory at Delft University of Technology the "Lange Speurwerk Goot" was used. The wave generator installed at the flume delivered a significantly more accurate wave pattern than the wave generator used by Lioutas (2010). However, still quite large differences were observed between the parameters that were used as input, and the measured parameters. See Figure H-1.

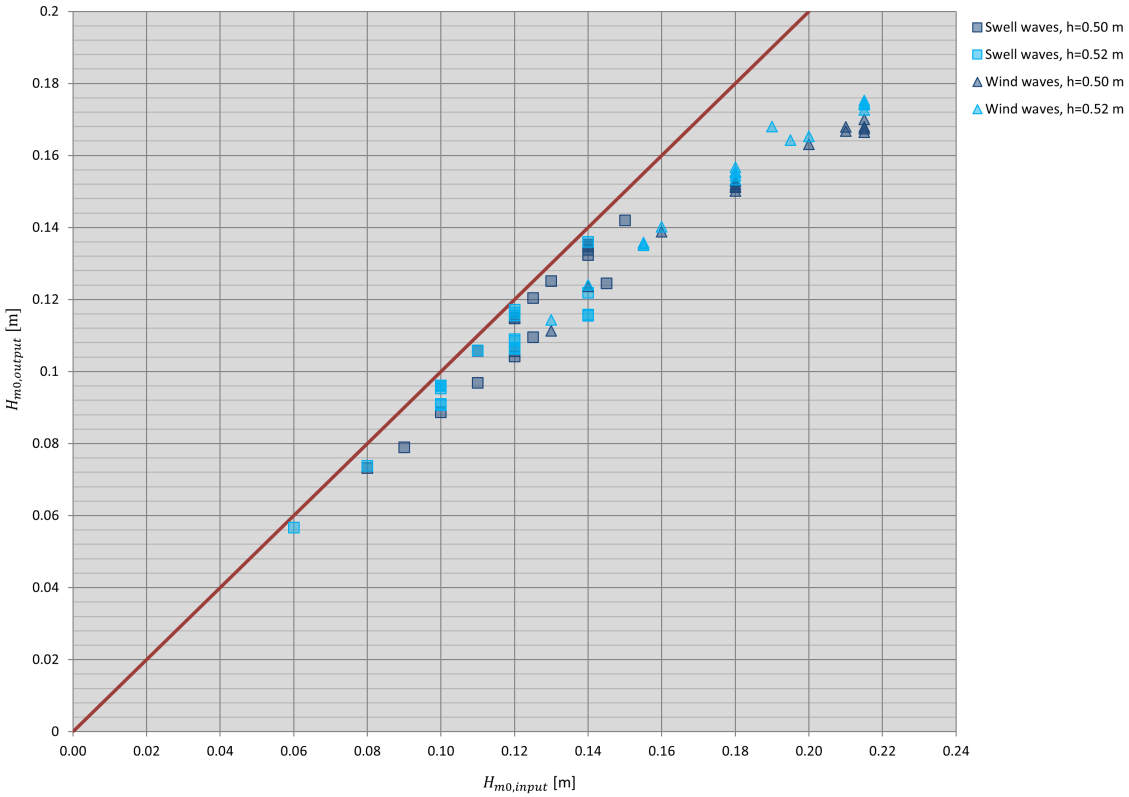


FIGURE H-1: WAVE GENERATOR INPUT, OUTPUT

# APPENDIX I. WAVE GAUGES MEASUREMENT FILE

To determine the wave conditions during a test, wave gauges were deployed in the flume. Every 0.01 second the voltage of the wave gauges was saved with DASYLab v 9.0. With a calibration step the voltage could be transformed to a water level. Later a Matlab routine – see Appendix J –was used to calculate the wave parameters describing the sea state during an experiment.

The data below is a fragment of a file as was delivered by DASYLab. Six channels were defined, each corresponding to a specific wave gauge.

DASYLab - V 9.00.00
WORKSHEET : Meten v1
Recording Date : 8/8/2012, 8:47:03 AM
Block Length : 64
Delta : 0.01 sec.
Number of Channels : 6
Elapsed Time[s];Write 0 [V];Write 1 [V];Write 2 [V];Write 3 [V];Write 4 [V];Write 5 [V];
0.00;0.416;0.348;0.298;0.095;0.147;0.225;
0.01;0.420;0.352;0.304;0.093;0.154;0.225;
0.02;0.418;0.352;0.305;0.095;0.149;0.225;
0.03;0.420;0.357;0.313;0.094;0.153;0.226;
0.04;0.417;0.356;0.313;0.095;0.148;0.225;
0.05;0.420;0.360;0.318;0.093;0.153;0.223;
0.06;0.416;0.359;0.320;0.096;0.150;0.225;
0.07;0.420;0.365;0.326;0.092;0.153;0.225;
0.08;0.416;0.362;0.327;0.096;0.149;0.225;
0.09;0.418;0.368;0.332;0.093;0.151;0.224;
0.10;0.414;0.363;0.334;0.097;0.150;0.226;
0.11;0.416;0.370;0.341;0.095;0.153;0.225;
0.12;0.413;0.367;0.339;0.095;0.149;0.226;
0.13;0.414;0.371;0.346;0.093;0.154;0.225;
0.14;0.410;0.368;0.347;0.096;0.148;0.224;
0.15;0.411;0.373;0.351;0.092;0.154;0.226;
0.16;0.406;0.369;0.351;0.095;0.150;0.225;
0.17;0.406;0.374;0.358;0.094;0.153;0.225;
0.18;0.401;0.370;0.359;0.096;0.149;0.225;
etc.

# APPENDIX J. WAVE GAUGE INTERPRETATION

To determine the parameters describing the sea state during an experiment, the wave gauge information was processed by a Matlab routine called “Decomp15”. The script decomposes incoming and reflecting waves using the method described by Zelt and Skjelbreia (1992). The routine uses a Least Squared Method to interpret the incoming and reflecting components for various wave periods, where for each period the computational weight of the three wave gauges is optimized.

The routine needs as input the position of the three wave gauges closest to the breakwater scale model, and the time series measurements of the wave gauges. Based on these, a calculation is made resulting in an energy variance spectrum of the incoming and reflecting waves. Also a file is printed containing important parameters such as the spectral wave height $H_{m0}$ and the peak period $T_p$. Unfortunately at the time of the experiments the Matlab routine was not set up to calculate the spectral wave period $T_{m-1,0}$. Instead the fixed ratio for a single-peaked spectrum was used to calculate this; $T_p$=1.1$T_{m-1,0}$. During the experiments only single-peaked spectra were generated and therefore it is not expected significant errors are introduced with this step.

# APPENDIX K. EXPERIMENTAL DATA

In the tables below the experiments measurements are presented. Results are sorted based on 1) berm configuration, 2) wave steepness, 3) water depth and 4) wave height.

Experiments where practical errors occurred during the execution are not included.

TABLE K-1: EXPERIMENTAL DATA

| | Test code | $B$ [m] | $d_B$ [m] | tan($\alpha$) | $A_C$ [m] | $h$ [m] | $H_{m0}$ [m] | $T_p$ [s] | $T_{m-1,0}$ [s] | $s_{m-1,0}$ [-] | $\xi_{m-1,0}$ [-] | Test Duration [s] | Water volume per bin [litre] | | | | | | | |
|---|---|---|---|---|---|---|---|---|---|---|---|---|---|---|---|---|---|---|---|---|
| | | | | | | | | | | | | | Bin 1 | Bin 2 | Bin 3 | Bin 4 | Bin 5 | Bin 6 | Bin 7 | Bin 8 |
| Validation | V10 | 0.00 | 0.00 | 1/2 | 0.20 | 0.50 | 0.0732 | 2.54 | 2.31 | 0.009 | 5.33 | 2460 | 58.90 | 0.04 | 0.03 | 0.04 | 0.09 | 0.02 | 0.06 | 0.00 |
| | V11 | 0.00 | 0.00 | 1/2 | 0.20 | 0.50 | 0.0790 | 2.69 | 2.45 | 0.008 | 5.44 | 2460 | 149.50 | 0.02 | 0.01 | 0.00 | 0.02 | 0.00 | 0.01 | 0.00 |
| | V12 | 0.00 | 0.00 | 1/2 | 0.20 | 0.50 | 0.0887 | 2.78 | 2.53 | 0.009 | 5.30 | 2640 | 345.20 | 6.45 | 0.00 | 0.00 | 0.01 | 0.00 | 0.00 | 0.00 |
| | V13 | 0.00 | 0.00 | 1/2 | 0.20 | 0.50 | 0.0968 | 2.91 | 2.65 | 0.009 | 5.31 | 2710 | 464.30 | 158.90 | 7.99 | 2.20 | 0.32 | 0.01 | 0.01 | 0.00 |
| | V04 | 0.00 | 0.00 | 1/2 | 0.20 | 0.50 | 0.1057 | 2.81 | 2.55 | 0.010 | 4.91 | 2580 | 670.20 | 90.30 | 23.30 | 10.30 | 4.60 | 0.00 | 0.00 | 0.00 |
| | V14 | 0.00 | 0.00 | 1/2 | 0.18 | 0.52 | 0.0567 | 2.19 | 1.99 | 0.009 | 5.22 | 2350 | 38.60 | 0.02 | 0.02 | 0.00 | 0.05 | 0.00 | 0.00 | 0.00 |
| | V15 | 0.00 | 0.00 | 1/2 | 0.18 | 0.52 | 0.0739 | 2.54 | 2.31 | 0.009 | 5.31 | 2460 | 262.70 | 0.01 | 0.00 | 0.00 | 0.02 | 0.00 | 0.00 | 0.00 |
| | V16 | 0.00 | 0.00 | 1/2 | 0.18 | 0.52 | 0.0906 | 3.05 | 2.77 | 0.008 | 5.75 | 2360 | 741.50 | 87.00 | 12.80 | 4.20 | 1.08 | 0.01 | 0.00 | 0.00 |
| | V01 | 0.00 | 0.00 | 1/2 | 0.18 | 0.52 | 0.1066 | 2.81 | 2.55 | 0.010 | 4.89 | 2670 | 941.20 | 309.10 | 79.00 | 44.30 | 42.90 | 18.00 | 1.45 | 0.00 |
| | V07 | 0.00 | 0.00 | 1/2 | 0.20 | 0.50 | 0.1680 | 2.13 | 1.94 | 0.029 | 2.95 | 1890 | 843.80 | 427.00 | 196.50 | 106.70 | 57.60 | 23.90 | 8.40 | 0.00 |
| | V05 | 0.00 | 0.00 | 1/2 | 0.20 | 0.50 | 0.1113 | 1.38 | 1.25 | 0.045 | 2.35 | 1260 | 29.90 | 0.20 | 0.00 | 0.00 | 0.00 | 0.00 | 0.00 | 0.00 |
| | V19 | 0.00 | 0.00 | 1/2 | 0.20 | 0.50 | 0.1237 | 1.51 | 1.37 | 0.042 | 2.44 | 1400 | 68.90 | 0.38 | 0.04 | 0.06 | 0.18 | 0.05 | 0.02 | 0.01 |
| | V20 | 0.00 | 0.00 | 1/2 | 0.20 | 0.50 | 0.1388 | 1.62 | 1.47 | 0.041 | 2.47 | 1500 | 197.20 | 2.36 | 0.25 | 0.34 | 0.55 | 0.16 | 0.05 | 0.02 |
| | V06 | 0.00 | 0.00 | 1/2 | 0.20 | 0.50 | 0.1631 | 1.68 | 1.53 | 0.045 | 2.36 | 1740 | 547.30 | 28.80 | 2.30 | 2.20 | 2.90 | 1.20 | 0.20 | 0.00 |
| | V02 | 0.00 | 0.00 | 1/2 | 0.18 | 0.52 | 0.1143 | 1.30 | 1.18 | 0.052 | 2.18 | 1290 | 186.50 | 1.10 | 0.00 | 0.00 | 0.00 | 0.00 | 0.00 | 0.00 |
| | V17 | 0.00 | 0.00 | 1/2 | 0.18 | 0.52 | 0.1240 | 1.54 | 1.40 | 0.041 | 2.48 | 1395 | 259.40 | 2.35 | 0.18 | 0.26 | 0.31 | 0.01 | 0.00 | 0.00 |
| | V18 | 0.00 | 0.00 | 1/2 | 0.18 | 0.52 | 0.1402 | 1.61 | 1.46 | 0.042 | 2.44 | 1500 | 505.90 | 26.90 | 1.02 | 1.08 | 1.49 | 0.56 | 0.02 | 0.03 |
| | V03 | 0.00 | 0.00 | 1/2 | 0.18 | 0.52 | 0.1653 | 1.69 | 1.54 | 0.045 | 2.36 | 1710 | 595.30 | 332.10 | 63.00 | 19.60 | 11.50 | 4.80 | 2.00 | 0.35 |
| Berm A | BA21 | 0.30 | 0.10 | 1/2 | 0.20 | 0.50 | 0.0841 | 2.52 | 2.29 | 0.010 | 4.94 | 2400 | 71.50 | 0.01 | 0.00 | 0.00 | 0.02 | 0.00 | 0.02 | 0.00 |
| | BA22 | 0.30 | 0.10 | 1/2 | 0.20 | 0.50 | 0.1056 | 2.81 | 2.55 | 0.010 | 4.91 | 2580 | 426.50 | 32.70 | 2.73 | 0.17 | 0.01 | 0.00 | 0.00 | 0.00 |
| | BA09 | 0.30 | 0.10 | 1/2 | 0.20 | 0.50 | 0.1204 | 3.05 | 2.77 | 0.010 | 4.99 | 2880 | 778.66 | 158.50 | 47.80 | 36.50 | 45.20 | 15.00 | 3.10 | 0.00 |
| | BA08 | 0.30 | 0.10 | 1/2 | 0.20 | 0.50 | 0.1338 | 3.27 | 2.97 | 0.010 | 5.08 | 2880 | 903.33 | 409.30 | 164.00 | 111.60 | 107.20 | 49.40 | 44.90 | 4.00 |
| | BA01 | 0.30 | 0.12 | 1/2 | 0.18 | 0.52 | 0.0952 | 2.81 | 2.55 | 0.009 | 5.17 | 2475 | 579.40 | 24.20 | 1.20 | 0.00 | 0.00 | 0.00 | 0.00 | 0.00 |
| | BA02 | 0.30 | 0.12 | 1/2 | 0.18 | 0.52 | 0.1090 | 3.11 | 2.83 | 0.009 | 5.35 | 1800 | 586.90 | 182.60 | 42.20 | 29.70 | 37.30 | 9.80 | 1.40 | 0.02 |
| | BA03 | 0.30 | 0.12 | 1/2 | 0.18 | 0.52 | 0.1158 | 3.20 | 2.91 | 0.009 | 5.34 | 600 | 220.10 | 105.80 | 48.70 | 46.10 | 30.10 | 20.10 | 18.20 | 2.76 |
| | BA18 | 0.30 | 0.10 | 1/2 | 0.20 | 0.50 | 0.1468 | 1.59 | 1.45 | 0.045 | 2.36 | 1740 | 141.10 | 0.56 | 0.05 | 0.06 | 0.18 | 0.06 | 0.07 | 0.03 |
| | BA11 | 0.30 | 0.10 | 1/2 | 0.20 | 0.50 | 0.1528 | 1.62 | 1.47 | 0.045 | 2.35 | 3000 | 288.80 | 3.60 | 0.00 | 0.00 | 0.00 | 0.00 | 0.00 | 0.00 |
| | BA19 | 0.30 | 0.10 | 1/2 | 0.20 | 0.50 | 0.1667 | 1.68 | 1.53 | 0.046 | 2.34 | 1500 | 292.20 | 2.98 | 0.25 | 0.35 | 0.59 | 0.19 | 0.05 | 0.03 |
| | BA12 | 0.30 | 0.10 | 1/2 | 0.20 | 0.50 | 0.1680 | 1.65 | 1.50 | 0.048 | 2.29 | 1602 | 349.60 | 4.60 | 0.00 | 0.00 | 0.00 | 0.00 | 0.00 | 0.00 |
| | BA04 | 0.30 | 0.12 | 1/2 | 0.18 | 0.52 | 0.1354 | 1.39 | 1.26 | 0.054 | 2.15 | 1380 | 264.10 | 1.50 | 0.00 | 0.00 | 0.00 | 0.00 | 0.00 | 0.00 |
| | BA15 | 0.30 | 0.12 | 1/2 | 0.18 | 0.52 | 0.1388 | 1.40 | 1.27 | 0.055 | 2.13 | 1590 | 353.50 | 1.31 | 0.07 | 0.08 | 0.15 | 0.03 | 0.08 | 0.09 |
| | BA16 | 0.30 | 0.12 | 1/2 | 0.18 | 0.52 | 0.1510 | 1.60 | 1.45 | 0.046 | 2.34 | 1845 | 597.30 | 12.36 | 0.40 | 0.49 | 0.62 | 0.13 | 0.08 | 0.03 |
| | BA05 | 0.30 | 0.12 | 1/2 | 0.18 | 0.52 | 0.1552 | 1.65 | 1.50 | 0.044 | 2.38 | 1500 | 536.10 | 40.60 | 0.90 | 0.90 | 1.40 | 0.50 | 0.00 | 0.00 |
| | BA17 | 0.30 | 0.12 | 1/2 | 0.18 | 0.52 | 0.1596 | 1.62 | 1.47 | 0.047 | 2.30 | 1506 | 553.10 | 43.70 | 0.98 | 0.69 | 0.92 | 0.25 | 0.06 | 0.04 |
| | BA06 | 0.30 | 0.12 | 1/2 | 0.18 | 0.52 | 0.1745 | 1.75 | 1.59 | 0.044 | 2.38 | 1560 | 579.00 | 186.40 | 5.00 | 3.90 | 5.10 | 2.20 | 1.00 | 0.30 |
| Berm B | BB14 | 0.30 | 0.00 | 1/2 | 0.20 | 0.50 | 0.0800 | 2.52 | 2.29 | 0.010 | 4.97 | 2400 | 61.80 | 0.08 | 0.02 | 0.01 | 0.01 | 0.00 | 0.00 | 0.00 |
| | BB15 | 0.30 | 0.00 | 1/2 | 0.20 | 0.50 | 0.0900 | 2.67 | 2.43 | 0.010 | 4.96 | 2505 | 171.10 | 0.08 | 0.00 | 0.00 | 0.00 | 0.00 | 0.00 | 0.00 |
| | BB07 | 0.30 | 0.00 | 1/2 | 0.20 | 0.50 | 0.1058 | 2.91 | 2.65 | 0.010 | 5.08 | 2700 | 429.20 | 36.60 | 2.64 | 2.60 | 2.00 | 0.30 | 0.60 | 0.60 |
| | BB16 | 0.30 | 0.00 | 1/2 | 0.20 | 0.50 | 0.1100 | 2.93 | 2.66 | 0.010 | 4.86 | 2700 | 620.80 | 88.40 | 27.00 | 14.80 | 10.70 | 0.86 | 0.03 | 0.03 |
| | BB08 | 0.30 | 0.00 | 1/2 | 0.20 | 0.50 | 0.1419 | 3.30 | 3.00 | 0.010 | 4.98 | 1620 | 571.70 | 297.20 | 114.20 | 88.50 | 83.00 | 38.50 | 32.50 | 0.18 |
| | BB11 | 0.30 | 0.02 | 1/2 | 0.18 | 0.52 | 0.0665 | 2.13 | 1.94 | 0.011 | 4.69 | 2160 | 38.80 | 0.02 | 0.00 | 0.00 | 0.00 | 0.00 | 0.00 | 0.00 |
| | BB12 | 0.30 | 0.02 | 1/2 | 0.18 | 0.52 | 0.0832 | 2.52 | 2.29 | 0.010 | 4.96 | 2430 | 257.20 | 0.00 | 0.00 | 0.00 | 0.01 | 0.02 | 0.00 | 0.00 |
| | BB13 | 0.30 | 0.02 | 1/2 | 0.18 | 0.52 | 0.1058 | 2.81 | 2.55 | 0.010 | 4.91 | 2235 | 668.30 | 63.90 | 10.50 | 2.32 | 0.09 | 0.00 | 0.00 | 0.00 |
| | BB01 | 0.30 | 0.02 | 1/2 | 0.18 | 0.52 | 0.1163 | 3.08 | 2.80 | 0.010 | 5.13 | 1680 | 570.70 | 147.20 | 32.60 | 27.90 | 33.30 | 7.70 | 1.60 | 0.06 |
| | BB17 | 0.30 | 0.00 | 1/2 | 0.20 | 0.50 | 0.1417 | 1.50 | 1.36 | 0.049 | 2.26 | 1500 | 64.10 | 0.28 | 0.02 | 0.04 | 0.05 | 0.02 | 0.02 | 0.00 |
| | BB18 | 0.30 | 0.00 | 1/2 | 0.20 | 0.50 | 0.1523 | 1.57 | 1.43 | 0.048 | 2.28 | 1470 | 118.70 | 0.68 | 0.06 | 0.08 | 0.09 | 0.02 | 0.01 | 0.01 |
| | BB09 | 0.30 | 0.00 | 1/2 | 0.20 | 0.50 | 0.1668 | 1.65 | 1.50 | 0.047 | 2.29 | 1620 | 264.90 | 3.20 | 0.41 | 0.44 | 0.46 | 0.12 | 0.07 | 0.00 |
| | BB10 | 0.30 | 0.00 | 1/2 | 0.20 | 0.50 | 0.1758 | 1.67 | 1.52 | 0.049 | 2.26 | 900 | 288.00 | 10.70 | 0.70 | 0.83 | 1.10 | 0.37 | 0.19 | 0.00 |
| | BB04 | 0.30 | 0.02 | 1/2 | 0.18 | 0.52 | 0.1533 | 1.58 | 1.44 | 0.048 | 2.29 | 1530 | 472.00 | 6.50 | 0.49 | 0.57 | 0.72 | 0.25 | 0.11 | 0.00 |
| | BB05 | 0.30 | 0.02 | 1/2 | 0.18 | 0.52 | 0.1745 | 1.70 | 1.55 | 0.047 | 2.31 | 1620 | 603.70 | 160.70 | 4.20 | 3.30 | 5.30 | 2.50 | 1.40 | 0.20 |
| Berm C | BC14 | 0.30 | -0.10 | 1/2 | 0.20 | 0.50 | 0.0824 | 2.52 | 2.29 | 0.010 | 4.99 | 2415 | 12.20 | 0.01 | 0.01 | 0.00 | 0.00 | 0.00 | 0.00 | 0.00 |
| | BC13 | 0.30 | -0.10 | 1/2 | 0.20 | 0.50 | 0.0880 | 2.60 | 2.36 | 0.010 | 4.98 | 2460 | 31.60 | 0.03 | 0.01 | 0.01 | 0.00 | 0.00 | 0.00 | 0.00 |
| | BC15 | 0.30 | -0.10 | 1/2 | 0.20 | 0.50 | 0.0911 | 2.71 | 2.46 | 0.010 | 5.10 | 2550 | 64.30 | 0.08 | 0.00 | 0.02 | 0.05 | 0.03 | 0.02 | 0.00 |
| | BC08 | 0.30 | -0.10 | 1/2 | 0.20 | 0.50 | 0.1042 | 2.99 | 2.72 | 0.009 | 5.26 | 2880 | 378.60 | 39.70 | 4.80 | 1.40 | 1.00 | 0.14 | 0.00 | 0.00 |
| | BC09 | 0.30 | -0.10 | 1/2 | 0.20 | 0.50 | 0.1095 | 3.02 | 2.75 | 0.009 | 5.18 | 2880 | 474.80 | 58.40 | 10.70 | 5.00 | 3.60 | 0.48 | 0.00 | 0.00 |
| | BC16 | 0.30 | -0.10 | 1/2 | 0.20 | 0.50 | 0.1143 | 2.99 | 2.72 | 0.010 | 5.10 | 2820 | 520.30 | 66.00 | 15.30 | 7.64 | 4.87 | 0.41 | 0.03 | 0.02 |
| | BC10 | 0.30 | -0.10 | 1/2 | 0.20 | 0.50 | 0.1244 | 3.24 | 2.95 | 0.009 | 5.22 | 1860 | 518.50 | 110.20 | 19.50 | 11.60 | 7.87 | 0.78 | 0.00 | 0.00 |
| | BC01 | 0.30 | -0.08 | 1/2 | 0.18 | 0.52 | 0.0909 | 2.79 | 2.54 | 0.009 | 5.25 | 2580 | 313.40 | 0.16 | 0.00 | 0.00 | 0.00 | 0.00 | 0.00 | 0.00 |
| | BC02 | 0.30 | -0.08 | 1/2 | 0.18 | 0.52 | 0.1062 | 3.02 | 2.75 | 0.009 | 5.26 | 1920 | 520.30 | 60.00 | 13.00 | 5.50 | 3.40 | 0.25 | 0.06 | 0.00 |
| | BC03 | 0.30 | -0.08 | 1/2 | 0.18 | 0.52 | 0.1218 | 3.26 | 2.96 | 0.009 | 5.30 | 1140 | 402.70 | 143.50 | 66.00 | 53.20 | 53.20 | 24.10 | 9.80 | 0.50 |
| | BC11 | 0.30 | -0.10 | 1/2 | 0.20 | 0.50 | 0.1501 | 1.55 | 1.41 | 0.048 | 2.27 | 1530 | 12.40 | 0.10 | 0.05 | 0.00 | 0.00 | 0.00 | 0.00 | 0.00 |
| | BC12 | 0.30 | -0.10 | 1/2 | 0.20 | 0.50 | 0.1665 | 1.62 | 1.47 | 0.049 | 2.26 | 1260 | 37.80 | 0.34 | 0.10 | 0.14 | 0.25 | 0.20 | 0.10 | 0.00 |
| | BC04 | 0.30 | -0.08 | 1/2 | 0.18 | 0.52 | 0.1350 | 1.48 | 1.35 | 0.048 | 2.29 | 1392 | 36.60 | 0.20 | 0.10 | 0.00 | 0.00 | 0.00 | 0.00 | 0.00 |
| | BC05 | 0.30 | -0.08 | 1/2 | 0.18 | 0.52 | 0.1555 | 1.62 | 1.47 | 0.046 | 2.33 | 1500 | 156.60 | 0.00 | 0.00 | 0.00 | 0.00 | 0.00 | 0.00 | 0.00 |
| | BC06 | 0.30 | -0.08 | 1/2 | 0.18 | 0.52 | 0.1742 | 1.67 | 1.52 | 0.048 | 2.27 | 1620 | 379.50 | 2.00 | 0.13 | 0.27 | 0.22 | 0.00 | 0.00 | 0.00 |

| | Test code | $B$ [m] | $d_B$ [m] | tan($\alpha$) | $A_C$ [m] | $h$ [m] | $H_{m0}$ [m] | $T_p$ [s] | $T_{m-1,0}$ [s] | $s_{m-1,0}$ [-] | $\xi_{m-1,0}$ [-] | Test Duration [s] | Water volume per bin [litre] | | | | | | | |
|---|---|---|---|---|---|---|---|---|---|---|---|---|---|---|---|---|---|---|---|---|
| | | | | | | | | | | | | | Bin 1 | Bin 2 | Bin 3 | Bin 4 | Bin 5 | Bin 6 | Bin 7 | Bin 8 |
| Berm D | BD16 | 0.60 | 0.10 | 1/2 | 0.20 | 0.50 | 0.0944 | 2.71 | 2.46 | 0.010 | 5.01 | 2550 | 132.10 | 0.21 | 0.03 | 0.08 | 0.09 | 0.04 | 0.08 | 0.02 |
| | BD15 | 0.60 | 0.10 | 1/2 | 0.20 | 0.50 | 0.1028 | 2.81 | 2.55 | 0.010 | 4.98 | 2580 | 271.20 | 1.91 | 0.04 | 0.04 | 0.10 | 0.05 | 0.10 | 0.03 |
| | BD09 | 0.60 | 0.10 | 1/2 | 0.20 | 0.50 | 0.1156 | 3.05 | 2.77 | 0.010 | 5.09 | 2880 | 572.40 | 69.80 | 14.00 | 6.30 | 4.20 | 0.65 | 0.12 | 0.00 |
| | BD14 | 0.60 | 0.10 | 1/2 | 0.20 | 0.50 | 0.1348 | 3.23 | 2.94 | 0.010 | 5.00 | 1740 | 574.90 | 152.70 | 42.10 | 28.60 | 30.80 | 16.50 | 4.60 | 0.14 |
| | BD10 | 0.60 | 0.10 | 1/2 | 0.20 | 0.50 | 0.1352 | 3.37 | 3.06 | 0.009 | 5.21 | 1710 | 554.20 | 198.60 | 50.70 | 37.40 | 36.40 | 17.70 | 13.30 | 0.16 |
| | BD01 | 0.60 | 0.12 | 1/2 | 0.18 | 0.52 | 0.0960 | 2.81 | 2.55 | 0.009 | 5.15 | 2580 | 459.80 | 5.45 | 0.08 | 0.00 | 0.00 | 0.00 | 0.00 | 0.00 |
| | BD02 | 0.60 | 0.12 | 1/2 | 0.18 | 0.52 | 0.1085 | 2.96 | 2.69 | 0.010 | 5.10 | 1260 | 529.00 | 77.60 | 25.20 | 21.90 | 14.90 | 3.70 | 0.40 | 0.00 |
| | BD03 | 0.60 | 0.12 | 1/2 | 0.18 | 0.52 | 0.1155 | 3.20 | 2.91 | 0.009 | 5.35 | 600 | 225.40 | 73.00 | 41.40 | 36.60 | 28.40 | 19.00 | 5.70 | 0.22 |
| | BD12 | 0.60 | 0.10 | 1/2 | 0.20 | 0.50 | 0.1512 | 1.62 | 1.47 | 0.045 | 2.37 | 1500 | 103.40 | 0.60 | 0.00 | 0.00 | 0.00 | 0.00 | 0.00 | 0.00 |
| | BD13 | 0.60 | 0.10 | 1/2 | 0.20 | 0.50 | 0.1700 | 1.65 | 1.50 | 0.048 | 2.27 | 1560 | 221.70 | 1.76 | 0.00 | 0.00 | 0.00 | 0.00 | 0.00 | 0.00 |
| | BD05 | 0.60 | 0.12 | 1/2 | 0.18 | 0.52 | 0.1357 | 1.45 | 1.32 | 0.050 | 2.24 | 1380 | 206.10 | 0.37 | 0.00 | 0.00 | 0.00 | 0.00 | 0.00 | 0.00 |
| | BD17 | 0.60 | 0.12 | 1/2 | 0.18 | 0.52 | 0.1418 | 1.52 | 1.38 | 0.048 | 2.29 | 1380 | 234.40 | 0.38 | 0.01 | 0.02 | 0.04 | 0.02 | 0.02 | 0.01 |
| | BD06 | 0.60 | 0.12 | 1/2 | 0.18 | 0.52 | 0.1567 | 1.62 | 1.47 | 0.046 | 2.32 | 1500 | 493.50 | 13.90 | 0.30 | 0.20 | 0.40 | 0.20 | 0.05 | 0.00 |
| | BD07 | 0.60 | 0.12 | 1/2 | 0.18 | 0.52 | 0.1742 | 1.75 | 1.59 | 0.044 | 2.38 | 1560 | 575.60 | 106.90 | 1.11 | 1.32 | 1.93 | 1.00 | 0.28 | 0.00 |
| Berm E | BE13 | 0.60 | 0.00 | 1/2 | 0.20 | 0.50 | 0.0934 | 2.69 | 2.45 | 0.010 | 5.00 | 2550 | 94.90 | 0.09 | 0.00 | 0.01 | 0.01 | 0.00 | 0.00 | 0.00 |
| | BE12 | 0.60 | 0.00 | 1/2 | 0.20 | 0.50 | 0.1067 | 2.83 | 2.57 | 0.010 | 4.92 | 2865 | 316.30 | 4.91 | 0.04 | 0.00 | 0.05 | 0.01 | 0.02 | 0.00 |
| | BE07 | 0.60 | 0.00 | 1/2 | 0.20 | 0.50 | 0.1149 | 2.99 | 2.72 | 0.010 | 5.01 | 2880 | 493.50 | 64.60 | 12.50 | 4.66 | 2.72 | 0.34 | 0.12 | 0.16 |
| | BE09 | 0.60 | 0.00 | 1/2 | 0.20 | 0.50 | 0.1251 | 3.24 | 2.95 | 0.009 | 5.20 | 1740 | 474.70 | 81.50 | 18.70 | 15.00 | 17.40 | 6.56 | 2.08 | 0.13 |
| | BE08 | 0.60 | 0.00 | 1/2 | 0.20 | 0.50 | 0.1347 | 3.27 | 2.97 | 0.010 | 5.06 | 1700 | 531.30 | 184.30 | 47.90 | 30.80 | 36.10 | 17.40 | 5.40 | 0.13 |
| | BE01 | 0.60 | 0.02 | 1/2 | 0.18 | 0.52 | 0.0961 | 2.78 | 2.53 | 0.010 | 5.09 | 2640 | 469.70 | 8.64 | 0.10 | 0.10 | 0.05 | 0.00 | 0.00 | 0.00 |
| | BE03 | 0.60 | 0.02 | 1/2 | 0.18 | 0.52 | 0.1058 | 2.91 | 2.65 | 0.010 | 5.08 | 2700 | 682.90 | 58.90 | 8.60 | 1.70 | 0.47 | 0.10 | 0.02 | 0.00 |
| | BE02 | 0.60 | 0.02 | 1/2 | 0.18 | 0.52 | 0.1172 | 3.02 | 2.75 | 0.010 | 5.01 | 2280 | 756.10 | 129.60 | 28.00 | 23.90 | 17.10 | 1.84 | 0.03 | 0.00 |
| | BE10 | 0.60 | 0.00 | 1/2 | 0.20 | 0.50 | 0.1514 | 1.58 | 1.44 | 0.047 | 2.31 | 1560 | 42.60 | 0.07 | 0.04 | 0.03 | 0.08 | 0.01 | 0.03 | 0.00 |
| | BE11 | 0.60 | 0.00 | 1/2 | 0.20 | 0.50 | 0.1680 | 1.62 | 1.47 | 0.050 | 2.25 | 1740 | 126.60 | 0.06 | 0.01 | 0.01 | 0.02 | 0.01 | 0.01 | 0.00 |
| | BE14 | 0.60 | 0.01 | 1/2 | 0.19 | 0.51 | 0.1547 | 1.54 | 1.40 | 0.051 | 2.22 | 1800 | 220.60 | 0.06 | 0.00 | 0.00 | 0.00 | 0.00 | 0.01 | 0.00 |
| | BE16 | 0.60 | 0.02 | 1/2 | 0.18 | 0.52 | 0.1054 | 1.32 | 1.20 | 0.047 | 2.31 | 1320 | 22.90 | 0.01 | 0.00 | 0.00 | 0.00 | 0.00 | 0.00 | 0.00 |
| | BE15 | 0.60 | 0.02 | 1/2 | 0.18 | 0.52 | 0.1214 | 1.39 | 1.26 | 0.049 | 2.27 | 2130 | 112.80 | 0.03 | 0.00 | 0.00 | 0.00 | 0.00 | 0.00 | 0.00 |
| | BE04 | 0.60 | 0.02 | 1/2 | 0.18 | 0.52 | 0.1554 | 1.68 | 1.53 | 0.043 | 2.42 | 1500 | 367.90 | 0.25 | 0.02 | 0.05 | 0.06 | 0.03 | 0.01 | 0.01 |
| | BE05 | 0.60 | 0.02 | 1/2 | 0.18 | 0.52 | 0.1643 | 1.72 | 1.56 | 0.043 | 2.41 | 1500 | 464.70 | 1.79 | 0.00 | 0.05 | 0.15 | 0.14 | 0.31 | 0.26 |
| | BE06 | 0.60 | 0.02 | 1/2 | 0.18 | 0.52 | 0.1726 | 1.75 | 1.59 | 0.044 | 2.39 | 1560 | 539.40 | 28.20 | 0.12 | 0.09 | 0.15 | 0.06 | 0.10 | 0.12 |
| Berm F | BF09 | 0.60 | -0.10 | 1/2 | 0.20 | 0.50 | 0.1148 | 2.99 | 2.72 | 0.010 | 5.01 | 3000 | 148.40 | 0.71 | 0.02 | 0.01 | 0.03 | 0.01 | 0.01 | 0.00 |
| | BF10 | 0.60 | -0.10 | 1/2 | 0.20 | 0.50 | 0.1324 | 3.24 | 2.95 | 0.010 | 5.06 | 2960 | 468.70 | 28.00 | 5.38 | 3.44 | 2.22 | 0.04 | 0.01 | 0.01 |
| | BF01 | 0.60 | -0.08 | 1/2 | 0.18 | 0.52 | 0.0961 | 2.78 | 2.53 | 0.010 | 5.09 | 2700 | 102.60 | 0.00 | 0.01 | 0.00 | 0.00 | 0.00 | 0.01 | 0.00 |
| | BF02 | 0.60 | -0.08 | 1/2 | 0.18 | 0.52 | 0.1156 | 2.99 | 2.72 | 0.010 | 4.99 | 2890 | 419.40 | 25.30 | 0.45 | 0.02 | 0.00 | 0.00 | 0.00 | 0.00 |
| | BF03 | 0.60 | -0.08 | 1/2 | 0.18 | 0.52 | 0.1360 | 3.24 | 2.95 | 0.010 | 4.99 | 2400 | 830.60 | 154.70 | 36.20 | 23.40 | 21.70 | 4.95 | 0.27 | 0.02 |
| | BF12 | 0.60 | -0.10 | 1/2 | 0.20 | 0.50 | 0.1520 | 1.52 | 1.38 | 0.051 | 2.21 | 1500 | 1.10 | 0.01 | 0.01 | 0.02 | 0.05 | 0.01 | 0.04 | 0.06 |
| | BF13 | 0.60 | -0.10 | 1/2 | 0.20 | 0.50 | 0.1674 | 1.51 | 1.37 | 0.057 | 2.10 | 1270 | 1.10 | 0.00 | 0.00 | 0.01 | 0.01 | 0.01 | 0.02 | 0.00 |
| | BF06 | 0.60 | -0.08 | 1/2 | 0.18 | 0.52 | 0.1544 | 1.62 | 1.47 | 0.046 | 2.34 | 1500 | 21.10 | 0.25 | 0.08 | 0.12 | 0.13 | 0.08 | 0.02 | 0.01 |
| | BF07 | 0.60 | -0.08 | 1/2 | 0.18 | 0.52 | 0.1753 | 1.65 | 1.50 | 0.050 | 2.24 | 1620 | 86.90 | 0.10 | 0.00 | 0.02 | 0.06 | 0.04 | 0.01 | 0.00 |

For the location of the different collection bins refer to Table 3-7.

# APPENDIX L. RECOMMENDED EXPERIMENT SETUP

When applying this experiment setup several points of consideration should be taken into mind. As already discussed in section 6.3, floating tanks and pumps need to be used as to prevent lowering of the water table. Plastic pipelines underneath the scale model should ensure water can be exchanged between both sides of the flume. Furthermore core/backfill material should be scaled such that internal flow is simulated correctly.

Chutes are used to collect overtopped water at a certain distance from the crest. The backfill material underneath the chute could still be used to store overtopped water, thereby leading to too high infiltration rates. This effect is illustrated in Figure L-1. One option to mitigate this model effect is to place an impermeable volume between chute and SWL, but this is only valid when the internal water table in prototype situation remains fairly constant at SWL during wave action.

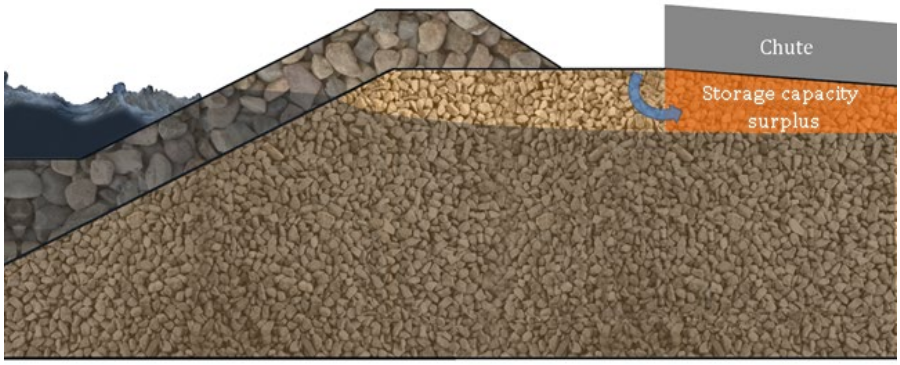


FIGURE L-1: EFFECT OF BACKFILL MATERIAL UNDERNEATH CHUTES

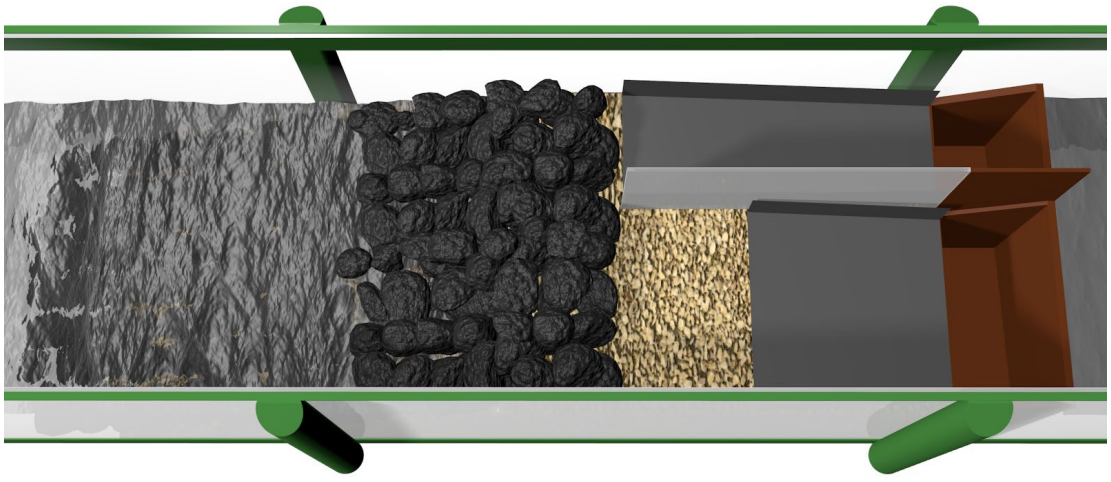

FIGURE L-2: 3D IMPRESSION OF RECOMMENDED EXPERIMENT SETUP

Construction drawings for the recommended experiment setup are provided on the next page.

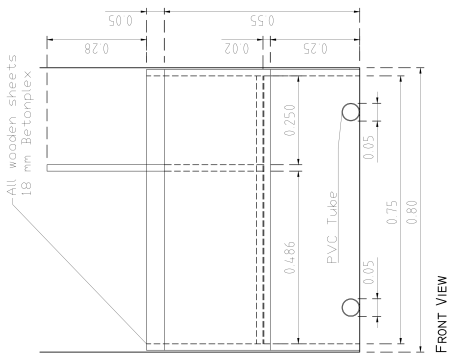


FRONT VIEW

Recommended Experiment Setup
Units: m

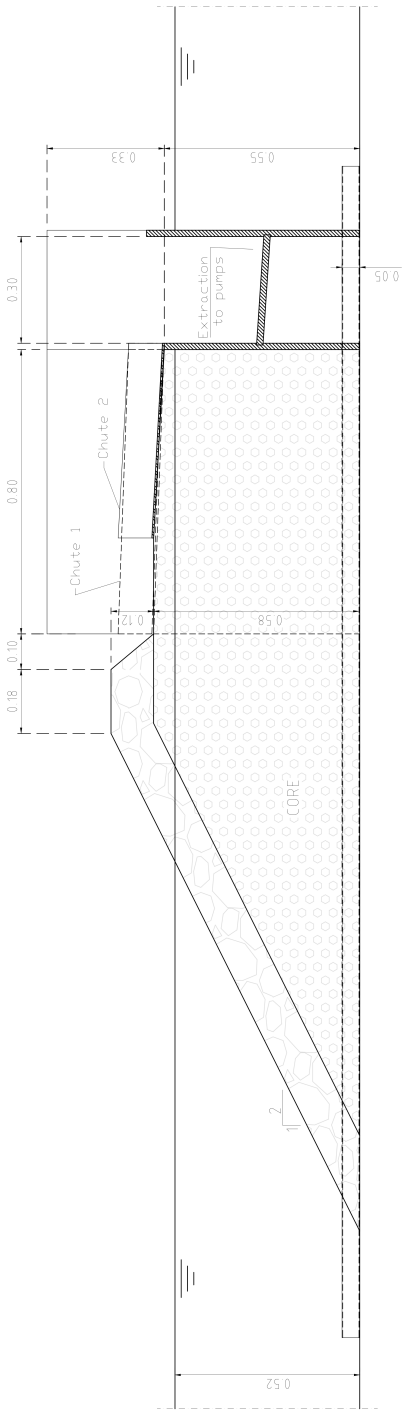


LONGITUDINAL CROSS SECTION A-A'

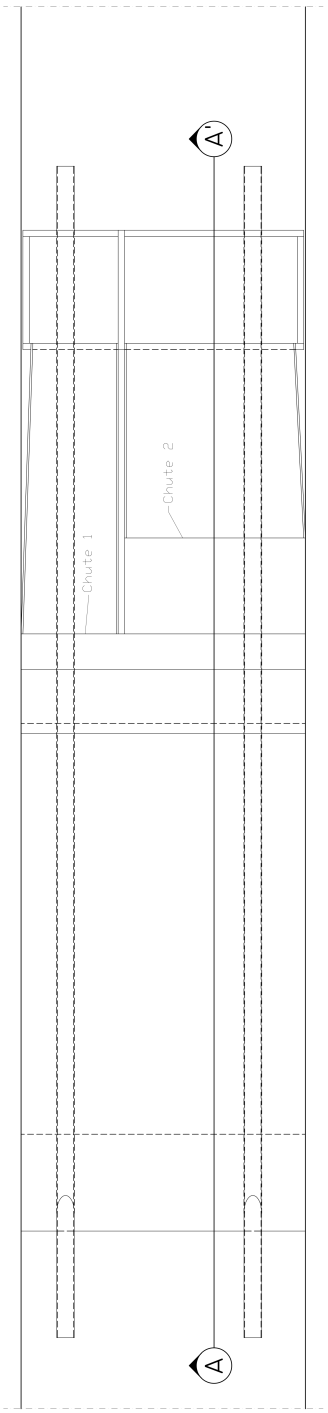


TOP VIEW